Adaptations of Principal Neurons in the Ventral Cochlear Nucleus with Upstream Perturbations

By

Samantha Wright

A dissertation submitted in partial fulfillment of the requirements for the degree of

Doctor of Philosophy

Neuroscience

at the

UNIVERSITY OF WISCONSIN-MADISON

2014

Date of final oral examination: 6.5.2014

The dissertation is approved by the following members of the Final Oral Committee:
Donata Oertel, Professor, Neuroscience
Tom Yin, Professor, Neuroscience
Robert Fettiplace, Professor, Neuroscience
Edwin Chapman, Professor, Neuroscience
Corinna Burger, Assistant Professor, Neurology

Acknowledgements

First and foremost, I would like to thank my horse, without whom I would never have the confidence or determination to begin the endeavor of a graduate education. Since she will never read this, the point seems moot; however, the gratitude and appreciation for the friendship and support still exist.

Secondly, I am grateful to Donata for the generous opportunity she afforded me by taking me into her lab. It was a gamble to accept me as a student and agree to support me throughout the process of gaining a graduate degree, one that I hope she can look back upon with a smile, a few laughs and little if any regrets. I am honored to have been trained by her, I am obliged for the professional good fortune that will arise because of my degree, and of course, I am delighted with our friendship.

Table of Contents

Abstract

The aim of this work is to understand how primary auditory neurons in the brainstem adapt to altered acoustically driven and prehearing spontaneous activity. It is well understood and documented that auditory pathologies result in the atrophy and death of principal neurons throughout the auditory pathway, but how do the surviving neurons respond and adjust to abnormal stimuli or to the lack of any sound evoked excitation?

To elucidate these answers we use a mouse model in which calcium induced exocytosis from inner hair cells to spiral ganglion neurons is absent. These mutant mice never hear and are thought to be lacking most if not all prehearing patterned spontaneous activity after P4. Here we investigate the innervation of cochlear nuclei by auditory nerve fibers, which are composed of the axons of spiral ganglion neurons, and how they maintain the precise topographic organization of frequency specific innervation within the cochlear nuclei; or in the case of a different mutant, how auditory nerve fibers fail to stereotypically infiltrate the cochlear nuclei due to an inability to bifurcate. We also examine the morphology of the specialized axon terminals of spiral ganglion neurons which contact bushy cells, end bulbs of Held, and study how deafness affects their structure. Additionally, the physiology of these mutant synapses, as well as the biophysically properties of the bushy cells themselves was compared with the wild type.

It is well known and characterized that neurons are plastic and can quickly adapt to changes in excitation, inhibition and innervation. In a sensory system where neuronal plasticity could alter the reliable encoding of sound, how do principal neurons regulate themselves to faithfully convey neuronal transmission in the face of altered excitability? We found that the principal auditory brainstem neurons and their connections are indeed modified in response to genetic and sensory manipulation.

We found that mice which lack typical acoustic excitation and most prehearing patterned spontaneous activation have alterations at the end bulb bushy cell interface. End bulbs that contact bushy cells of the deaf mutant mice are less robust with shrunken morphologies compared to wild type hearing mice; however, the synaptic currents which are delivered through these wispy mutant end bulbs are larger than the synaptic currents of hearing animals with larger end bulb terminals. In addition, the bushy cells from deaf mice had more auditory nerve fibers innervating each bushy cell compared to the hearing animals, as well as having larger maximal and individually evoked synaptic currents delivered to bushy cells in the deaf animals compared to the hearing mice. The biophysical properties of the bushy cells themselves reveal a major difference between hearing and deaf animals, such that the rate of depolarization threshold in bushy cells is reduced in deaf animals compared to hearing littermates, indicating that they may be less effective coincidence detectors than bushy cells of hearing mice. All of these alterations are likely adaptation mechanisms that principal neurons in a primary sensory system undertake to maintain optimal levels of excitation to ensure survival of these neurons in the face of diminished acoustically driven activity.

Chapter 1

Introduction

Aim of Research

The goal of this research is to understand exactly how the end bulb terminals of auditory nerve fibers and their bushy cell targets adapt to the lack of most acoustically driven excitation and most, if not all, patterned spontaneous activity before the onset of hearing. We know that neurons actively and dynamically modify their shapes and their biophysical properties in response to synaptic activation (Shah et al. 2010). Specifically, cells regulate ion channels in their membranes, they regulate the number and type of neurotransmitter receptors and they also modulate neurotransmitter release in order to maintain an optimal level of activity specific for each cell (Turrigiano 1999). The absence of sound driven activity modifies the auditory pathway (Trune 1982 a&b; Lustig et al. 1994; Harris and Rubel 2006) and we aim to better understand and characterize how deafness and the lack of most prehearing patterned spontaneous activity results in specific neural adaptations.

Hair Cells of the Cochlea

Mechanotransduction occurs in the cochlea. Sound pressure waves reach the tympanic membrane of the middle ear, or the temporal bone, and propagate into the fluid of the inner ear via the auditory ossicles. As the fluid of the inner ear is displaced it creates a traveling wave along the basilar membrane which runs throughout the entire length of the cochlea. Inner and outer hair cells reside along the basilar membrane. At the base of the cochlea the basilar membrane is narrow and stiff and drives hair cells that respond to high frequencies, while at the apex the basilar membrane is wide and floppy and drives hair cells that respond to low frequencies. Bundles of stereocilia at the top of each inner hair cell are deflected by fluid movement and shearing forces between the basilar membrane and tectorial

membrane (Dallos 1996; Slepecky 1996). Transducer channels are attached to the bottoms of tip links at the tips of all but the tallest stereocilia and they open when stereocilia are deflected toward the tallest stereocilia, allowing the influx of ions. The process of mechanotransduction thus converts mechanical energy to electrical signals. The inward current though the transducer channels creates a depolarizing, graded receptor potential and stimulates calcium (Ca^{2+}) induced exocytosis and neurotransmitter release.

Inner hair cells are the acoustic transducers from the outside world to our brains, but outer hair cells also play a critical role. Outer hair cells improve the sharpness of tuning of the cochlea, affecting the mechanics of the cochlea with every cycle of the sound. The lateral walls of outer hair cells are densely packed with a molecule called Prestin which, as its name implies, responds rapidly to changes in voltage with changes in length, a process called electromotility, which affects the mechanical properties of the Organ of Corti. This process allows the outer hair cells to act as the cochlear amplifier by creating mechanical feedback via regulating the distance between the basilar membrane and the tectorial membrane and thus tuning the inner hair cells (Dallos 1996; Dallos et al. 1997). Electromotility of the outer hair cells can be recorded as otoacoustic emissions and the presence of otoacoustic emissions is a measure of the health of the outer hair cells as the cochlear amplifier (Brownell 1990).

Efferent Innervation

Efferent fibers innervate the hair cells of the cochlea, providing feedback from the superior olivary complex. Efferent activation of hair cells comes from two neuronal populations, the lateral olivocochlear and medial olivocochlear systems (Warr 1992; Smith and Spirou 2002). Lateral olivocochlear neurons reside laterally around the lateral superior olive and project ipsilaterally; they are believed to protect the cochlea from noise damage and they also balance auditory nerve fiber excitation between the two ears (Darrow et al. 2006; Darrow et al. 2007). Medial olivocochlear neurons reside

ventral and medial to the medial superior olive and ventral nucleus of the trapezoid body, with the majority of their projections being contralateral; they also protect the cochlea by reducing its sensitivity and are involved in acoustic adaptations for sound localization (Irving et al. 2011; Rajan 1988). The lateral olivocochlear efferents are either myelinated or unmyelinated fibers which contact either the inner hair cells or the dendrites of afferent auditory nerve fibers through GABAergic and/or peptidergic synapses. The medial olivocochlear efferents contact outer hair cells through myelinated cholinergic fibers that contact groups of outer hair cells (Slepecky 1996; Smith and Spirou 2002). Innervation by medial olivocochlear efferents hyperpolarizes outer hair cells and thereby affects electromotility.

Auditory Nerve Fibers and Afferent Innervation

Auditory nerve fibers are the axons of bipolar spiral ganglion neurons that form the auditory part of cranial nerve eight, the vestibulocochlear nerve. Spiral ganglion neurons are the direct link for acoustic communication between inner hair cells and the brain. Auditory nerve fibers release glutamate onto their postsynaptic targets in the cochlear nucleus. Afferent excitation from the cochlea to the cochlear nucleus is communicated though myelinated and unmyelinated spiral ganglion neuron axons. The large, myelinated axons that receive input from inner hair cells account for >90% of the afferent projections from the inner hair cells; they are called type I fibers or spiral ganglion neurons (Dallos 1996; Slepecky 1996). Approximately 10-20 type I fibers contact each inner hair cell but each type I auditory nerve fiber receives excitation from only one inner hair cell. In contrast, unmyelinated axons of small diameter fibers receive input from outer hair cells and account for <10% of the afferent projections; they are called type II fibers or type II spiral ganglion neurons (Smith and Spirou 2002). Type II fibers end in the cochlear nuclei but little is known about their function (Brown and Ledwith III 1990).

All auditory nerve fibers terminate in the cochlear nucleus. Type I fibers enter at the nerve root and bifurcate sending an ascending branch to the anterior ventral cochlear nucleus (aVCN) and a descending branch through the posterior ventral cochlear nucleus (pVCN) and on to innervate the dorsal cochlear nucleus (DCN). Type II auditory nerve fibers also enter the cochlear nucleus and bifurcate, but only occasionally enter the DCN (Smith and Spirou 2002). Auditory nerve fibers maintain the topographic organization of frequency from the cochlea, in both the VCN and DCN; where low frequency fibers innervate the most ventral and lateral regions of the nucleus and the high frequency fibers innervate more dorsal and medial portions of the nucleus (Bourk et al. 1981; Osen 1970b).

In cats, but not in mice, distinct and separate characteristics of auditory nerve fibers have been distinguished. In cats, type I fibers have been shown to have different rates of spontaneous firing, different thresholds of activation that vary with fiber thickness, different mitochondrial content, different synapse morphologies and different contact sites upon inner hair cells (Liberman 1978). These fundamentally different characteristics may endow auditory nerve fibers with distinct morphologies and patterns of activity. Auditory nerve fibers with low or medium spontaneous firing rates (discharge less than 18 spikes/seconds), they have high activation thresholds, and large dynamic ranges, while high spontaneous firing fibers have lower activation thresholds and smaller dynamic ranges and their end bulb terminals are less branched (Liberman 1991; Ryugo and Spirou 2009). Low and medium spontaneous rate fibers tend to terminate in more rostral and dorsal parts of the aVCN, while high spontaneous rate fibers generally innervate the caudal and ventral regions of the aVCN (Liberman 1991).

End Bulbs

Typically auditory nerve fiber axon terminals have normal synaptic bouton endings; however, in the VCN, type I fibers end in specialized synaptic terminals called end bulbs of Held (Held 1893). These

calyceal terminals have highly branched, finger-like projections containing numerous varicosities that wrap around the soma of bushy cells in the aVCN (Cajal 1909; Lorente de No 1933; Brawer and Morest 1975). End bulbs have diverse sizes and shapes. Generally, the largest end bulbs are found in the most anterior region of the aVCN, while smaller end bulbs are located more caudally; this is due to the distribution of the sub-types of postsynaptic cells on which they terminate and the types of fibers themselves.

Functionally, the morphology of each end bulb is diverse. End bulb area is correlated to characteristic frequency of the auditory nerve fiber. Larger end bulbs are attached to auditory nerve fibers tuned to lower frequencies, <4 kHz, and smaller end bulbs arise from auditory nerve fibers pertaining to any frequency (Sento and Ryugo 1989). Also noteworthy, is that end bulb area is not directly correlated with spontaneous firing rate of the auditory nerve fibers but spontaneous rate is related to the complexity and fine structure of the terminal branching. Sento and Ryugo (1989) described this by dividing the end bulb area by its perimeter, the form factor. End bulbs of high spontaneous firing rate auditory nerve fibers have larger and fewer terminal branches and swellings, while the low-medium spontaneous firing rate fibers were more 'lacey' in their appearance with delicate, fine structures. Importantly, end bulbs of different spontaneous firing rates do not converge onto the same bushy cell (Ryugo and Sento 1991). Additionally, postsynaptic soma size was usually smaller for low-medium spontaneous firing rate fibers than for high (Sento and Ryugo 1989). In mice auditory nerve fibers have not been shown to fall into clear groups on the basis of their spontaneous firing rate (Taberner and Liberman 2005).

The end bulb is a dynamic structure that can release unusually large amounts of neurotransmitter. The end bulb is reported to have anywhere from 400 to 1500 release sites with clear, round synaptic vesicles approximately 50 nm in diameter. A single auditory nerve fiber can activate from 2,000 to 10,000 α-amino-3-hydroxy-5-methyl-4-isoxazolepropionic acid (AMPA) receptors on a spherical bushy cell (Ryugo and Spirou 2009). The electrical hallmark of this synapse in extracellular, *in vivo* recordings

is the prepotential that occurs about 0.5 msec before the excitatory postsynaptic potential (EPSP) and represents the depolarization of the end bulb (Pfeiffer 1966; Kopp-Scheinpflug et al. 2002). Direct patch-clamp recordings of end bulbs reveal their functional characteristics, in combination with simultaneous recordings from spherical bushy cells show the membrane and discharge properties of end bulbs. In addition, measurements of the presynaptic voltage-gated Ca^{2+} channels reveal that the predominant Ca^{2+} current in end bulbs is through P/Q-type channels which may be developmentally regulated (Lin et al. 2011). The number of voltage-gated Ca^{2+} channels opened upon peak depolarization was estimated at 5,500 and the total number expressed at each end bulb was 6,400. In brain slices from P 9-11 mice, Ca^{2+} current inactivation was absent from end bulbs in trains of stimulation and even showed facilitation during short trains; however the readily releasable pool was diminished after stimulations lasting longer that 40 msec. The size of the readily releasable pool was calculated to be ~ 1,064 vesicles with single action potentials releasing ~40 vesicles, so that the Ca^{2+} entering the end bulb releases ~10% of the vesicle population. Estimates reveal 8 voltage-gated Ca^{2+} channels are associated with one docked vesicle, and upon arrival of the action potential ~3-4 voltage-gated Ca^{2+} channels open. Lin et al. report that depression at this synapse is from vesicle depletion or receptor desensitization rather than voltage-gated Ca^{2+} channel inactivation. Most importantly, they estimate that even at very depolarized membrane potentials single voltage-gated Ca^{2+} channels had open probabilities substantially lower than one and that the probability of release at the end bulb terminal is also very low. It should be noted that data from other groups indicate different probabilities of release at the end bulb, which may be due to age, hearing experience and other experimental conditions (Brenowitz and Trussell 2001a &b). Additional experiments indicate that probability of release is high from end bulbs in mature mice (Wang and Manis 2008).

Deafness and End bulbs

In a well-studied case of hearing loss in cats, it is clear that the morphology of end bulbs is significantly distorted in the absence of auditory activity. Deaf white cats have a form of non-syndromic, congenital deafness that reveals how auditory nerve fibers respond to early-onset cochlear degeneration. Deaf white cat pathology involves loss of hair cells, collapse of the organ of Corti, spiral ganglion neuron loss and atrophy of the primary neurons in the ventral cochlear nucleus and superior olivary complex (Ryugo et al. 1997). Compared to normally hearing cats, the end bulbs from deaf white cats had fewer arborizations, less tertiary branching, with meager networks of fine filamentous processes, they also had fewer and smaller *en passant* and terminal swellings, this is in combination with encompassing much less of the soma compared to normally hearing animals. Ultrastructurally, end bulbs in deaf white cats lacked the typical numerous round, clear synaptic vesicles, but instead had huge variability in synaptic vesicle density at the presynaptic active zones (Redd et al. 2000). Interestingly, in deaf white cats the active zones with few or no vesicles were associated with extremely large mitochondria. Deaf white cats had postsynaptic densities that were unusually long and thick, consistent with an upregulation of receptors, and they did not form the convex bulges into the active zone of the end bulb as in hearing cats. Overall the normally hearing cats had approximately double the synaptic area per end bulb as deaf white cats. Additionally, smaller end bulbs that contact globular bushy cells in deaf white cats revealed that they were about half the size compared to hearing cats, with relatively normal complexity but there was a loss of the extracellular synaptic space which may be required for efficient uptake of glutamate in the synaptic cleft.

Principal Cells of the Ventral Cochlear Nucleus

The principal neurons of the ventral cochlear nucleus comprise bushy, stellate and octopus cells. Bushy and stellate cells each have specialized subtypes. Bushy cells come in both large and small

spherical cells, along with globular bushy cells and the stellate cells have both T and D subtypes. Each principal cell type projects its axons out of the cochlear nucleus to distinctively different targets, each carrying unique acoustic aspects of the sound stimuli.

Bushy cells

Bushy cells are named for the prominent tuft of spineless dendrites that emanates from one side of the soma; however some have two primary dendrites. When two dendrites are present on a bushy cell the dendritic trees are always on opposite sides of the cell body (Gomez-Nieto & Rubio 2009). They are generally contacted by auditory nerve fibers tuned to narrow frequency ranges. Bushy cells come in three varieties; the large spherical bushy cell (large SBC), small spherical bushy cell (small SBC) and globular bushy cell (GBC). In cats it is clear that each subtype is distinct in its morphology, location within the VCN, its innervation and projections and its biophysical characteristics (Brawer et al. 1974; Cant and Morest 1974; Osen 1969; Hackney et al. 1990; Cant and Benson 2003; Brawer and Morest 1975; Ryugo and Sento 1991). However, in mice bushy cells are not distinguishable based on these qualities and the sub-types can only be determined by the projection patterns of their axons exiting the cochlear nucleus.

All bushy cell axons leave the cochlear nucleus through the trapezoid body. Small SBCs generally do not cross the midline, they innervate the ipsilateral lateral superior olive (Cant and Casseday 1986), large SBCs innervate the medial superior olive bilaterally (Cant and Benson 2003; Cant and Casseday 1986; Osen 1970a; Osen 1970b). Medial superior olive principal cells act as coincidence detectors, where they serve a major role in sound localization by calculating interaural timing differences (Yin 2002). GBCs cross the midline and project to principal cells in the contralateral medial nucleus of the trapezoid body where they form the largest synapses in the mammalian brain, the calyces of Held (Tolbert et al. 1982; Tolbert and Morest 1982a; Tolbert and Morest 1982b). Principal neurons in the

medial nucleus of the trapezoid body are glycinergic and inhibitory and they project to the ipsilateral lateral superior olive where stimulus intensities are compared for interaural level differences.

Generally, GBCs have more oval shaped somas than the rounder somas of SBCs. Small SBCs lie in the posterior part of the aVCN, while large SBCs are located in the anterior aVCN; GBCs on the other hand are more concentrated in the posterior aVCN (Tolbert et al. 1982; Tolbert and Morest 1982a; Tolbert and Morest 1982b). All sub-types of bushy cells are involved in sound localization in the azimuth (Yin 2002). Each bushy cell is innervated by at least one specialized, axosomatic synaptic terminal from an auditory nerve fiber, an end bulb of Held, but each bushy cell can also be innervated by many end bulbs. In cats, the largest, calyceal endings innervate large SBCs in the most rostral aVCN that are tuned to low frequencies. Mice have poor low frequency hearing and as such have few large SBCs (Webster and Trune 1982; Yin 2002). Other large end bulb terminals innervate small SBCs which are numerous in mice (Cant and Casseday 1986). Smaller, less complex, 'modified' end bulbs terminate on to GBCs that are also numerous in mice.

Physiologically, the characteristics of SBCs and GBCs are slightly different; however the main function of bushy cells is the same, to convey and even sharpen the information from auditory nerve fibers. End bulbs faithfully transmit rapid acoustic signals with temporal precision from inner hair cells to bushy cells (Yin 2002), with the timing of the EPSPs in bushy cells reflecting the timing of firing in auditory nerve fibers. SBCs and GBCs can even improve encoding of the phase of low frequency sounds compared to auditory nerve fibers by the coincident excitation of multiple auditory nerve fibers converging onto each cell (Joris et al. 1994). SBCs respond to tones with firing patterns that are 'primary like' (Brawer and Morest 1975; Ryugo and Sento 1991). The responses of GBCs have been characterized as "primary-like-with-notch" (Smith et al. 1991). The consistent and precisely timed firing at the onset of sound results in a consistent and sharply timed first action potential from trial to trial that is followed by a refractory period whose timing is also consistent, giving peristimulus time histograms their characteristic

large initial peak followed by a notch (Spirou et al. 2005). Bushy cells have low input resistances and short time constants, in the range of 0.5-2 msec, in the physiological voltage range, allowing them to convert excitatory postsynaptic currents (EPSCs) into brief, sharply timed EPSPs (Oertel 1983; Cao et al. 2007). The rapid decay of the EPSPs minimizes the temporal summation of synaptic inputs, EPSCs. Bushy cells' EPSPs' fast kinetics are endowed by their AMPA receptor subunit composition of GluR3 and GluR4, flop isoforms, and the absence of GluR2 allows them to flux Ca^{2+} ions and facilitate fast synaptic transmission with rapid desensitization for precise onset and decay responses (Gardner et al. 2001; Wang et al. 2011; Whiting, Moiseff and Rubio 2009). Their low input resistance make the bushy cells firing temporally precise but also leads to a requirement for large synaptic currents which are delivered through enormous synaptic terminals; the end bulbs of Held (Brawer and Morest 1975; Sento and Ryugo 1989; Oertel 1983).

Convergence of End bulbs onto bushy cells

Generally more than one end bulb converges onto a single bushy cell. This convergence of auditory nerve fibers helps to improve the temporal precision of firing in bushy cells compared to the auditory nerve fibers themselves, due to the short time constants in bushy cells and the necessity of synchronous summation of EPSCs. In mice, we have found that between one and four end bulbs innervate SBCs (Cao and Oertel 2010). We have also shown that the smaller, modified end bulbs which innervate GBCs do so in groups of five or more, and we have seen as many as twelve auditory nerve fibers contacting a single GBC, estimated by the number of current steps present in a recording of evoked EPSCs (Cao and Oertel 2010). In cats, some estimates are as great as fifteen to twenty-three auditory nerve fibers innervating one GBC (Spirou et al. 2005; Liberman 1991). The estimates of convergence of auditory nerve fibers onto bushy cells vary greatly in the literature due to differences between species and

are also complicated by the difficulty in clearly distinguishing between the different types of bushy cells (Ryugo and Spirou 2009; Spirou et al. 2005).

Bushy cells also receive additional dendritic innervation from auditory nerve fibers, and inhibitory somatic and dendritic innervation, some from the ipsilateral DCN (Gomez-Nieto & Rubio 2009; Gomez-Nieto & Rubio 2011; Wickesberg & Oertel 1990; Kopp-Scheinpflug et al. 2002). Synaptic integration is important for the accurate encoding of acoustic information. Synaptic inputs have different effects on the output of neurons depending on the size of their currents, their location along the dendritic tree, as well as the geometry of the dendrites themselves influencing the propagation of electrical signals. Ultrastructurally, numerous types of excitatory and inhibitory synapses were identified along the length of the dendrites of bushy cells (Cant and Morest 1979). Excitatory synapses are characterized by asymmetric synaptic contacts that contain round synaptic vesicles. While inhibitory synapses are characterized by symmetric synaptic contacts with flattened or pleomorphic synaptic vesicles. Four main types of excitatory and inhibitory synapses, each, were identified based on the size of the ending and the synaptic vesicles; one excitatory synaptic type identified was associated with end bulbs (Gomez-Nieto & Rubio 2009). Convergence of these distinct types of excitatory synapses on bushy cell dendrites was also differentiated by the separate distribution of vesicular glutamate transporters 1 and 2. A distinct distribution was found that vesicular glutamate transporter 1 labeled inputs are from cochlear origins, while vesicular glutamate transporter 2 labeled inputs were non-cochlear in origin, likely from somatosensory innervation (Gomez-Nieto & Rubio 2009).

The end bulb ensures faithful transmission of high-fidelity acoustic signals from the auditory nerve, but it is still unknown how bushy cells can sharpen and modify the timing of acoustic signals compared to those of the auditory nerve. One possibility is that convergence of inputs from multiple, similarly tuned auditory nerve fibers essentially averages out temporal jitter (Joris et al. 1998). It has also been proposed that the synaptic dyads and triads from auditory nerve fibers and inhibitory inputs,

including axodendrosomatic and axodendrodendritic synaptic contacts innervate groups of bushy cells, where a single input will contact two or three different bushy cells in synaptic dyads or triads (Gomez-Nieto & Rubio 2009). This can also include one bushy cell projecting its distal dendrites to contact four to five other bushy cell bodies that reside in clusters (Gomez-Nieto & Rubio 2009). Another neuroanatomical method of improving the synchronization of bushy cells to that of auditory nerve fibers is electrical coupling of bushy cells. Gap junctions between bushy cell somas were identified ultrastructurally, indicating another intricate method for bushy cells to synchronize themselves (Gomez-Nieto & Rubio 2009). Interestingly, these finding were shown to be evident in both rats and non-human primates from rhesus monkeys (Gomez-Nieto & Rubio 2011).

Stellate cells

T Stellate cells form a major output pathway from the cochlear nuclei. The dendrites of T stellate cells are aligned in parallel with the auditory nerve fibers innervating them, resulting in T stellate cells being narrowly tuned as they are only contacted by auditory nerve fibers representing a narrow range of frequencies (Cant and Benson 2003; Young and Oertel 2004). T Stellate cells are excitatory and respond to the phasic excitation from auditory nerve fibers in a tonic manner, so that their firing rates reflect the intensity of sounds to which they are tuned relative to intensities at other frequencies. They have been termed ‘choppers’ (Smith and Rhode 1989; Oertel et al. 2011). Individual T stellate cells signal the duration and intensity of sound energy to which they are tuned, while the collective population of T stellate cells conveys the spectrum of the sound (Blackburn and Sachs 1990). Excitation of T stellate cells comes from auditory nerve fibers and also from other T stellate cells; inhibition arises from glycinergic innervation from the D stellate cells and the tuberculoventral cells projecting from the DCN (Wickesberg and Oertel 1990). Glutamatergic excitation and glycinergic inhibition generate large, sharply

timed postsynaptic potentials, indicating that it arises on the proximal dendrites of the T stellate cells; while more subtle neuromodulation may occur more distally on dendrites (Oertel et al. 2011). The axons of T stellate cells typically branch within the cochlear nucleus, sending collateral branches to the vicinity of the cell's dendrites and to the DCN. The main axon exits the cochlear nucleus through the trapezoid body, and innervates the vicinity of the ipsilateral lateral superior olive, the ventral nucleus of the trapezoid body that is the source of cholinergic medial olivocochlear efferents, the contralateral ventral nucleus of the lateral lemniscus and the inferior colliculus (Smith et al. 1993). Axon collaterals from T stellate cells also innervate tuberculoventral cells and possibly fusiform cells in the ipsilateral DCN.

D stellate cells are inhibitory. The dendrites of D stellate cells radiate across numerous bands of auditory nerve fibers and they receive both somatic and dendritic innervation from auditory nerve fibers (Oertel et al. 1990; Cant and Benson 2003). D stellate cells can thus be innervated by many auditory nerve fibers from multiple frequencies and as such are broadly tuned (Smith and Rhode 1989; Oertel et al. 1990). D stellate cells respond to pure tones with an 'onset chopper' firing pattern (Smith and Rhode 1989; Rhode and Greenberg 1992). The axons of D stellate cells project out of the cochlear nucleus through the dorsal acoustic stria to the contralateral VCN and DCN but they also innervate the ipsilateral VCN and DCN.

Octopus cells

Octopus cells are named for their extension of dendrites off one side of the soma. Their cell bodies are located in the dorsal portion of the pVCN. Octopus cell dendrites are innervated by auditory nerve fibers perpendicularly such that they receive acoustic information from a wide range of frequencies as the auditory nerve fibers themselves converge before innervating the DCN (Osen 1969; Cant and Benson 2003; Young and Oertel 2004). We estimate that in mice octopus cells are contacted by at least

60 auditory nerve fibers (Golding et al. 1995). Octopus cells have extreme temporal precision in the timing of their action potentials. They require the synchronous summation of EPSPs to fire action potentials (Golding et al. 1999). Octopus cells respond to tones with a single action potential in an 'onset' manner to the synchronous firing of auditory nerve fibers. They respond best to increases in acoustic stimuli such as increases in intensity at the onset of speech syllables (Oertel et al. 2000; Rhode and Smith 1986). The axons of octopus cells leave the VCN through the intermediate acoustic stria and project to the contralateral superior paraolivary nucleus and the contralateral ventral nucleus of the lateral lemniscus where they end in calyceal terminals (Cant and Benson 2003). Both of these intermediate brainstem nuclei are major inhibitory inputs to the inferior colliculus.

Otoferlin

Implicated as the putative Ca^{2+} sensor of inner hair cells, otoferlin is a multi- Ca^{2+} binding domain protein, whose function is required for hearing. First described in humans by the Yasunaga group in 1999, genetic screening revealed a nonsense mutation in otoferlin resulting in a premature stop codon which resulted in DFNB9 an autosomal recessive, non-syndromic form of prelingual hearing loss. Since then numerous studies have investigated the functional role of otoferlin in Ca^{2+} induced exocytosis. To date, over 92 mutations in the otoferlin protein have been identified which cause deafness in humans (Mahdieh et al. 2012).

Otoferlin is a member of the ferlin family of proteins. The ferlin family was originally founded after the gene discovered in *C. elegans* that encodes the FER-1 protein, which is required for maturation of spermatozoa. The ferlin family also includes myoferlin and dysferlin, amongst others. Myoferlin has been implicated in endocytosis in muscle and endothelial cells (Bernatchez et al. 2009), and dysferlin is a protein required for normal skeletal muscle repair (Han and Campbell 2007). Both proteins are

membrane-anchored cytosolic proteins. Also included in the ferlin family, is misfire, a Drosophila protein required for fertilization and embryonic development, a sea urchin ferlin involved in wound-activated Ca^{2+} intracellular ATP signaling and three other mammalian proteins, which are not yet characterized. The entire ferlin family of proteins has multiple Ca^{2+} binding domains (C2) domains. All of the characterized members of the ferlin family are membrane-anchored, cytosolic proteins and have been implicated in vesicle fusion and membrane trafficking (Yasunaga et al. 2000). Otoferlin can be traced far back in unicellular eukaryotic lineages which have no synaptotagmin isoforms (Lek et al. 2011).

My studies are focused on a mouse line with a missense mutation in the OTOF gene that results in a single non-conserved amino acid substitution in the second C2 domain of otoferlin. These mice have abnormal auditory brainstem responses (ABRs) while their vestibular evoked potentials showed no deficit even though otoferlin is present in vestibular hair cells (Longo-Guess et al. 2007). For our experiments we used the otoferlin mutant mouse model *Otof* ^{deaf5Jcs}*/Kjn*. Two breeding pairs were purchased from Jackson Labs stock #006128; these animals are on the mixed background of C57Bl/6J and C3HeB/FeJ mice. Chemical mutagenesis, *N*-ethyl-*N*-nitrosourea (ENU) created this missense mutation causing a single point mutation from thymine to adenine in exon 10 of otoferlin. This resulted in a non-conservative amino acid change from isoleucine to asparagine. Altering the amino acid from a non-polar to a polar one leads to protein misfolding, instability and a total loss of function in the highly conserved second C2 domain of otoferlin, C2B.

Otoferlin has both long and short isoforms; the short isoforms of otoferlin lack the first 19 coding exons and are located in human non-neural tissues. These include the adult human tissues of the heart, placenta, liver, pancreas, skeletal muscle, kidney and brain; the last of which also contains the long form of the protein (Yasunaga et al. 2000). Mice only have the long isoform that has been localized to the eye, cochlea, vestibular organ, brain, cerebellum, heart, skeletal muscle, liver, kidney, lung and testes (Roux et

al. 2006; Yasunaga et al. 1999). The sequences of the long isoforms of otoferlin are almost identical in human and murine nervous tissues. The predominant long isoform of otoferlin comprises 1997 amino acids with six C2 domains, many of which bear homology to the C2 domains of synaptotagmin-1 (Yasunaga et al. 2000). Besides the six C2 domains which bind phospholipids in a Ca^{2+} dependent manner, otoferlin also has a coiled-coil domain in the center of the protein and a C terminal transmembrane domain. Several putative phosphorylation sites for cAMP-dependent protein kinase, casein kinase II, tyrosine kinase, protein kinase C and putative N-glycosylation sites were predicted in the murine and human sequences (Yasunaga et al. 2000).

The long form of otoferlin has six C2 domains, C2A thru C2F, the majority of which contain five aspartyl residues with similar proximity to those that bind Ca^{2+} in the C2A domain of synaptotagmin-1, suggesting that otoferlin might be involved in Ca^{2+} mediated vesicle exocytosis (Yasunaga et al. 2000). Otoferlin senses Ca^{2+} and has accelerated membrane permissively in its presence. In addition, otoferlin can aggregate liposomes in a Ca^{2+} dependent manner to facilitate membrane fusion. Immunoprecipitation revealed that otoferlin has the ability to bind to syntaxin1A and SNAP-25B hererodimers with its 4 C-terminal, C2C-C2F domains, which is enhanced by Ca^{2+} (Johnson and Chapman 2010). All 6 C2 domains bind to liposomes in the presence of Ca^{2+} but only C2A and C2B, the N-terminal C2 domains, bound to liposomes without Ca^{2+}. Tests of whether otoferlin can aggregate membranes in the presence of Ca^{2+} reveal the 5 most C-terminal C2 domains, C2B-C2F, showed reactivity with membranes but only in the presence of Ca^{2+}. A critical ability of otoferlin is to be able to accelerate Soluble N-ethylmaleimide-sensitive factor Attachment protein REceptor (SNARE) mediated membrane fusion in the presence of Ca^{2+} and regulate the folding and activity of SNARE proteins. Similarly, the C2B-C2F domains were able to fuse the v- and t-SNARE proteoliposomes through a SNARE-dependent pathway (Johnson and Chapman 2010). Studies of the specific single point mutation from isoleucine to asparagine in the C2B domain were performed to elucidate its functional characteristics. They revealed that this mutant form of

otoferlin is incapable of performing the functions of a Ca^{2+} sensor, that the loss of Ca^{2+} sensing activity results in a failure to aggregate membranes in the presence of Ca^{2+} and an inability to accelerate SNARE mediated membrane fusion (Johnson and Chapman 2010).

A recent molecular study definitively demonstrated that otoferlin can indeed bend membranes (Marty et al. 2013). This ability to sculpt lipid bilayers appears to be a common feature of dysferlin and myoferlin. Remarkably, Ca^{2+} is not required for alterations in the structural state of lipid membranes by the C2 domains of these ferlin proteins; although Ca^{2+} does enhance this activity (Marty et al. 2013). This is in stark contrast with synaptotagmin-1, which requires Ca^{2+} for its interaction with membranes. Also, in the presence of high salt concentrations, synaptotagmin-1 cannot perform membrane bending while otoferlin can (Marty et al. 2013). Studies with truncated otoferlin constructs reveal that multiple C2 domains at both the N- and C- terminal portions of the protein can directly perturb the structural state of the lipid bilayers, and inclusions of each additional C2 domain seems to be additive in membrane manipulation effect, with the last three C-terminal C2 domains appearing most potent in membrane bending activity (Marty et al. 2013). The final requirement for membrane sculpting permissivity was the presence of negatively charged lipids.

The functional role of otoferlin still remains unclear. Numerous investigations have exposed convincing yet sometimes contradictory results. Some of the conflict may result from otoferlin's numerous C2 domains' individual abilities, various splice sites and different isoforms. Furthermore, otoferlin could have multiple functions related to its Ca^{2+} sensing abilities; facilitating Ca^{2+} mediated exocytosis, expediting Ca^{2+} mediated endocytosis, and Ca^{2+} dependent synaptic vesicle replenishment on rapid time scales, along with other possible Ca^{2+} dependent vesicle trafficking functions. Evidence exists for all of the above.

In hair cells of the inner ear, otoferlin localizes to the specialized ribbon synapses associated with synaptic vesicles, binds Ca^{2+} and co-immunoprecipitates with the t-SNARE proteins, syntaxin 1 and SNAP 25 (Roux et al. 2006). Otoferlin is also present near the presynaptic membrane, in the cytoplasm, in the Golgi and endoplasmic reticulum. In inner hair cells, Ca^{2+} mediated exocytosis was almost completely abolished in the absence of otoferlin, even in the presence of normal Ca^{2+} currents (Roux et al. 2006). The conflict deepens when otoferlin is shown to overlap with, but not co-localize with the synaptic ribbon marker, C-terminal binding protein 2 (CtBP2) as well as with the presynaptic Ca^{2+} channel Ca_v 1.3 (Schug et al. 2006). In a pull down assay from another group, several C2 domains bound to Ca_v 1.3 channels and this interaction was Ca^{2+} dependent (Ramakrishnan et al. 2009). Additionally, a decoupling of CtBP2 and Ca_v 1.3 channels has been found in otoferlin mutants and could account for the reduced Ca^{2+} mediated exocytosis (Heidrych et al. 2009). Moreover, in inner hair cells it has been suggested that otoferlin is involved in endosome transport and vesicle recycling because of co-localization with the cytosolic Golgi matrix protein 130 (Schug et al. 2006). In support of this claim, otoferlin interacts with myosin VI at the basolateral membrane of inner hair cells, which is also associated with the trans Golgi network. Eliminating either protein resulted in diminished basolateral pole volume, reduction in normal presynaptic proteins, and failure of proper intracellular membrane targeting in inner hair cells, indicating that otoferlin may be involved in endocytosis and transport of intracellular compartments to the basolateral membrane (Heidrych et al. 2009). It has also been suggested that otoferlin is involved in the replenishment and or tethering/docking of synaptic vesicles to the ribbon-type active zones of inner hair cells, because in another study, otoferlin mutants maintain the normal amplitude and kinetics of Ca^{2+} activated neurotransmitter release of the readily releasable pool but have a reduction in the sustained phase of exocytosis, especially at high stimulus levels (Pangrsic et al. 2010). Congruently, a study in developing chick hair cells showed that vesicle replenishment was Ca^{2+} insensitive in immature hair cells while mature hair cells had efficient Ca^{2+} sensitive vesicle recruitment that correlated tightly to otoferlin up-regulation during development (Levic et al. 2011). Moreover,

otoferlin has been shown to be responsible for the linear Ca^{2+} dependence of exocytosis in immature outer hair cells and vestibular hair cells (Beurg et al. 2008; Dulon et al. 2009). The results come from studies involving separate mutations in different C2 domains, C2C, C2D, C2F, a full knock out and an avian homolog, which may account for differing interpretations, and as such otoferlin may assume multiple roles in vesicle trafficking and recycling.

Functional studies have compared otoferlin and synaptotagmin; neither protein can restore function, nor recover exocytosis in mutations of the other (Reisinger et al. 2011). Synaptotagmin-1 viral transduction could not restore inner hair cell Ca^{2+} triggered exocytosis neither *in vitro* nor hearing *in vivo*. Neurons overexpressing otoferlin were neither able to rescue synchronous neurotransmitter release nor alter the kinetics of the fast component of release in synaptotagmin-$1^{-/-}$ cells (Reisinger et al. 2011). It is however possible that the appropriate binding partners for each protein were not present so that rescue functions were not possible (Rutherford and Pangrsic 2012). These data indicate that otoferlin and synaptotagmin cannot replace one another even though they are both implicated as Ca^{2+} sensors.

Are normal neuronal SNARE proteins even required for exocytosis from inner hair cells? Reports that exocytosis in inner hair cells is insensitive to neurotoxic cleavage of SNARE proteins, SNAP-25, syntaxin 1 and synaptobrevin 1, by the appropriate botulinum toxin stereotypes which are known to cleave and render neuronal SNARE proteins non-functional did not disrupt Ca^{2+} induced exocytosis in inner hair cells (Nouvian et al. 2011). Nouvian et al. also reveal that none of the neuronal SNARE proteins were synaptically located in in inner hair cells, leading them to conclude that neurotransmitter release in inner hair cells may function without the typical neuronal SNAREs. However, *in situ hybridization* and immunohistochemistry revealed that SNAP-25 and syntaxin1A proteins are present in inner hair cells. They were not, however, only concentrated at the basolateral membrane but were distributed throughout the in inner hair cells (Safieddine and Wenthold 1999). A plausible conclusion is that there might be the analogs to the conventional SNARE machinery inherent in otoferlin

itself, where otoferlin may be dimerizing with syntaxin 1A, SNAP 25 and synaptobrevin in these studies. In support of this, the presence of synaptic transmission in SNARE-deficient mice suggests there is no need for neuronal SNAREs in inner hair cells (Rutherford and Pangrsic 2012).

It is certain that otoferlin operates at the vesicle release sites of inner hair cells and that when the protein is disrupted, mice are profoundly deaf (Roux et al. 2006; Longo-Guess et al. 2007; Pangrsic et al. 2010). Remarkably, Ca^{2+} induced exocytosis in inner hair cells is otoferlin independent until P4 (Beurg et al. 2010). At P7 inner hair cells of otoferlin knockout mice require 3 continuous seconds of depolarization for Ca^{2+} induced vesicle release, measured as an increase in membrane capacitance; in hearing mice the fast component of release, the readily releasable pool of synaptic vesicles, occurs after tens of milliseconds of depolarization and the slow component of exocytosis or slow releasable pool appears after just hundreds of milliseconds (Beurg et al. 2010). Synaptotagmin-1 and 2, the typical central nervous system Ca^{2+} sensors, are not present in inner hair cells of post hearing mice. However, several synaptotagmin isoforms are present during the prehearing period but none tested was responsible for Ca^{2+} induced vesicle release before P3 (Beurg et al. 2010). It is possible that multiple Ca^{2+} sensors are required in inner hair cells to give individual auditory nerve fibers that contact a single inner hair cells, different thresholds, dynamic ranges and spontaneous release (Gregory and Quinones 2011). In line with this is that hypothyroid rats which lack otoferlin mRNA and protein in inner hair cells, still exhibit Ca^{2+} induced exocytosis before and after hearing onset, with post hearing animals exhibiting larger Ca^{2+} induced changes in capacitance that controls (Brandt et al. 2007).

Otoferlin does not operate alone; it has a plethora of accessory proteins with which it performs physiological functions. Some of these proteins have been identified while others remain incognito. Of the ones which have been identified, only a portion have known functions, many of which are implicated in exocytosis, endocytosis and vesicle recycling in the trans-Golgi network. These interacting protein partners exist as a functional unit in a complex of proteins referred to as an ‘interactome’ (Zak et al.

2011). Additionally, functional defects in any one of these proteins which result in deficits in exocytosis at the hair cell synapse and cause deafness are termed 'synaptopathies' (Pangrsic et al. 2012). Interestingly, it has been shown that otoferlin has several binding partners which are important for clathrin-mediated endocytosis. It was thought that clathrin-mediated endocytosis was too slow to be effective in inner hair cell endocytosis. However by pharmacologically inhibiting clathrin-mediated endocytosis, real time membrane capacitance changes were impaired in synaptic vesicle replenishment in mature inner hair cells (Duncker et al. 2013). Therefore it is possible that otoferlin participates in the retrieval of membrane as well as playing a role in the late stages of exocytosis in inner hair cells. This compound ability could help the auditory system maintain the indefatigable sustained exocytosis required for the accurate perception of sound.

Patterned spontaneous activity

Before the onset of hearing, patterned spontaneous activity originating in the immature Organ of Corti propagates throughout the entire auditory pathway (Johnson et al. 2011; Tritsch et al. 2007; Tritsch and Bergles 2010). This patterned spontaneous activity is likely required for normal neuronal survival, organization, maturation and function of the auditory system. While the developing auditory system is still naive to sound, inner supporting cells in Köllikers organ within the cochlea, spontaneously release ATP resulting in crenation of small groups of inner hair cells and inner supporting cells due to osmosis, inward currents and transient intracellular Ca^{2+} waves that propagate radially in groups of electrically coupled inner supporting cells and adjacent inner hair cells (Tritsch et al. 2007). As Köllikers organ develops, the spontaneous inward currents in inner hair cells and inner supporting cells grow larger and slower and the transient intracellular Ca^{2+} waves become more prominent, but both eventually disappear after the onset of hearing (Tritsch et al. 2010b; Tritsch and Bergles 2010). The crenation is thought to be

the result of osmotic effects from increases in extracellular Cl^- and K^+ concentrations and correlates with large increases in intracellular Ca^{2+} leading to Ca^{2+} activated Cl^- efflux and K^+ influx, generating the inward currents in inner hair cells and inner supporting cells (Tritsch et al. 2010b). Additionally, the secretion of water by osmosis may contribute to formation of endolymph or perilymph and the crenation may be large enough to cause displacement of inner hair cells and stereociliary deflection, leading to additional depolarization from mechanotransduction during development (Tritsch and Bergles 2010).

Focally released ATP from inner supporting cells binds to purinergic P2 receptors on the inner hair cells, causing the inner hair cells to depolarize and fire Ca^{2+} spikes which facilitate neurotransmitter release from immature ribbon synapses (Tritsch and Bergles 2010). ATP-mediated inward currents in inner hair cells do not become prominent until P4 whereafter the amplitude and frequency increase until the onset of hearing, when they cease. After P4, mini-bursting activity was recorded in inner hair cells occurring at frequencies resembling theta oscillations. Interestingly, P4 is the same age at which otoferlin becomes up-regulated in inner hair cells (Beurg et al. 2010).

Waves of spiking activity in neighboring inner hair cells and in their corresponding auditory nerve fibers have a high probability for being synchronized, likely helping neurons encoding similar frequencies to 'fire together and wire together' (Tritsch et al. 2007; Tritsch et al. 2010). Whole-cell patch clamp recordings of neighboring inner hair cells have more correlated spontaneous inward currents than distant pairs of inner hair cells (Tritsch and Bergles 2010). Inner hair cells are not spontaneously active before the onset of hearing and require extracellular ATP-mediated input to fire Ca^{2+} spikes.

Calcium action potentials generated from prehearing inner hair cells initiate the release of glutamate from immature ribbon synapses, depolarizing the spiral ganglion neurons, and allowing them to fire action potentials in discrete mini bursts that disseminate to the cochlear nucleus, medial nucleus of the trapezoid body and inferior colliculus recorded *in vivo* (Tritsch et al. 2007; Tritsch et al. 2010).

Spiking activity patterns in spiral ganglion neurons are related to the development of inner hair cells, around P2 inner hair cells become sensitive to ATP, initiating some spiral ganglion neurons to be depolarized enough to fire tonic, low-frequency action potentials (Tritsch and Bergles 2010). Bursting activity in prehearing spiral ganglion neurons averages 1 to 6 action potentials every 100-300 msec followed by short periods of quiet, representative of theta frequencies which may potentiate developing synapses and induce signaling cascades. Bursting activity propagates through the auditory pathway (Brugge and O'Connor 1984; Crins et al. 2011). These results suggest that focal synchronized activity could help to perfect and sustain synaptic connections throughout the developing auditory system.

Series Resistance and its Compensation

Good series resistance compensation in voltage clamp is an important factor for acquiring accurate recordings of current measurements. It is a particularly serious problem when measuring the large synaptic currents in bushy cells of mice in the strain used in this study. As one is recording synaptic or membrane currents through the recording electrode, the recording electrode is serving two purposes, injecting enough current to assure that the holding potential of the cellular membrane is constant at the set determined/command level and measuring the voltage in the cell. The amplifier compares the measured voltage to the desired "command" voltage and then injects current as a function of the difference between the measured and the command voltage. The recording electrode in the Axon Multiclamp 700B amplifier does this in a 'time sharing' manner, whereby for one moment it is fluxing current into or out of the cell and in the next moment it is recording the voltage. The amplifier measures the voltage when the cell's membrane voltage has settled back after current was injected. It is important, therefore, that the time constant of the electrode be short so that the measured membrane voltage is not contaminated by the voltage drop caused by current passing through the electrode. If the measured voltage differs from the

command voltage, the amplifier reduces the difference by injecting current proportional to the difference. By measuring how much current is required to keep the cell's voltage constant is thus a measure of how much current the synapse has contributed. Time delays in the circuits of the amplifier result in a slight lag between reading the cellular voltage and injecting the correct amount of current to maintain the command potential and can lead to voltage oscillations.

Another issue is that the recording electrode has a resistance in series with the cell's resistance. The amplifier measures the summed voltage across the pipette resistance as well as across the cell's resistance but meaningful measurements of synaptic currents require that voltage be kept constant across the cell's membrane in the face of large changes in current flow. The series resistance compensation is positive feedback system, by which the amplifier adds a fraction of the output to compensate for the electrode's resistance (Barbour 2011). The fraction of the output is set by the investigator. When the currents fluxing through the pipette are small and when the pipette resistance is small, the voltage drop across the pipette resistance is not very large so the series resistance compensation is not a major concern for accurate measured physiological currents. However, when the currents are large, small errors in compensation for pipette resistance result in large errors in the actual membrane potential of the cell. For example, if only 80% of the resistance of a 5 MΩ pipette is compensated in the measurement of a 20 nA synaptic current, the holding potential will have an error of 20 mV. In this case excitatory synaptic currents being measured are reduced because the cell's membrane voltage, which should stay constant, shifts from a holding potential of -65 mV to -45 mV. It is generally impossible to compensate the series resistance 100% because positive feedback combined with electronic delays cause the voltage to oscillate and kill the recorded cell. If settings are on the verge of oscillation, the synaptic currents include an oscillatory component and are artifactually large. In my experiments the best I could do was to compensate 75-80%. Compensating for the series resistance in voltage clamp can be a tricky business.

In current clamp the series resistance is not an issue because the amplifier delivers either no current or current pulses. While current pulses are delivered, the measured voltage has a constant error which equals the pipette resistance multiplied by the current. These constant errors are generally small because injected currents are small (for example, 5MΩ x 1 nA = 5 mV) and can be subtracted (by the bridge balance correction) either during the experiment or offline after the experiment because they are constant (Barbour 2011). Bridge balance is the current clamp equivalent of the voltage clamp series resistance compensation. In current clamp constant current pulses are injected that result in a constant voltage drop across the electrode that can easily be subtracted whereas in voltage clamp the amount of current being injected varies as a function of changes in the physiological currents. The bridge balance allows the amplifier to measure the resistance of the electrode so it can be corrected for.

Finally, for accurate recordings, especially in voltage-clamp, capacitance needs to be compensated. In the MultiClamp 700B amplifier, the fast and slow capacitance compensation adjustments are used in voltage clamp and the pipette capacitance neutralization is used in current clamp. In voltage clamp these are true corrections for pipette capacitance, while in current clamp capacitance neutralization can only partially compensate for that capacitance (Molecular Devices 2010). Appropriate settings allow the amplifier to correct for capacitance of the pipette in the voltage-clamp feedback to minimize oscillations and to separate the pipette's from the cell's capacitance.

Chapter 2

Mutation of Npr2 Leads to Blurred Tonotopic Organization of Central Auditory Circuits in Mice

[*1]Cindy C. Lu, [*2]Xiao-Jie Cao, [2]Samantha Wright, [3]Le Ma, [2]Donata Oertel, and [1]Lisa Goodrich

*These authors contributed equally to this manuscript

[1]Department of Neurobiology, Harvard Medical School, Boston, MA 02115

[2]Department of Neuroscience, University of Wisconsin School of Medicine and Public Health, Madison, WI 53706

[3]Department of Cell and Neurobiology, Keck School of Medicine, University of Southern California, Los Angeles, CA 90089

Abstract

Tonotopy is a fundamental organizational feature of the auditory system. Sounds are encoded by the spatial and temporal patterns of electrical activity in spiral ganglion neurons (SGNs) and are transmitted via tonotopically ordered processes from the cochlea through the eighth nerve to the cochlear nuclei. Upon reaching the brainstem, SGN axons bifurcate in a stereotyped pattern, innervating target neurons in the anteroventral cochlear nucleus (aVCN) with one branch and the posteroventral and dorsal cochlear nuclei (pVCN and DCN) with the other. Each branch is also tonotopically organized, thereby distributing acoustic information along multiple parallel pathways for processing in the brainstem. In mice with a mutation in the receptor guanylyl cyclase Npr2, this spatial organization is disrupted. Peripheral SGN processes appear normal, but central SGN processes fail to bifurcate and are disorganized, resulting in blurred tonotopic organization within the VCN, underinnervation of the aVCN, and reduced convergence of SGN inputs onto target neurons. Secondary circuits within the cochlear nuclei are also degraded, as revealed by changes in the topographic mapping of tuberculoventral cell projections from DCN to VCN. Nonetheless, *Npr2* mutant SGN axons are still able to transmit acoustic information with normal sensitivity and timing, as revealed by auditory brainstem response recordings and electrophysiological recordings from VCN neurons. Although most features of signal transmission are normal, intermittent failures were observed in responses to trains of shocks, likely due to a failure in action potential conduction at branch points in *Npr2* mutant afferent fibers. Our results show that *Npr2* is necessary for sharp tonotopic organization of cochlear nuclear circuitry and for the proper convergence of SGNs onto their targets, but that signals are still transmitted with normal timing, and that mice can hear even with these deficits.

Author Summary

Millions of people suffer from debilitating hearing defects, ranging from a complete inability to detect sound to more subtle changes in how sounds are encoded by the nervous system. Many forms of deafness are due to mutations in genes that impair the development or function of hair cells, which are responsible for changing sound into electrical signals that can be processed by the brain. Both mice and humans carrying these mutations fail standard hearing tests. In contrast, very little is known about the genetic basis of central auditory processing disorders, which are poorly defined and difficult to diagnose, since these patients can still detect sounds. One alternative approach is to find genes that are required for the normal wiring of central auditory circuits in mice and to use these genes as entry points to understand how changes at the circuit level affect circuit function. Here, we show that the natriuretic peptide receptor Npr2 is required to establish frequency maps in the mouse central auditory system. Surprisingly, despite the dramatic change in circuit organization, *Npr2* mutant mice are still able to respond to sounds with normal sensitivity and timing, underscoring the need for better hearing diagnostic methods in mice as in humans.

Introduction

The sense of hearing is mediated by precisely organized neural circuits that encode the frequency content, timing, and intensity of sounds. Frequency information is coded by the spatial organization of hair cells in the cochlea, with high frequencies detected in the base and low frequencies in the apex. SGNs transmit this information to the cochlear nuclei, where their axons bifurcate into an ascending branch that innervates the aVCN and a descending branch that targets the pVCN and DCN. In each of these regions, the systematic innervation by SGN fibers forms frequency maps that maintain the tonotopic order of hair cells in the cochlea. This imposes a tonotopic organization that is preserved along the auditory pathway. For example, tonotopy governs intrinsic connections between neurons in the cochlear nuclei, such as tuberculoventral cell projections from the DCN to the VCN (Wickesberg and Oertel 1988; 1990).

Bifurcation of SGN axons plays a key role in the delivery of information from the cochlea to the cochlear nuclei. By contacting a variety of target neurons with distinct projection patterns, each SGN feeds information to parallel pathways in the brainstem (Cant and Benson 2003). Through their ascending branches, SGNs convey auditory signals to bushy cells that are involved in comparing interaural time and intensity for localizing sounds in azimuth (Cant and Morest 1979; Yin 2002; Spirou et al. 2005; Lauer et al. 2013), as well as to some T stellate cells. Through their descending branches, SGNs innervate T stellate cells that encode the spectrum of sounds (Blackburn and Sachs 1990; Alibardi 1998; Oertel et al. 2011), octopus cells that mark the onset of sounds (Rhode and Smith 1986; Golding et al. 1995; McGinley et al. 2012), and fusiform and giant cells of the DCN that use spectral cues to localize sounds monaurally in the vertical plane (Oertel and Young 2004). Together, the activation of these diverse populations of cochlear nuclear neurons by SGN axons enables animals to detect, recognize, and locate sounds in their environment.

Although the mechanisms of cochlear wiring are beginning to be elucidated, much less is known about how the precise pattern of functionally diverse connections in the cochlear nuclei is generated (Appler and Goodrich 2011). Indeed, a growing number of genes affecting hair cell development or function and SGN connectivity in the cochlea in the mouse have been identified, many of which have been implicated in sensorineural deafness in humans (Dror and Avraham 2009). These animal models have provided a useful entry point for understanding the cellular and molecular bases for hearing loss arising from cochlear defects. In contrast, the molecular mechanisms that govern establishment of central auditory circuits are still largely unknown, as are the effects that miswiring of these circuits may have on hearing. Notably, it is estimated that ~1% of people with normal hearing sensitivity, and therefore normal cochlear function, have defects in their ability to process sound (Hind et al. 2011). Unambiguously identifying and characterizing patients with these central auditory processing disorders (CAPD) is challenging, because multimodal sensory, language, and attention deficits can accompany or mimic CAPD, thereby complicating diagnosis (Ahmmed et al. 2014). One alternative approach to uncover the mechanisms underlying these types of disorders is to characterize mouse mutants with central auditory defects. Identification of genes that control central SGN wiring would represent a first step towards developing such models.

During the course of a screen to identify genes required for auditory circuit assembly, we discovered that the natriuretic peptide receptor Npr2 is required for central axon bifurcation in SGNs (Lu et al. 2011). Much of the Npr2 signaling pathway has been elucidated in dorsal root ganglion (DRG) and other sensory neurons, which also exhibit axon bifurcation defects (Schmidt et al. 2007; Schmidt et al. 2009; Ter-Avetisyan et al. 2014). Upon binding to its ligand, the C-type natriuretic peptide (CNP), which is expressed throughout the embryonic midline (Schmidt et al. 2009), Npr2 activates a cGMP-dependent protein kinase 1 (*PrkG1*) signaling cascade that regulates cytoskeletal-associated proteins (Schmidt et al. 2009; Zhao et al. 2009; Zhao and Ma 2009; Schmidt and Rathjen 2010; Xia et al. 2013). This may

promote axon bifurcation by causing growth cone splitting (Schmidt et al. 2007), but how Npr2 signaling regulates axon branching is unclear, as CNP can also act as a chemoattractant (Zhao and Ma 2009). Although Npr2 regulates SGN bifurcation during early development, the long-term effects of *Npr2* mutation on auditory circuit assembly and function remain poorly understood. Here, we address this question by examining the anatomical and functional properties of neural circuits in the auditory system of *Npr2* mutant mice.

Results

SGNs appear normal in the auditory periphery of Npr2 mutant mice

As a first step toward understanding how loss of Npr2 activity affects auditory circuit assembly and function, we characterized the peripheral wiring of SGNs in the cochlea, as visualized using *Neurog1-CreER*^{T2} and *RC::rePe* GFP reporter mice. Connections between SGNs and hair cells appeared normal in *Npr2* mutants at postnatal day 0 (P0) (Fig. 1A, B). In both wild-type and *Npr2* mutant cochleae, well-defined bundles of peripheral processes extended toward the organ of Corti. In addition, SGN central processes in the auditory nerve peripheral to the bifurcation in the nerve root seemed normal in *Npr2* mutant mice at P21, as assessed by electron microscopy (Fig. 1C, D). The g-ratio, which is the ratio of the axon diameter to the total myelinated fiber diameter, did not differ significantly between control and *Npr2* mutant animals (Fig. 1E). In both groups of animals, the observed ratio was near the optimal for conduction (Rushton 1951). Hence, development of the peripheral auditory system appears normal in *Npr2* mutant mice.

SGN projections are disorganized in Npr2 mutant cochlear nuclei, with persistent defects in axonal bifurcations

Previously, we showed that *Npr2* is expressed in SGNs and is required for the bifurcation of central SGN axons at E12.5 (Lu et al. 2011). To determine how this early failure in bifurcation affects subsequent development, we characterized SGN central projections in *Npr2* mutants at E16.5, when both branches have formed and projected tonotopically within the developing cochlear nuclei (Fig. 2A) (Koundakjian et al. 2007). Lipophilic dye labeling revealed that in *Npr2* mutants, the cochlear nerve root lacks the Y-shaped morphology typical of wild-type animals (Fig. 2B,C), consistent with a persistent bifurcation defect. In addition, whereas SGN axons were neatly bundled both proximal and distal to the bifurcation of the nerve in control animals, *Npr2* mutant axons were disorganized in the region where they would normally branch (Fig. 2B, arrow), resembling the first exploratory SGN axons that reach the hindbrain at E11.5 in wild-type embryos (Lu et al. 2011).

We next examined SGN central projections in *Npr2* mutant animals between P14-P18, after the auditory circuit is fully formed and functional hearing has begun. To label SGN axons, *Neurog1-creER^{T2}* mice were crossed to *AI14 tdTomato* reporter mice, resulting in offspring with tdTomato expression in a random subset of SGNs due to leaky Cre activity in the absence of tamoxifen. In *Neurog1-CreER^{T2};AI14* mice, tdTomato expression in SGNs is sparse enough that neuronal morphology can be examined, but is distributed uniformly along the length of the cochlea so that the overall pattern of SGN innervation throughout the intact cochlear nucleus complex can be visualized in cleared tissue. In control animals, auditory nerve fibers projected in a highly stereotyped and ordered manner to the aVCN, pVCN, and DCN (Fig. 2D). In *Npr2* mutants, SGN afferents were able to reach all three divisions, but appeared disorganized (Fig. 2E). Notably, some patches of the aVCN appeared to be underinnervated compared to controls (Fig. 2E, arrowheads). Indeed, sections through the cochlear nuclei revealed a severe disorganization of projections in the aVCN and pVCN in *Npr2* mutants (Fig. 2G) compared to controls

(Fig. 2F). Control axons exhibited clear bifurcations in the VCN (Fig. 2H), resulting in neat bundles of axonal branches in the aVCN (Fig. 2H'). In contrast, *Npr2* mutant SGN axons generally turned instead of bifurcating (Fig. 2I) and often followed aberrant paths in the aVCN (Fig. 2I'). Thus, loss of axon bifurcation and abnormal trajectories persist even after the onset of hearing in *Npr2* mutant mice.

Although the overall pattern of innervation was clearly abnormal, SGNs projected to all divisions of the *Npr2* mutant cochlear nuclei. To determine whether SGNs innervating the aVCN can still form branches that project to the pVCN, we labeled fibers with biocytin injections into the aVCN and searched for labeled fibers in the pVCN. In control animals, such injections labeled the ascending branch retrogradely to the nerve root and they labeled the descending branch anterogradely through the pVCN and into the DCN (Fig. 3A). The labeled descending branches formed a tight bundle in the octopus cell area, where the SGN fibers converge on their way to the DCN (Fig. 3A'). In *Npr2* mutant animals, obvious bundles were not seen. However, a few widely spread fibers in the octopus cell area were consistently labeled (Fig. 3B,B'), indicating that some individual SGN fibers manage to innervate both regions in spite of the axon bifurcation defect. Bifurcations are distinct from interstitial branches in that they are usually the first branch points within the cochlear nuclei, are found in a predictable location, and exhibit a characteristic Y-shaped morphology (Fig. 3C). Although a minority of SGN axons branched in approximately the correct location in *Npr2* mutants, the branch point did not exhibit the morphology typical of a bifurcation. Branches exhibited more varied angles and one branch was often abnormally thin (Fig. 3D, arrows). As in controls (Fig. 3E, arrowheads), *Npr2* mutant SGN axons were able to form interstitial branches (Fig. 3G, arrowheads). Thus, it seems likely that the branches that SGN axons form in *Npr2* mutant mice are interstitial branches rather than true bifurcations. Nonetheless, axonal branches in the aVCN terminated in endbulbs of Held with the usual range of sizes and shapes in both controls (Fig. 3F) and mutants (Fig. 3H), indicating that despite their defective branching patterns and trajectories,

Npr2 mutant SGN axons are still able to find appropriate targets and make specialized synapses with normal morphology.

Disruption of tonotopic organization in Npr2 mutants

Since the peripheral organization of SGN projections in the cochlea appeared unaffected in *Npr2* mutants, SGNs are likely able to receive sharply tuned frequency information from hair cells. However, given the disorganization of SGN central axons in *Npr2* mutants, we wondered whether mutant SGN axons preserve the tonotopic order of their projections as they exit the cochlea and find their way into the cochlear nuclei. Crystals of the lipophilic dyes, DiI and DiD, were inserted into the apical and basal turns of the cochlea in fixed E16.5 mouse heads and the dye was allowed to diffuse anterogradely through SGN axons to the hindbrain (Fig. 4A). In wild-type animals, SGN axons are tonotopically segregated within the eighth nerve, and their bifurcation points fan out in tonotopic order within the cochlear nuclei with axons from more basal SGNs bifurcating more dorsally than apical SGNs. This pattern is evident even at E16.5, with segregation of basal and apical SGN axons visible in the eighth nerve as well as in the developing cochlear nuclei (Fig. 4B). The gross tonotopic segregation observed in control embryos was maintained in *Npr2* mutants (Fig. 4C,C'). However, in some *Npr2* mutant embryos (n=2/4), obvious intermingling of apical and basal projections was observed (Fig. 4C,C', arrowheads), suggesting imprecise tonotopy. Moreover, mutant axons appeared to project more strongly towards what will become the pVCN and DCN, quantified by comparing the fluorescence intensity of the branches projecting rostrally vs. caudally (Fig. 4D). Apical SGNs were more strongly affected than basal SGNs and showed a stronger bias towards the developing pVCN and DCN.

To determine whether the blurring of tonotopy persists through postnatal stages, similar dye labeling of SGNs was performed at P14 by placing DiI and DiD crystals in the apical and mid-turns of the

cochlea, respectively (Fig. 4E). Clear segregation of the two dyes was observed in both the eighth nerve (Fig. 4F) and in the aVCN (Fig. 4F') and pVCN (Fig. 4F'') in controls. In contrast, in *Npr2* mutants, the axons from apical and mid-turn SGNs were appropriately segregated within the eighth nerve (Fig. 4G, H), but their projections often overlapped extensively in the aVCN (Fig. 4G', H') and/or pVCN (Fig. 4G'', H''). Thus, tonotopic segregation appears normal in the auditory nerve, but is lost to some degree within the cochlear nuclei of *Npr2* mutants.

The abnormal tonotopic organization of SGN projections raised the question of whether the second-order tonotopic organization of intrinsic neuronal circuits within the cochlear nuclei is similarly disorganized. Tuberculoventral (TV) cells are glycinergic neurons that reside in the deep layer of the DCN and innervate targets in the aVCN and pVCN, forming a negative feedback circuit. They are tonotopically arranged, receiving input from the same auditory nerve fibers as their targets and therefore exhibiting similar tuning (Wickesberg and Oertel 1988; Wickesberg and Oertel 1990; Zhang and Oertel 1993). The pattern of TV cell connectivity was examined by injecting biocytin into the aVCN, which normally labels TV cell bodies in the DCN as well as SGN afferent fibers that project to that isofrequency band (Wickesberg and Oertel 1988) (Fig. 5A-B). Labeling follows the tonotopic organization of the cochlear nuclei: dorsal injections labeled bands of TV cells dorsally in DCN, whereas ventral injections labeled TV cells in a more ventral position in the DCN. In control animals, a few labeled cells in the DCN were located ventral to the isofrequency band, because their axons crossed the injection site to innervate more ventral regions of the aVCN (Fig. 5A, arrowhead). However, labeled cells dorsal to the band in the DCN were not observed in normal animals, indicative of the sharp tonotopic organization (Fig. 5A,D). In contrast, in *Npr2* mutant mice, the labeled cell bodies were found over a large span of the DCN (Fig. 5B, D), even when the injections were made ventrally in the aVCN. To quantify this result, the distribution of labeled cells along the tonotopic axis was measured in reconstructions of 37 slices with injections into the ventral half of aVCN (Fig. 5C). In control mice, the distribution of labeled cells aligned at their peaks

showed a sharp peak that tapered ventrally toward the granule cell lamina. In *Npr2* mutants, the distributions lacked sharp peaks. The average distribution of labeled cells, aligned on the median, was broader, reflecting the more diffuse organization observed within individual slices. These findings indicate that the tonotopic organization of the TV cell projection in mutant cochlear nuclei is less precise than in wild-type animals.

The abnormal wiring pattern in Npr2 mutants does not noticeably affect auditory brainstem responses (ABRs)

To investigate how the change in the branching of SGN inputs to the cochlear nuclei affects hearing, we compared auditory brainstem responses (ABR) in six-week old wild-type and *Npr2* mutant mice. ABRs are generated by the synchronous firing of groups of aligned axons. In cats, the first large positive and negative waves reflect the firing of axons of SGNs, the second positive wave reflects the firing of neurons in the VCN that lie near the nerve root, the third positive wave reflects activation of the VCN rostral and caudal to the nerve root and the superior olivary complex, and later waves reflect the summation of activity at many stages of the auditory pathway (Melcher 1996). No significant difference was observed between control (n=6) and *Npr2* mutant (n=15) mice in the amplitude or shape of ABRs in responses to 16 kHz tones (Fig. 6A, B). The normal average ABR waveforms suggest that the timing of firing of SGNs and of their targets in the VCN and in the superior olivary complex is apparently normal. In addition, ABR thresholds did not differ significantly between wild-type and *Npr2* mutant mice (Fig. 6C). Thus, within the resolution of these measurements, the sensitivity and timing of firing of auditory neurons in the brainstem seem normal in *Npr2* mutants.

It should be noted that *Npr2* mutant mice exhibit additional abnormalities, including dwarfism and cardiac deficits (Tsuji 2005), that compromise their health and often cause them to die within the first

postnatal month. Thus, it is possible that no ABR phenotype was observed because the animals that survived to the testing stage were the healthiest and least abnormal. However, cochlear nuclear innervation defects were fully penetrant and varied only in severity. Moreover, since it is difficult to establish behavioral baselines in these animals, we were unable to use pre-pulse inhibition of the acoustic startle reflex to test for deficits in specific hearing tasks, such as frequency discrimination, gap detection, and sound localization.

Auditory signal transmission has many normal features in Npr2 *mutants*

Since ABRs did not reveal any obvious changes in auditory responsiveness in *Npr2* mutant mice, we next asked whether the loss of spatial organization affects signal transmission at the level of single cells by performing intracellular recordings in slices. Cochlear nuclear neuronal responses to sound depend on the pattern of convergence of synaptic inputs, the physiological properties of those inputs, and the electrical properties of target neurons that shape the voltage responses to synaptic currents. Whole-cell patch recordings in slice preparations of the cochlear nuclei confirmed that the three principal cell types of VCN (bushy, octopus, and T stellate cells), recognizable by the differences in their intrinsic electrical properties, are present in *Npr2* mutants. In *Npr2* mutants as in control animals, bushy and octopus cells fire transiently in response to depolarizing current pulses, whereas T stellate cells respond with trains of action potentials that last for the duration of the depolarization, in both wild-type and mutant animals (Oertel et al. 2011; Golding et al. 1995; Oertel et al. 1990; Cao et al. 2007) (data not shown). The absence of any measurable differences in the intrinsic properties indicates that mutant neurons are capable of signaling as rapidly and precisely as the wild type.

Given the obviously abnormal trajectories of SGN axons within the cochlear nuclei, we asked whether SGNs would still converge normally on principal cells of the VCN in *Npr2* mutants. The number

of excitatory inputs that converge on a recorded cell can be estimated by measuring the growth of synaptic responses to shocks of fiber bundles as the shock strength is gradually increased; the synaptic response grows in steps as additional fibers are brought to threshold (Cao and Oertel 2010). The number of steps in the increase in synaptic current is thus an estimate of the number of excitatory inputs. Bushy cells receive converging input from a small number of SGNs through endbulbs of Held or through smaller synaptic boutons. In the mutant, as in control animals, some jumps were small and others were large, reflecting the fact that bushy cells in mice receive input from small bouton endings as well as large endbulbs (Lauer et a. 2013; Cao and Oertel 2010; Chanda and Xu-Friedman 2010) (Fig. 7A). The number of converging inputs to bushy cells in *Npr2* mutants fell into the normal range, between 1 and 6 (Cao and Oertel 2010). However, a surprisingly large proportion had only a single input (5/7 in *Npr2* mutants, compared with 5/21 similar bushy cells in a wild type strain (Cao and Oertel 2010). Interpretation of these findings is complicated by the fact that there are multiple types of bushy cells: globular bushy cells that project to the medial nucleus of the trapezoid body and spherical bushy cells that project to the lateral or medial superior olivary nuclei. The sole electrophysiological distinction between these cell types in slices is the number of converging inputs (Lauer et al. 2013; Cao and Oertel 2010). Especially when the aVCN is disorganized, it is impossible to know whether populations of different types of bushy cells were sampled equally. However, our results suggest that bushy cells in the aVCN in *Npr2* mutants likely receive input from fewer SGNs than normal.

Shock-evoked synaptic responses in T stellate cells normally grow with between five and eight steps, each delivering roughly equal steps of current of between 100 and 300 pA (Cao and Oertel 2010; Ferragamo et al. 1998) (Fig. 7B). Many of these responses are likely to arise from SGNs but some could also arise from other T stellate cells (Ferragamo et al. 1998). In control mice, no differences have been reported between T stellate cells in pVCN, where they are most abundant, and in the aVCN (Oertel et al. 1990; Wu and Oertel 1984; Doucet and Ryugo 1997). In *Npr2* mutants, 6/10 of the T stellate cells we

recorded were in the pVCN, near the octopus cell area. Convergence of inputs in these cells was normal averaging 7.5±1 (n=6). In contrast, in the 4/10 T stellate cells that were recorded more anteriorly, evoked responses grew in only three or four, larger current steps (Fig. 7B). These data suggest that in *Npr2* mutants, convergence of SGNs onto targets in the aVCN is reduced, while in the pVCN, convergence is normal. This subtle change in circuit organization is consistent with our finding that SGN projections are biased towards the pVCN and DCN at embryonic stages.

Octopus cells receive converging input from larger numbers of inputs whose numbers cannot be estimated from the growth of synaptic responses with shock strength (Golding et al. 1995; McGinley et al. 2012; Cao and Oertel 2010). Synaptic responses generally grow in steps so small that the growth appears graded. In *Npr2* mutant mice, the growth of synaptic responses shows more irregularity than we have observed in CBA or ICR mice (Golding et al. 1995; Cao and Oertel 2010), but this irregularity was also observed in control mice. In octopus cells, no differences in convergence between wild-type and mutant mice could be resolved (Fig. 7C).

To gain additional insights into the nature of transmission between SGNs and their cochlear nuclear targets, we examined the pattern of synaptic responses to trains of shocks. In wild-type mice, repeated stimulation of the auditory nerve consistently evokes synaptic responses, although when driven at high rates, synaptic responses show depression, with a stronger effect in bushy than in T stellate cells (Cao and Oertel 2010; Wu and Oertel 1987; Yang and Xu-Friedman 2008). Synapses between SGNs and principal neurons in the VCN in *Npr2* mutants exhibited the expected synaptic depression observed in wild-type and heterozygous animals (Fig. 8A, A'). However, *Npr2* mutants differed from wild-type animals in that shocks intermittently failed to evoke any responses in some neurons. For instance, in 7/12 bushy cells, some of the shocks in a train failed to evoke a response (Fig. 8A). Failures were sporadic and complete, with no synaptic response at all in the target neuron (Fig. 8A''). A similar phenotype was also detected in T stellate cells (Fig. 8B), with 3/10 cells sporadically failing to respond to shocks; in contrast,

0 of 10 wild type and heterozygote responses failed. One reason failures may have been detected in relatively fewer T stellate cells than in bushy cells is that failures of small inputs are difficult to detect. Indeed, in T stellate cells failure was often incomplete in that small (<10%) synaptic current remained, presumably because the larger of two inputs failed while the smaller one did not.

For both bushy and T stellate cells, failures occurred even after the first shock in the train, when depletion of neurotransmission is not an issue (Fig. 8C). Together with the all-or-none character of the failures, these findings suggest that action potentials sometimes fail to invade the SGN synaptic terminals. To test whether a conduction block could be overcome by making action potentials in the parent axon taller and/or wider, we applied a low concentration of 4-aminopyridine (4-AP), a non-specific blocker of K^+ channels used to relieve conduction block in patients with multiple sclerosis (Dunn and Blight 2011). Indeed, 0.1 mM 4-AP eliminated synaptic failures reversibly in both bushy and T stellate cells (Fig. 8D, E). These results support the idea that *Npr2* mutant auditory nerve axons suffer from blocks in action potential conduction. Importantly, the responses that did occur showed normal, precise temporal tracking of inputs. Our data indicate that *Npr2* mutant mice exhibit altered spatial organization of the auditory circuit and unreliable action potential conduction, yet still maintain the overall temporal precision of auditory signal transmission.

Discussion

The sense of hearing depends on accurate transmission of frequency and timing information from the cochlea to the brain by SGNs. Hence, SGN projections are organized spatially according to frequency and form synapses that preserve the timing of sound stimuli. Using a combination of anatomical and physiological methods, we find that these two fundamental characteristics are differentially affected in *Npr2* mutant mice, which exhibit blurred tonotopy in the cochlear nuclei but still form functional

connections with largely normal electrophysiological features. Although there is a slight reduction in the convergence of inputs and occasional failures in transmission, the timing of neuronal firing at a population level and sound detection thresholds, as assessed by ABR, do not differ significantly between *Npr2* mutant and control mice. Taken together, these data indicate that central auditory circuits with defective spatial organization are still capable of normal signal transmission and hence auditory responsiveness, though it is unlikely that auditory processing in *Npr2* mutant mice is entirely normal. These findings highlight the importance of *Npr2* for central auditory circuit assembly and underscore the challenges of understanding the genetic basis of central auditory processing disorders.

Disruption of SGN wiring patterns in Npr2 *mutants during development*

Although recent studies have uncovered a number of genes required for cochlear wiring (Coate and Kelley 2013), how SGN central axons navigate to the cochlear nuclei is poorly understood. SGN axons reach the hindbrain and start to bifurcate by E12 in mice (Lu et al. 2011). When the aVCN is not present, SGN axons still project to the brainstem and bifurcate (Maricich et al. 2009), likely because the Npr2 ligand CNP is expressed along the entire rostral-caudal axis of the hindbrain. In addition, since SGN axons enter the hindbrain at the level of rhombomere 4, which gives rise to the pVCN and DCN, this region may provide attractive cues and may be primarily responsible for early SGN guidance decisions. Indeed, we find that *Npr2* mutant axons preferentially extend towards the developing pVCN and DCN, indicating that when required to make a directional choice without bifurcating, SGN axons show a caudal bias. Nevertheless, their projections follow aberrant trajectories, suggesting that *Npr2* is also required for normal responsiveness to cues in the environment. Whether these guidance defects are secondary to the loss of bifurcation remains to be determined.

After bifurcating, developing SGN axon branches must navigate towards distinct regions of the cochlear nuclei while retaining the tonotopic organization established in the cochlea. This fundamental feature of the auditory pathway is established during embryogenesis (Koundakjian et al. 2007; Molea and Rubel 2003). Tonotopy in brainstem auditory nuclei thus depends on molecular guidance during development and does not require hearing, although it is later refined by activity-dependent mechanisms that need not be driven by sound (Kandler et al. 2009; Tritsch et al. 2007). Disruption of peripheral SGN connections in the cochlea can affect tonotopy, as evidenced in mice lacking the transcription factor Neurod1 (Jahan et al. 2010). However, in these animals, auditory afferents are intermingled with projections from the vestibular endorgans, suggesting that disrupted tonotopic organization is secondary to a general change in neuronal identity. Eph/Ephrin signaling may play a more specific role in central topographic projections, with *ephrin-B2* mutants exhibiting abnormally broad frequency bands in the DCN (Miko et al. 2007). However, since EphA4/ephrin-B2 signaling is also involved in bundling of peripheral SGN projections extending towards the organ of Corti (Coate et al. 2012), the change in frequency responses in these mutants could also arise from peripheral disorganization.

Npr2 mutant mice offer an unusual example where defects in the tonotopic organization in the cochlear nuclei occur without obvious defects in cochlear organization. SGN axons are topographically ordered in the eighth nerve in *Npr2* mutants, but exhibit disorganization in the nerve root and blurred tonotopy in the cochlear nuclei, indicating that trajectories become disarrayed as they enter the cochlear nuclei. Since SGN bifurcation points are tonotopically ordered within the nerve root, with small bundles of SGN axons bifurcating together, it is possible that the abnormal guidance behavior of *Npr2* mutant axons exiting the eighth nerve disrupts this bundling, thereby perturbing the local tonotopic order. Indeed, proper fasciculation during axon guidance is known to play a key role in topographic mapping of axons in other systems (Clandinin and Feldheim 2009; Imai et al. 2009). Alternatively, mutant axons may be unable to detect guidance cues in the environment, either because Npr2 plays a role in guidance or

because key receptors are not trafficked properly to the branches that do form.

Functional consequences of abnormal innervation of the cochlear nuclei

Unexpectedly, the striking loss of tonotopic organization in the central auditory circuits of *Npr2* mutant mice does not result in any detectable changes in auditory function. ABRs are generated by the summation of coherent currents, and thus largely reflect synchronous firing in bundles of axons (Melcher et al. 1996), whereas intracellular recordings assay transmission to a single post-synaptic target. The absence of any obvious ABR defect is consistent with our anatomical studies, which revealed no abnormalities in peripheral wiring, myelination, axon diameter, or synaptic morphology. It is also consistent with whole-cell patch-clamp recordings from individual neurons. These recordings show that the principal cells of the VCN in *Npr2* mutants retain the ability to signal rapidly and with temporal precision. Most features of synaptic transmission were unaffected, with normal EPSC amplitudes, kinetics, depression, and delays in the VCN of *Npr2* mutants. Occasional failures in transmission do not alter the timing of signaling in the population of neurons. Moreover, since wave one amplitudes do not differ significantly between mutants and controls, either roughly similar numbers of neurons are activated, or the smaller heads of mutants compensate for slightly reduced numbers of active neurons. Our physiological studies suggest that *Npr2* mutant SGNs are still able to respond to sounds with normal sensitivity and timing, despite the loss of spatial organization. Normal ABRs are also observed in animals in which reorganization of central tonotopic maps is induced by persistent, moderate noise (Pienkowski and Eggermont 2012). While this might mean that ABRs are not sensitive enough to detect such changes, it may also reflect the plasticity of central auditory circuits, as has also been described by others (Kandler et al. 2009).

Although *Npr2* mutants exhibit blurred spatial organization, it is unclear whether this represents a

functional blurring at the level of frequency discrimination. In wild-type animals, the tuning of bushy and T stellate cells shows similar sharpness to that of auditory nerve fibers (Rhode and Smith 1986), indicating that SGNs that converge onto a single target neuron are similarly tuned. Since frequency coding is likely intact in the cochlea, activity-dependent synapse elimination, not only in the aVCN but also in TV cells of the DCN, could select for appropriate inputs with similar tuning in *Npr2* mutant mice even when they are not in the correct spatial location. Thus, the broadening of TV cell isofrequency mapping in *Npr2* mutants might reflect appropriate functional connections between cohorts of neurons that transmit similar frequency information, but that are no longer spatially confined to a tight band due to the disorganization of SGN afferents. Although pre-pulse inhibition of the acoustic startle response can be used in mice to test for frequency discrimination (Clause et al. 2011), such experiments are not possible with *Npr2* mutants, which have dwarfism and cardiac defects, and therefore await generation of *Npr2* conditional knockout animals. Interestingly, humans with *NPR2* mutations also exhibit achondroplasia (Bartels et al. 2004), suggesting that closer examination of auditory function may be warranted in such patients.

Although the basic features of synaptic transmission were unaffected by the loss of Npr2 function, auditory signal transmission became unreliable, with some shocks to SGNs failing to produce any response in post-synaptic targets. Since the failures sometimes occurred in the first response of a train, they could not have resulted from the depletion of neurotransmitter. Furthermore, EPSC failures were all-or-none, indicating that some action potentials did not reach the SGN terminals. Additionally, *Npr2* mutant axons showed no loss of myelin and did not exhibit the increased spike latency or jitter associated with dysmyelinated SGNs (Kim et al. 2013). Given the changes in SGN axon branching patterns in *Npr2* mutants and our ability to reverse failures with a K^+ channel blocker that strengthens action potentials, it is likely that failure occurred at branch points, which have long been recognized as being weak points in conduction (Moore and Westerfield 1983). Although a similar functional phenotype

has not yet been described in other sensory neurons in *Npr2* mutants, DRG neurons do exhibit mildly impaired ability to activate target neurons upon capsaicin treatment (Schmidt et al. 2007), indicating the need for a more detailed analysis of these neurons.

In summary, the spatial organization of connections of SGNs is disrupted in the cochlear nuclei but not in the cochleae of *Npr2* mutant mice. Despite abnormalities in convergence and intermittent conduction failures, there was no obvious loss of temporal precision in acoustic signaling, with postsynaptic responses tracking the activation of SGNs with precision and ABRs indicating grossly normal responses at a population level. It is unlikely that *Npr2* mutant mice have completely normal hearing, but more subtle behavioral tests will be required to reveal deficits. Overall, our results suggest that the development of the auditory circuit is robust enough that surprisingly normal synaptic connections can be made even in the face of disorganized tonotopy.

Materials and Methods

Mice

The following mouse strains were used: *Neurog1-creER^{T2}* mice (Koundakjian et al. 2007), *AI14-tdTomato* mice (Jackson Laboratories, Stock Number 007908); *RC::rePe* mice (Bang et al. 2011; Ray et al. 2011); and *Npr2^{cn}* mice which carry a missense point mutation (L885R) in the guanylyl cyclase domain of the *Npr2* gene that prevents the protein from catalyzing cGMP formation (Tsuji 2005) (Jackson Laboratories, Stock Number 003913). Animals were maintained on a mixed genetic background. Mice were genotyped using previously described PCR protocols (Jackson Laboratories, (Zhao et al. 2009; Koundakjian et al. 2007), or in the case of *RC::rePe*, the presence of DsRed fluorescence prior to Cre recombination. For timed pregnancies, embryonic day 0.5 (E0.5) was defined as noon on the day of a copulatory plug. All mice were maintained in accordance with institutional and National Institutes of Health (NIH) guidelines approved by the Institutional Animal Care and Use Committee (IACUC) at Harvard Medical School, University of Wisconsin, and University of Southern California.

Tonotopic dye labeling

E16.5 embryo heads were fixed in 4% paraformaldehyde (PFA) in PBS overnight and rinsed in PBS. The cochlea was exposed so that basal and apical turns were visible. In some cases, a small crystal of DiI (Life Technologies) was placed in the base of the cochlea, while a crystal of DiD (Life Technologies) was placed in the apex. In other cases, a picospritzer was used to inject a small amount of DiI or DiD dissolved in DMSO into the base or apex of the cochlea, respectively. Tissue was incubated at 37ºC in PBS for 3-4 days to allow the dye to diffuse along axons. The hindbrain was then dissected out, cleared in ScaleA2 (Hama et al. 2011) at 37ºC for 1 h, mounted on a slide, and imaged by confocal

microscopy to obtain z-projection images. To determine caudal/rostral bias of projections, the bifurcation zone was demarcated with a 100 pixel (px) diameter circle, and the intensity of caudal and rostral projections was measured by defining 100 px diameter circles adjacent to this zone. The ratio of caudal to rostral projections was calculated for each image and averaged for controls (n=2 wild-type + n=2 heterozygote embryos) and *Npr2* mutants (n=4 embryos).

For P14-P18 animals, mice were perfused transcardially with 4% PFA in PBS (n=2 control and 4 mutants). Their heads were bisected sagittally and fixed overnight in 4% PFA in PBS at 4ºC. Tissue was rinsed in PBS and dissected so that the cochlea was exposed, with the brain still attached, then decalcified in 0.1 M EDTA in PBS at room temperature for 3 days. The decalcified bone covering the organ of Corti was removed so that mid and apical turns were visible, and small crystals of DiI and DiD were placed in the apical and mid-turns of the cochlea, respectively, using a 30-gauge needle to first create a small slit into which the dye crystal could be inserted. The tissue was incubated at 37ºC in 4% PFA in PBS for 1 week, at which point most of the dye had diffused along projections. Since the axons are heavily myelinated at this stage and require a large amount of dye to reach the central projections in the cochlear nucleus, an additional crystal of DiI or DiD was at this time placed in the same slit, and allowed to diffuse for another week. The cochlea and cochlear nuclei were then dissected out, embedded in 5% low melt agarose in PBS, and sectioned by vibratome at 150 µm. For the cochlea, transverse sections of the cochlear nerve were collected, and for the cochlear nucleus, transverse sections of the aVCN and pVCN were collected. These were mounted on a slide and imaged by confocal microscopy (Zeiss SP8 X).

Visualization of cochlear afferents

To label SGN central axons at E16.5, embryo heads were fixed in 4% PFA in PBS overnight, and the cochlea was exposed. A picospritzer was used to injected DiI dissolved in DMSO into the

cochlea, and then treated as described above for tonotopic dye labeling. Labeling of SGN central axons at P21 was performed by biocytin injections into the aVCN, as described below. SGN peripheral projections in the cochlea were labeled by crossing *Npr2*$^{cn/+}$ mice with *Npr2* heterozygotes also carrying the *Neurog1-creER*^{T2} and *RC::rePe* alleles. Tamoxifen was administered by gavage to the mothers when embryos were at E10.5 to induce CreER^{T2} activity in SGNs, as previously described (Koundakjian et al. 2007). Cochleae from P0 pups were collected and fixed in 4% PFA, and the mid-turn, which is most strongly labeled by E10.5 tamoxifen administration, was isolated and mounted on a slide. Fluorescence from the *RC::rePe* GFP reporter allele was then examined by confocal microscopy.

To visualize the overall pattern of SGN projections in the cochlear nuclei at postnatal stages, *Npr2*$^{cn/+}$ mice were mated with *Npr2* heterozygotes also carrying the *Neurog1-creER*^{T2} and *Ai14: tdTomato* alleles. P18 animals were perfused transcardially with 4% PFA in PBS, and their brains were drop fixed overnight in 4% PFA in PBS. Cochlear nuclei were then dissected out and cleared overnight in ScaleA2. The entire cochlear nucleus was mounted in ScaleA2 on a glass slide and imaged by confocal microscopy using a Leica SP8 X microscope. Tiled confocal stacks (~300 µm thick) were obtained at 10x so that the entire cochlear nucleus was covered. These tiled images were stitched together by ImageJ and z-projected to generate a single, large image of the cochlear nucleus including aVCN, pVCN, and DCN. For examination of projections in just the aVCN and pVCN, animals were processed as above, and then cochlear nuclei were embedded in 5% low melt agarose in PBS and cut sagittally at 150 µm using a vibratome. Regular confocal stacks were obtained at 20x and 40x and z-projected.

Biocytin Injections

To assess the morphology of auditory nerve fibers and topographic organization of tuberculoventral cell projections, biocytin injections were made into the aVCN in parasagittal slices in

mice aged between P14 and P26. With a single, parasagittal cut, the cochlear nuclei were removed from the brainstem in a single "slice" of up to 400 μm either with a vibratome or with scissors. The slice was maintained *in vitro* as in electrophysiological experiments. With a picospritzer, normal saline containing 1% biocytin (Sigma) was injected into the aVCN through a pipette with a tip diameter of ~5 μm. Movement of the pipette through the slice disrupted processes that crossed the injection site as pulses of pressure released biocytin. Biocytin was allowed to spread through the tissue for 1.5 to 2 hours as slices continued to be superfused with warmed, oxygenated saline. Slices were then fixed in 4% PFA, stored at 4°C, embedded in a gelatin-albumin mixture, and resectioned at 40 to 60 μm in frozen sections. Biocytin in cells and fibers was visualized with horseradish peroxidase (Vectastain ABC Elite Kit, Vector Laboratories) (Golding et al. 1995). Photomicrographs were taken through a Zeiss Axioskop with a Zeiss Axiocam.

Quantification of TV cell tonotopic mapping

After being processed histologically, sections were analyzed with a *camera lucida*. Each section was reconstructed and marked with the locations of labeled neurons and landmarks. Landmarks were used to reconstruct slices as illustrated in Figure 5D. The distribution of labeled cells in the reconstructed slice was measured by means of a transparent grid that was laid parallel to an isofrequency band. Cells were then counted within parallel rows of squares as illustrated by the histograms in Figure 5D. Comparisons between genotypes were made by lining up peaks in histograms and summing cells in bands.

Electron microscopy

P21 animals were perfused transcardially with 4% PFA in PBS, and bisected heads were fixed

overnight at 4ºC in fixative (2.5% PFA, 5% glutaraldehyde, 0.06% picric acid in 0.2 M sodium cacodylate buffer). The cochlear nuclei were dissected out with the eighth nerve attached, and the region where the eighth nerve enters the cochlear nuclei was cut into a 1-2 mm cube in the fixative. The tissue was washed in 0.2 M sodium cadocylate buffer three times, followed by incubation in 1% osmium tetroxide/1.5% potassium ferrocyanide in water for 1 hour in the dark at room temperature. After three washes in malelate buffer (pH 5.15) three times, the tissue was placed in 1% Uranyl Acetate or maleate buffer for 30 minutes, washed in water three times, and then dehydrated through an ethanol series (70% ethanol for 15 min, 90% ethanol for 15 min, and 100% ethanol twice for 15 min). Tissue was incubated in propyleneoxide solution for 1 hour, and then infiltrated with Epon resin mixed 1:1 with propyleneoxide for 2-3 hours at room temperature. Samples were embedded in freshly mixed Epon and polymerized for 24-48 hours at 60°C. Thin sections were cut transverse to the eighth nerve using a Reichert Ultracut-S and were imaged using a Technai G2 Spirit BioTWIN transmission electron microscope with an AMT 2k CCD camera. To calculate the g-ratio, EM images of the eighth nerve were obtained for control (n=3) and *Npr2* mutant (n=3) mice, and Fiji (ImageJ) was used to demarcate the area encompassed by each axon, as well as the area of the entire myelinated fiber. The g-ratio for each axon was calculated for ~200 axons for each animal by dividing the diameter of the entire myelinated fiber by the diameter of the axon proper, and averages for controls and mutants were calculated.

Auditory brainstem recordings

Auditory brainstem responses (ABRs) were recorded in 6-week-old mice in a soundproof chamber, as previously described (del Rio et al. 2013). Average ABR waveforms were plotted using a MATLAB (MathWorks) script written by Ann E. Hickox in the laboratory of Dr. Charles Liberman (EPL Laboratories, Massachusetts Eye and Ear Infirmary, Boston, MA).

Preparation of slices

Coronal slices of the cochlear nuclei were made from mice between P17 and P25. Slices (220 μm thick) were cut with a vibrating microtome (Leica VT 1000S) in normal physiological saline or in saline with reduced Na^+ at 24-27^oC, and then transferred to a recording chamber (~0.6 ml) and superfused continually at 5-6 ml/min. Temperature was controlled with a Thermalert thermometer (Physitemp) the input of which comes from a small thermistor (IT-23, Physitemp, diameter: 0.1 mm) placed between the inflow of the chamber and the tissue. The output of the Thermalert thermometer was fed into a custom-made, feedback-controlled heater that heated the saline in glass tubing (1.5 mm) just before it reached the chamber to maintain the temperature at 33°C. Biocytin injections were made under the control of a Wild (M5) dissecting microscope. For electrophysiological recordings, the tissue was visualized through a compound microscope (Zeiss Axioskop) with a 63X water immersion objective and CCD Camera (Hamamatsu), with the image displayed on a video screen.

Electrophysiological recordings

Whole-cell patch clamp recordings were made by using an Axopatch 200A amplifier (Axon Instruments, Burlingame, CA). Patch electrodes whose resistances ranged between 3.5 and 8 MΩ were made from borosilicate glass. All recordings of eEPSCs were digitized at 40 kHz and low-pass filtered at 10 kHz. The series resistance was compensated by 85-90% in recordings from octopus cells and by 70-80% in recordings from T stellate and bushy cells with a 10-μsec lag (Cao and Oertel 2010). EPSCs were evoked by shocks through a Master-8 stimulator and Iso-flex isolator (AMPI, Jerusalem, Israel), delivered

through an extracellular-saline-filled glass pipette (~5 µm tip). Analysis of EPSCs was performed by using pClamp (Clampfit 9.0, Axon Instruments).

For solutions, all chemicals were from Sigma-Aldrich, unless stated otherwise.

Normal saline: The normal extracellular physiological saline comprised (in mM) 130 NaCl, 3 KCl, 1.2 KH_2PO_4, 2.4 $CaCl_2$, 1.3 $MgSO_4$, 20 $NaHCO_3$, 6 HEPES, 10 glucose, and 0.4 ascorbic acid saturated with 95% O_2-5% CO_2, pH 7.3-7.4, between 24 and 33 °C. The osmolality was 306 mOsm/kg (3D3 Osmometer, Advanced Instruments Inc, Norwood, MA). *Cutting solution:* Some dissections were performed in a special cutting solution that contained (in mM) 99 NaCl, 3 KCl, 1.2 KH_2PO_4, 1 $CaCl_2$, 1.3 $MgSO_4$, 20 $NaHCO_3$, 6 HEPES, 10 glucose, and 72 sucrose.

Pipette solution: Recording pipettes were filled with a solution that consisted of (in mM) 90 Cs_2SO_4, 20 CsCl, 5 EGTA, 10 HEPES, 4 Mg-ATP, 0.3 GTP, 5 Na-phosphocreatine, 5 mM QX314, and was adjusted to pH 7.3 with CsOH (~298 mOsm). Voltages were corrected for a -10 mV junction potential.

Acknowledgements

We thank Dr. Charles Liberman for assistance with ABR recordings (facility supported by a P30 core center grant, DC02509) as well as the Harvard Neurobiology Imaging Facility (P30 core center grant, NS072030), Harvard Medical School Electron Microscopy Facility, and the Harvard NeuroDiscovery Center Enhanced Neuroimaging Core for access to equipment and technical advice. We gratefully acknowledge Anna Kowalkowski at the University of Wisconsin for her help with the histology and its analysis.

Figure 1

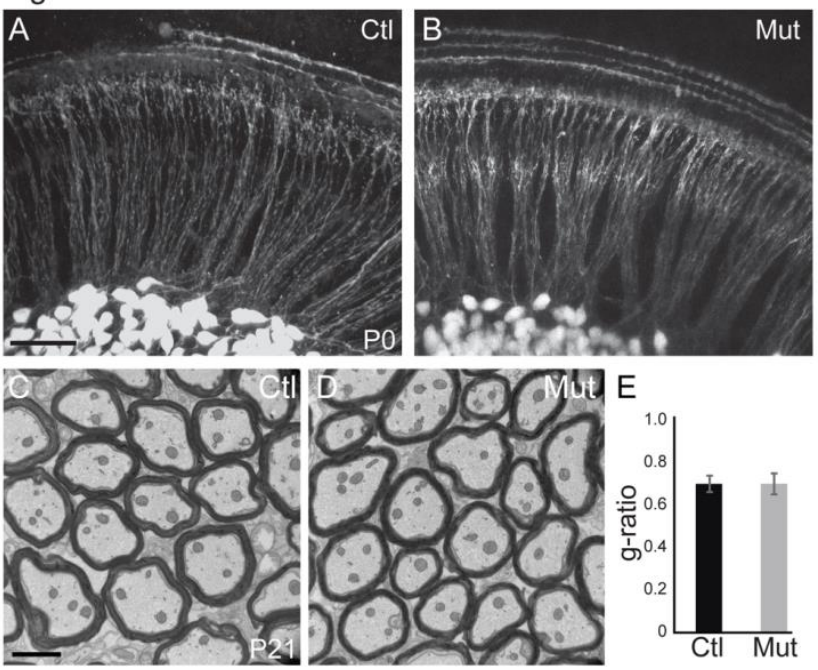

Figure 1: Peripheral SGN connectivity is normal in *Npr2* mutant mice.

(**A,B**) Genetic labeling of SGN projections in P0 cochlea using *Neurog1-CreER*^{T2} and the *RC::rePe* GFP reporter. No obvious difference in the peripheral pattern of connections was observed between control (Ctl) (**A**) and *Npr2* mutant (Mut) (**B**) animals. (**C**) Electron micrograph of a transverse section of myelinated SGN axons in the eighth nerve in a control P21 animal. (**D**) Similar electron micrograph of the eighth nerve of an *Npr2* mutant at P21 shows normal axonal diameters and normal myelination. (**E**) The g-ratio of *Npr2* mutants did not differ from controls and was near optimal. Scale bars in A, 50 µm; C, 2 µm.

Figure 2

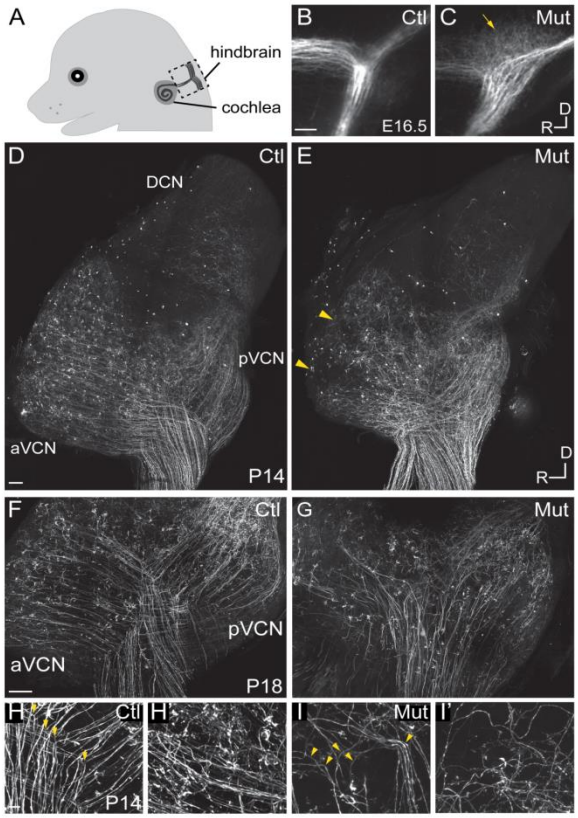

Figure 2: *Npr2* mutant mice show SGN central axon guidance and bifurcation defects.

(**A**) Schematic diagram of E16.5 embryo head showing SGN axons projecting from the cochlea into the hindbrain. The boxed area indicates the hindbrain region shown in **B** and **C**. (**B,C**) Dye labeling of SGN central axons in the hindbrain at E16.5. (**B**) SGN axons normally exhibited a stereotyped bifurcation pattern in the developing brainstem at E16.5, as shown in a control heterozygous embryo (Ctl). (**C**) In *Npr2* mutants, axons appeared disorganized in the region where they would normally bifurcate (arrow), and the nerve root lacked the distinctive Y-shape. Dorsal (D) is up and rostral (R) is to the left. (**D-I**) Genetic labeling of SGN central axons at postnatal stages (P14-18) using *Ngn1-cre*^{ERT2} and *AI14-tdTomato*, which allows random, relatively sparse labeling of SGNs. (**D-E**) Tiled confocal stack projections showing the entire cochlear nucleus of control (Ctl) (**D**) and *Npr2* mutant (Mut) (**E**) animals at P14. (**D**) Control SGN axons projected in a highly organized fashion to the aVCN, pVCN, and DCN. (**E**) In an *Npr2* mutant, SGN axons still projected to aVCN, pVCN, and DCN, but in a disorganized pattern. Yellow arrowheads indicate regions in the aVCN that appear under-innervated. (**F-G**) Confocal stack projections of vibratome-sectioned control and *Npr2* mutant cochlear nuclei at P18. (**F**) Control SGN axons showed stereotypical Y-shaped branch points and orderly projections to aVCN and pVCN. (**G**) In contrast, SGN projections to aVCN and pVCN were disarrayed in *Npr2* mutants. (**H-H'**) Control SGN axons exhibited characteristic bifurcations (yellow arrowheads, **H**) and formed organized bundles of axonal branches in aVCN (**H'**) at P14. (**I-I'**) *Npr2* mutant SGN axons turned instead of bifurcating (yellow arrowheads, **I**), and followed aberrant trajectories in aVCN (**I'**). Scale bar in **A**, 50 µm. Scale bars in **D** and **F**, 100 µm. Scale bar in **H**, 10 µm.

Figure 3

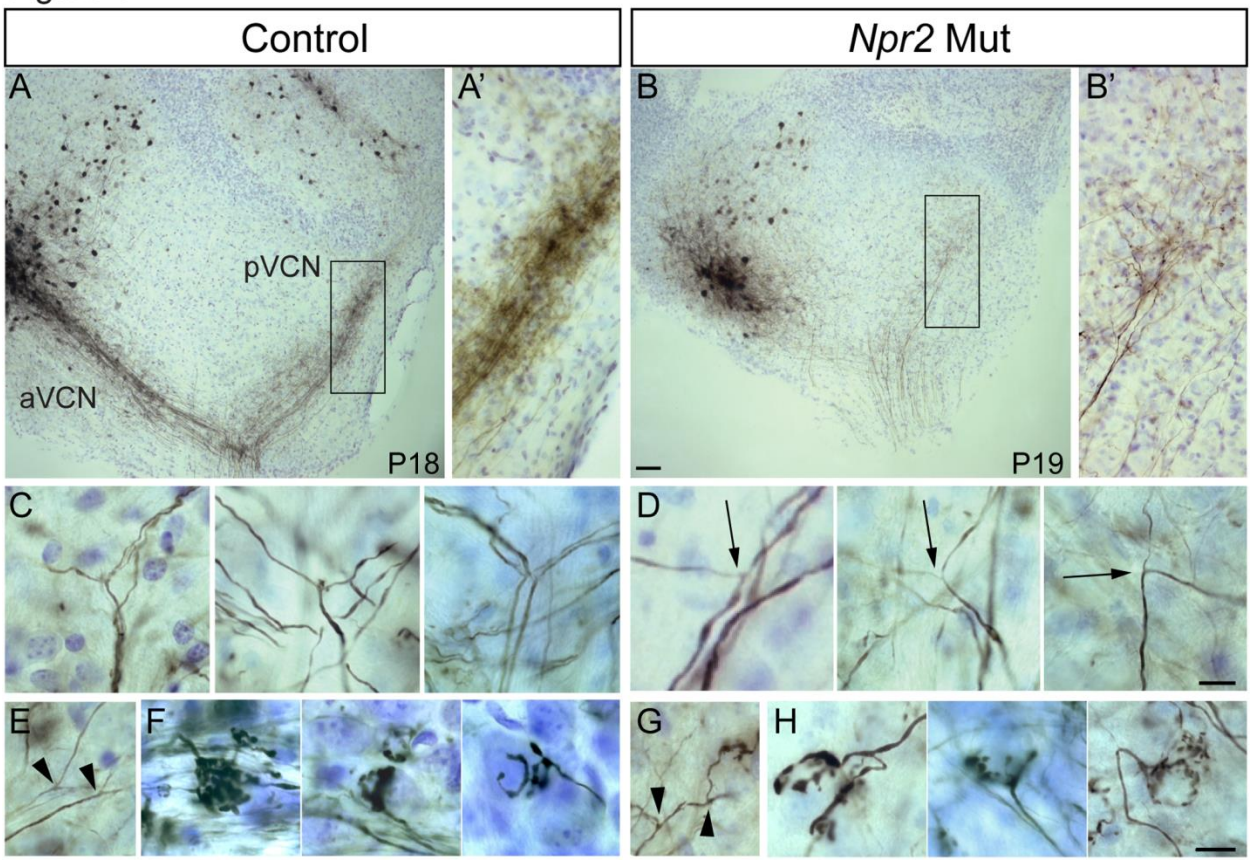

Figure 3: *Npr2* mutant SGN axons do not bifurcate properly but can form interstitial branches and morphologically normal synapses.

(**A**) Injection of biocytin into the aVCN (left) in a parasagittal slice of the cochlear nuclei labeled fibers not only in the nerve root but also in the pVCN (right) in control (Ctl) animals at P18. (**A'**) A close up view of boxed region in **A** showing labeled descending branches of SGNs. (**B**) In an *Npr2* mutant (Mut) at P19, biocytin injection into the aVCN also labeled fibers in the nerve root and in the pVCN, showing that at least some fibers branched at the nerve root. (**B'**) A close up view of the boxed region in B shows labeled SGN fibers and terminals in the pVCN. (**C,D**) Magnified views of bifurcation zone in control (**C**) and mutant (**D**) animals. (**C**) Examples of stereotyped bifurcations in control animals. (**D**) In mutants, rare fibers that do branch in the appropriate region do so at irregular angles and with one thinner and one thicker branch (arrows). (**E-H**) SGN axons can still form interstitial branches and elaborate morphologically normal synaptic endings in *Npr2* mutants. Interstitial SGN axon branches, which are distinct from bifurcations, are present in both control (**E**, arrowheads) and mutant (**G**, arrowheads) animals. Similarly, endbulbs of Held, which are one terminal whereby SGNs contact bushy cells, show the same types of branching patterns in the control (**F**) and *Npr2* mutants (**H**). Scale bars in B, 50 µm. Scale bars in D and H, 10 µm. Dorsal is up and rostral is to the left in all panels.

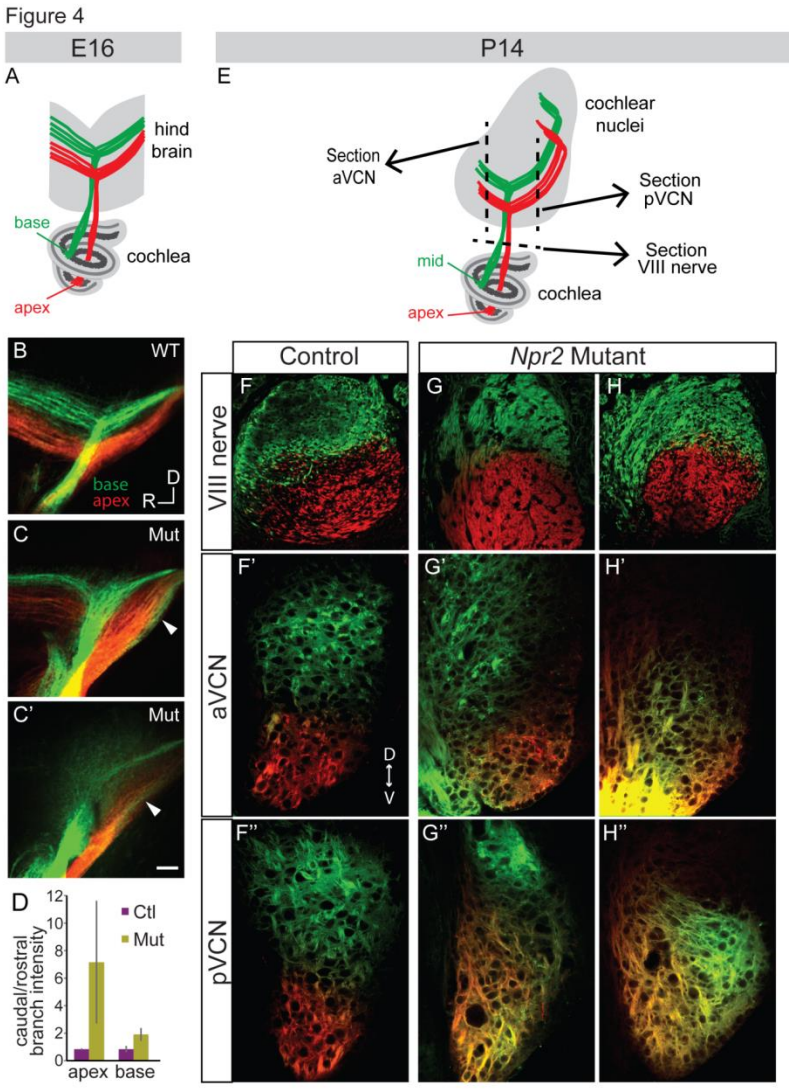

Figure 4: Tonotopy of SGN axons in the cochlear nuclei is blurred in *Npr2* mutants.

(**A**) Schematic diagram illustrating tonotopic dye labeling at E16. Labeling of SGNs in the cochlea with red (apex) and green (base) lipophilic dyes allowed their relative positions to be traced to the hindbrain. (**B**) In a wild-type (WT) E16 embryo, fibers from the base and apex bifurcated in the nerve root in separate bundles. (**C-C'**) Similar labeling in two different *Npr2* mutants (Mut) shows that fibers from the base and apex were incompletely segregated in the hindbrain. The gross tonotopy was preserved, but some overlap in dye labeling was seen between axons from basal and apical SGNs (arrowheads). Scale bar, 50 µm. (**D**) The intensity of labeling of SGN axons revealed a caudal bias in *Npr2* mutants, with more axons projecting towards the developing pVCN than the aVCN. (**E**) Schematic diagram illustrating tonotopic dye labeling at P14. The planes of sections illustrated in F-H are indicated by dotted lines. (**F-F''**) In a control animal, axons arising from the middle and from the apex of the cochlea were segregated in the auditory nerve and in the aVCN and pVCN. (**G-G'', H-H''**) Two examples of *Npr2* mutants. Although axons arising from the middle and apical turns of the cochlea remained segregated in the VIII nerve (**G**,**H**), they were intermingled in the aVCN (**G'**, **H'**) and pVCN (**G"**, **H"**).

Figure 5

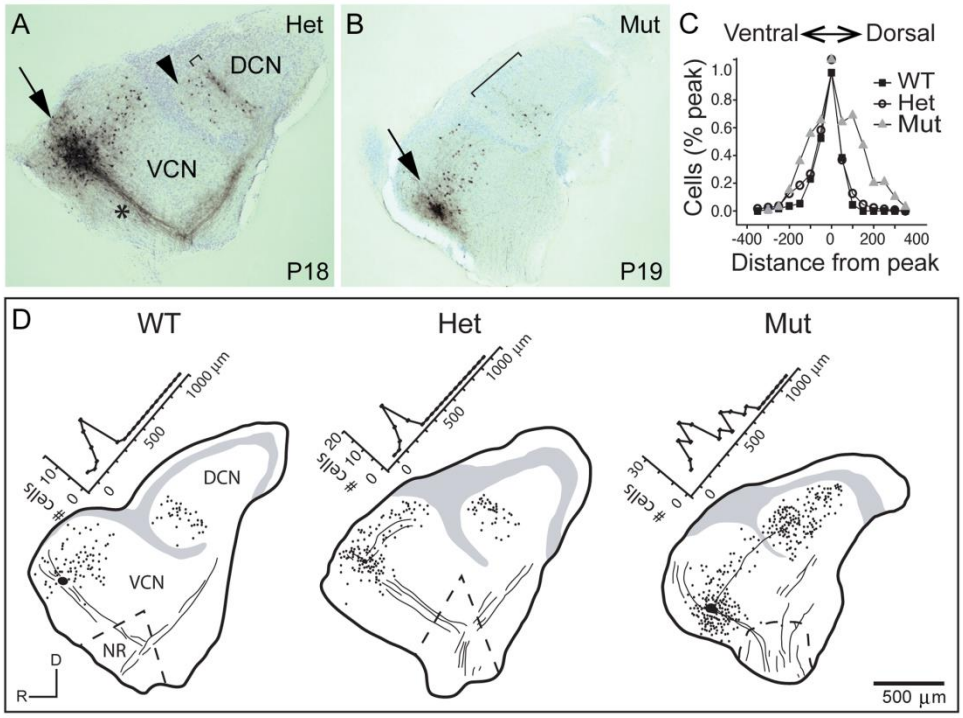

Figure 5: Tonotopy of TV neuron projections from the DCN to the aVCN is also blurred.

(**A**) Photomicrograph of a section of a parasagittal slice from a P18 heterozygote control animal with a biocytin injection into the aVCN (arrow). Biocytin labeled processes and cell bodies of neurons that passed through the injection site. Labeled processes included auditory nerve fibers (asterisk), the axons and terminals of TV cells whose cell bodies lie in the DCN (bracket), and the dendrites and local axonal collaterals of T stellate and D stellate cells whose cell bodies formed a halo around the injection site. Labeled TV cells clustered in a band (bracket) among terminals of auditory nerve fibers that were labeled by the same injection, showing that the TV cells lie in the same isofrequency lamina as their VCN targets. A few TV cells whose axons crossed the injection site on their way to more ventral regions were labeled ventral to (arrowhead) the labeled band of TV cells. No cell bodies were labeled in the DCN dorsal to the labeled band, indicative of the sharp tonotopic organization of the projection. (**B**) A similar injection of biocytin into the aVCN of a P19 *Npr2* mutant animal labeled a more diffuse bundle of auditory nerve fibers, a halo of neurons in the aVCN, and TV cells that were more scattered than in the heterozygote (bracket). (**C**) To compare the distribution of labeled neurons between control and mutant animals, peaks of distributions were lined up and normalized. In WT (n=6 slices, 258 cells) and Hets (n=20 slices, 914 cells), labeled cells were distributed in a sharp band, with no labeled cells more than 150 µm from the peak on the dorsal side. Since no clear bands were observed in *Npr2* mutants (Mut) (n=11 slices, 858 cells), histograms were aligned along their medians, at which half of the labeled cells lay more dorsal and half more ventral. The bands were sharp in both WT and Het animals, but were broader in *Npr2* mutant mice. No differences were detected over the age range examined between P14 and P26. (**D**) Examples of reconstructed slices, with labeled cells marked with dots, gray regions denoting areas containing granule cells in the largest section, and lines indicating the location of some of the labeled fibers. Numbers of labeled TV cell bodies were plotted as a function of distance along the tonotopic axis of the DCN, as illustrated. Scale bar, 500 µm.

Figure 6

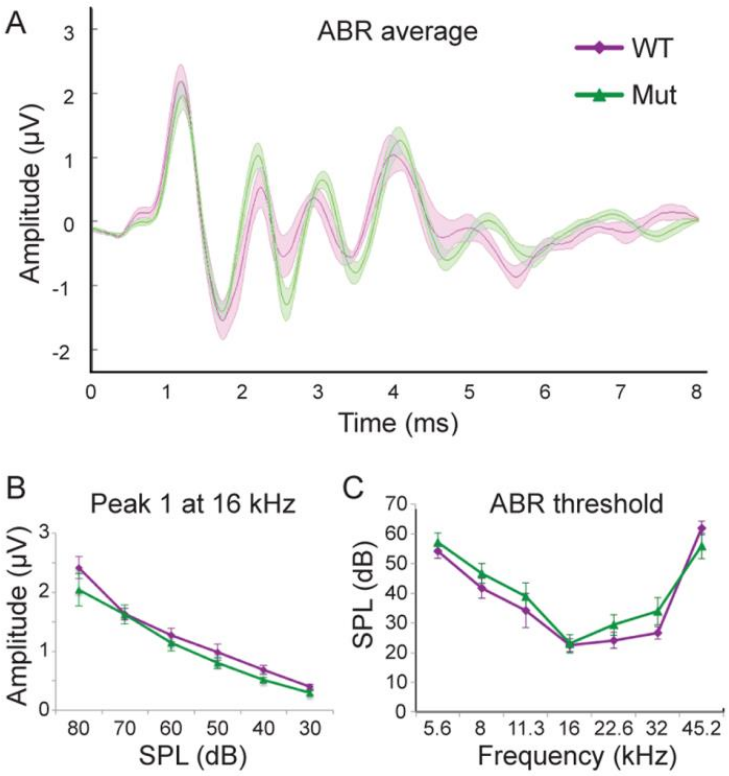

Figure 6: *Npr2* mutants detect sounds normally.

(**A**) Average ABR waveforms at 16 kHz for wild-type (WT) (purple, n=6) and *Npr2* mutant (Mut) (green, n=15) animals. The average is shown by the dark lines, and the shaded areas show the standard error of the mean. (B) Wave 1 reflects the synchronous firing of auditory nerve fibers. Its amplitude decreased with sound level similarly in WT (purple) and Mut (green). (**C**) Average ABR thresholds for WT (purple) and *Npr2* mutant (green) animals. No significant difference was observed between WT and *Npr2* mutants.

Figure 7

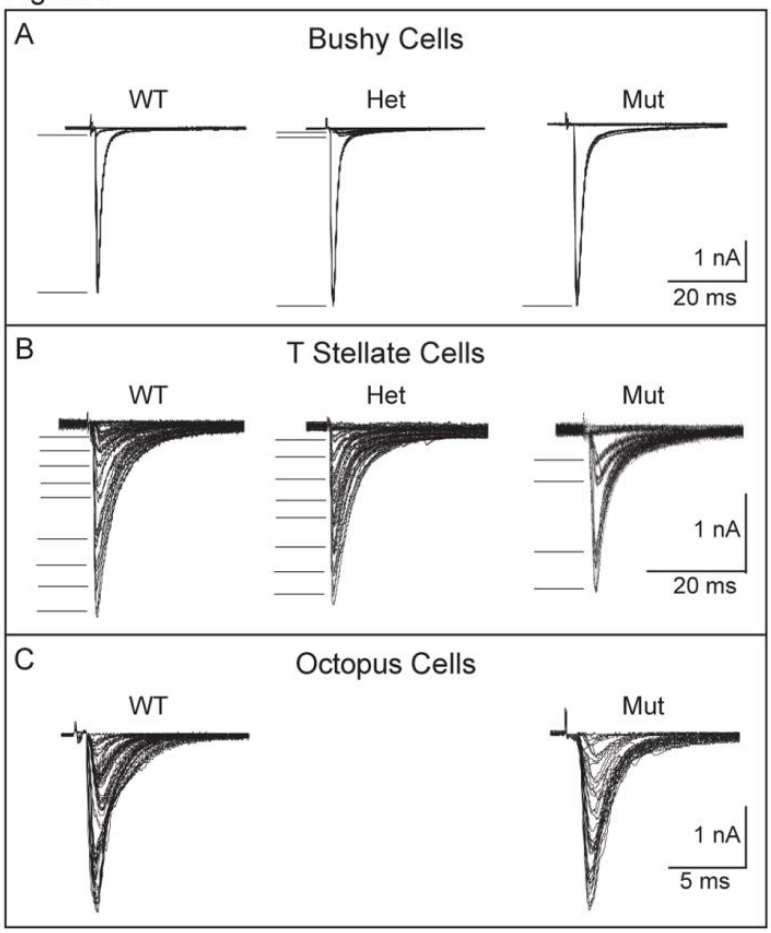

Figure 7: Convergence of SGNs onto bushy and T stellate cells tends to be lower in *Npr2* mutants.

(**A**) Voltage-clamp recordings (-65 mV) from individual bushy cells showed that in wild-type and heterozygote controls, gradual increase in the strength of shocks applied to auditory nerve fiber bundles evoked first one or two small jumps in current, presumably from bringing to threshold one or two fibers that contacted the recorded bushy cells, and then a large jump likely from bringing to threshold a fiber that contacted the bushy cell with an endbulb of Held. In the mutant, the response was all-or-none, increasing in a single step. In all genotypes, at least one of the steps was >1 nA. There was no obvious difference in the amplitudes of steps between mutant, heterozygote and wild type mice (P17-19). Five out of seven mutant bushy cells likely received one input through an endbulb. (**B**) Recordings from individual control T stellate cells showed that the synaptic current grew in 8 or 9 small steps, but that in a T stellate cell recorded anteriorly in an *Npr2* mutant, the response grew in only 4, larger steps. Small numbers of steps were recorded in 4 of 10 mutant T stellate cells, all of which lay anteriorly. (**C**) Recordings from individual octopus cells grew in more steps that were too numerous to count both in the wild type and in mutants. There was no discernible difference between them.

Figure 8

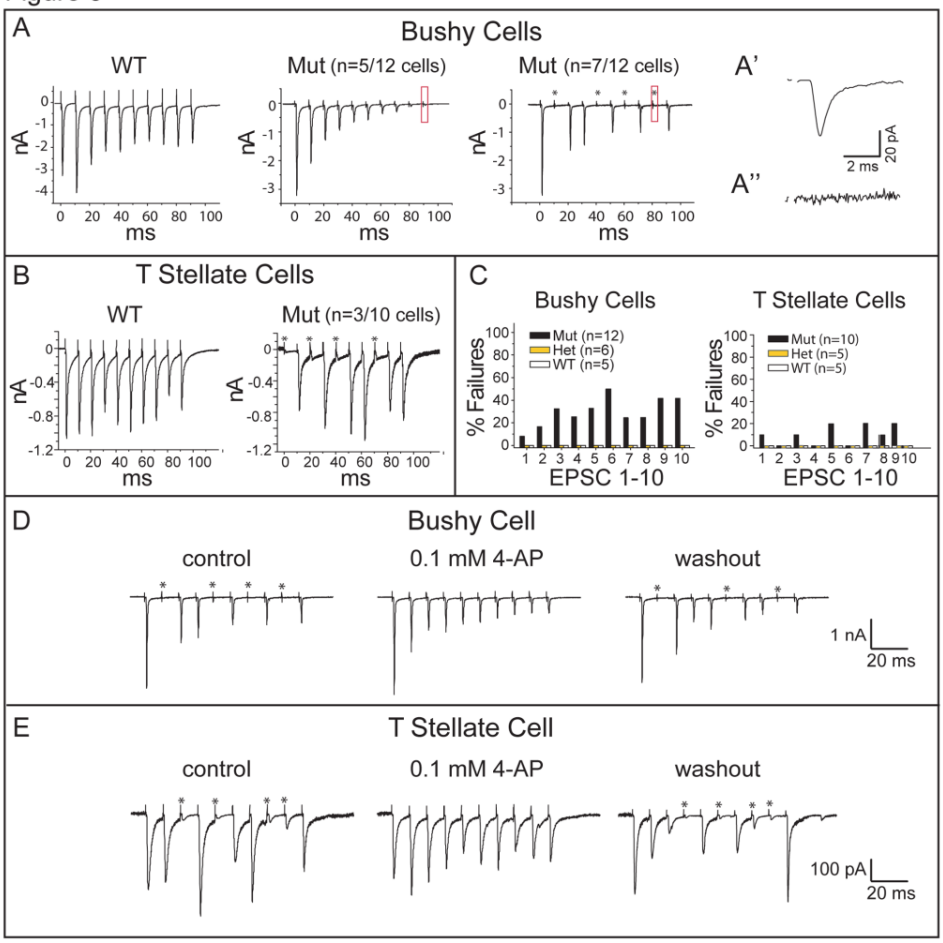

Figure 8: *Npr2* mutants exhibit normal synaptic depression but abnormal intermittent synaptic failures.

(**A**) Trains of shocks delivered at 100 Hz evoked synaptic responses that tended to diminish in amplitude, confirming synaptic depression in both control and *Npr2* mutant animals. However, some mutant bushy cells failed to respond to some of the shocks in the train. (**A'**) The small response (boxed) in the middle panel is shown at higher magnification to show that this cell had strong synaptic depression but that every shock evoked a synaptic current. 7 of 12 bushy cells showed synaptic failures such as those shown in the right panel. (**A''**) At higher magnification, no response was detected in the boxed region, indicating that this was a synaptic failure. (**B**) In T stellate cells, trains evoked responses with less synaptic depression than in bushy cells in the WT as well as in mutants. Failures in transmission were observed in mutant but not in WT animals. (**C**) Quantification of EPSC failures in control (WT and Het) and *Npr2* mutant (Mut) bushy and T stellate cells in response to the first 10 shocks in a train. No failures were observed in WT or Het cells, whereas in *Npr2* mutants, failures sometimes occurred, even in responses to the first shock. (**D, E**) Synaptic failures in *Npr2* mutants were reversibly eliminated by 4-aminopyridine (4-AP). In a bushy cell (**D**) and in a T stellate cell (**E**), failure to evoke EPSCs was reversibly abolished by 0.1 mM 4-AP. Blocking K^+ channels heightens and lengthens action potentials, making them less susceptible to conduction block.

Chapter 3

The Multiple Functions of T Stellate/Multipolar/Chopper Cells in the Ventral Cochlear Nucleus

Donata Oertel[1], Samantha Wright[1], Xiao-Jie Cao[1], Michael Ferragamo[2], Ramazan Bal[3]

[1]Department of Physiology, School of Medicine and Public Health, University of Wisconsin, 1300 University Avenue, Madison, WI 53706, USA
[2]Department of Biology, Gustavus Adolphus College, 800 West College Avenue, Saint Peter, MN 56082, USA
[3]Department of Physiology, Firat University, Faculty of Medicine, 23119 Elazig, Turkey

This Review was published in Hearing Research 2011 (276).

Abstract

Acoustic information is brought to the brain by auditory nerve fibers, all of which terminate in the cochlear nuclei, and is passed up the auditory pathway through the principal cells of the cochlear nuclei. A population of neurons variously known as T stellate, type I multipolar, planar multipolar, or chopper cells forms one of the major ascending auditory pathways through the brain stem. T Stellate cells are sharply tuned; as a population they encode the spectrum of sounds. In these neurons, phasic excitation from the auditory nerve is made more tonic by feed forward excitation, coactivation of inhibitory with excitatory inputs, relatively large excitatory currents through NMDA receptors, and relatively little synaptic depression. The mechanisms that make firing tonic also obscure the fine structure of sounds that is represented in the excitatory inputs from the auditory nerve and account for the characteristic chopping response patterns with which T stellate cells respond to tones. In contrast with other principal cells of the ventral cochlear nucleus (VCN), T stellate cells lack a low-voltage-activated potassium conductance and are therefore sensitive to small, steady, neuromodulating currents. The presence of cholinergic, serotonergic and noradrenergic receptors allows the excitability of these cells to be modulated by medial olivocochlear efferent neurons and by neuronal circuits associated with arousal. T Stellate cells deliver acoustic information to the ipsilateral dorsal cochlear nucleus (DCN), ventral nucleus of the trapezoid body (VNTB), periolivary regions around the lateral superior olivary nucleus (LSO), and to the contralateral ventral lemniscal nuclei (VNLL) and inferior colliculus (IC). It is likely that T stellate cells participate in feedback loops through both medial and lateral olivocochlear efferent neurons and they may be a source of ipsilateral excitation of the LSO.

Introduction

Acoustic information flows into the brain through the cochlear nuclei where the auditory pathway is subdivided into multiple, parallel ascending pathways. An important and interesting one is through stellate (or multipolar) cells of the VCN. Recent findings indicate that these cells and the synapses that feed acoustic information to them are specialized, allowing them to carry different acoustic information than the bushy and octopus cells, the two other major groups of principal cells of the VCN. Individual T stellate cells encode the envelope of sounds in the band of frequencies to which they are tuned, cues that are known to be critical for the understanding of speech (Shannon et al. 1995). As a population, T stellate cells encode spectrum, acoustic information that is used not only for understanding but also for localizing sounds (Blackburn and Sachs 1990; May et al. 1998).

Most T stellate cells occupy the multipolar cell region of the VCN between the nerve root and the octopus cell area, with a few sitting anterior to the nerve root (Osen 1969; Lorente de Nó 1981; Brawer et al. 1974; Oertel et al. 1990; Doucet and Ryugo 1997; Doucet and Ryugo 2006). T Stellate cells contact numerous targets in the brainstem, including the olivocochlear efferent neurons, ventral and intermediate nuclei of the lateral lemniscus and inferior colliculus. Here we summarize what functions T stellate cells perform and how cellular features support those functions.

Definitions of stellate/multipolar/chopper cells

T Stellate cells were identified in a variety of ways and were eventually found to correspond to a single cell type. Early studies named them “multipolar” (on the basis of Nissl staining) and “stellate” (on the basis of Golgi impregnation) cells (Osen 1969; Brawer et al. 1974; Lorente de Nó 1981). It then became clear that there were two distinct types of multipolar/stellate cells. Cant showed that “type I” and

"type II" multipolar cells in cats differed in their somatic innervation (Cant 1981). Smith and Rhode made the correlation between anatomical features and responses to tones. They showed that in cats type I multipolar/stellate cells responded to tones with sustained "chopping" whereas type II responded with "onset-chopping," firing a few times at regular intervals at the onset of a tone but then stopping firing in the continued presence of the tone (Smith and Rhode 1989). Choppers have been subdivided into "sustained" and "transient" choppers, defined below. There is no evidence to suggest that sustained and transient choppers represent different anatomical cell types. Studies in slices revealed that the axons of some multipolar/stellate cells project through the Trapezoid body (hence T stellate) whereas others project Dorsalward (D stellate) (Oertel et al. 1990). Those multipolar cells whose main axon projects through the trapezoid body, T stellate cells, have axon collaterals that innervate the same isofrequency lamina in the VCN and in the deep layer of the DCN (Fig. 1). The projection patterns of T and D stellate cells in slices corresponded to projection patterns of choppers and onset choppers, respectively (Rhode et al. 1983; Smith and Rhode 1989). We conclude, therefore that T stellate cells correspond to type I multipolar/choppers and D stellate cells with type II multipolar/onset-choppers. Doucet and Ryugo confirmed the differences in dendritic morphology and projection patterns with extracellular dye injections *in vivo* but gave them yet other, albeit more elegant, names: "planar" (type I/T stellate/chopper) and "radial" (type II/D stellate/onset chopper) multipolar cells (Doucet et al. 1997; Doucet et al. 2006).

T Stellate cells respond to sound by firing tonically

Tones evoke regular, tonic firing in T stellate cells whose rate increases monotonically with intensity (Rhode and Smith 1986; Young et al. 1988; Blackburn and Sachs 1989) (Fig. 2A). The timing of action potentials is so reproducible that peristimulus time histograms have modes that are strong and sharp at the onset of the response and weaken as temporal jitter accumulates over the duration of the

response to tones (Rhode et al. 1983; Smith et al. 1989; Blackburn et al. 1989) (Fig. 2B). This pattern was termed chopping (Pfeiffer 1966). Most (70%) choppers respond to tones with regular firing at a constant rate for the duration of the tone as "sustained choppers" (Fig. 2C) (Young et al. 1988; Blackburn et al. 1989). For these neurons, the interspike interval histograms are sharp. In a small proportion of choppers (30%), the "transient choppers," firing is less regular and the firing rate decreases in the continued presence of a tone. The two populations were distinguished by the coefficient of variation (CV), the ratio of the mean firing rate/standard deviation of the interspike interval. Those with a CV < 0.3 were defined as "sustained choppers"; those with CV >0.3 as "transient choppers" (Young et al. 1988; Blackburn et al. 1989). The chopper whose responses are illustrated in Figure 2C fired with great temporal regularity; the CV remained essentially constant at 0.15. Auditory nerve fibers and the other types of principal cells fire relatively rapidly at the onset of a tone and the rate of their irregular firing decreases to a lower rate over time in the continued presence of a tone, reflecting adaptation (Fig. 2D) (Kiang 1965; Young et al. 1988).

Inhibition shapes the temporal response patterns and the tuning of choppers. Glycinergic and GABAergic inhibition that is tuned similarly as excitation reduces peak excitation (Caspary et al. 1994). Choppers also have inhibitory sidebands; sound energy that falls near but outside the frequency range to which choppers increase firing, can cause the firing rate to decrease (Rhode et al. 1986; Palombi and Caspary 1992; Nelken and Young 1994; Paolini et al. 2005). Inhibitory sidebands, like the center-surround organization of visual receptive fields, enhance the encoding of spectral peaks and spectral edges. Inhibitory sidebands are produced, at least in part, by input from the more broadly tuned, glycinergic D stellate cells (Ferragamo et al. 1998b) with possible contributions from the periolivary regions (Adams and Warr 1976; Shore et al. 1991; Ostapoff et al. 1997).

The rate of tonic firing increases monotonically with level both at the onset of tones as well as during the steady state. The firing rate of choppers thus signals level. In contrast, other cells fire more

phasically, that is, they fire rapidly at the onset of a tone and then more slowly (primary-like) or stop firing (onset) in the continued presence of a tone. Phasically firing neurons (Fig. 2D) signal changes in level. The tonic firing of choppers is well suited for neurons that encode the spectrum of sounds as a population because the encoding of spectral peaks and valleys is relatively independent of the time after the onset of a sound (Blackburn et al. 1990; May et al. 1998). In neurons whose firing rate slows after the onset, level is encoded not only in the firing rate but also depends on the time after the onset of a sound.

The tonic firing of T stellate cells also makes them well suited for encoding the envelope of sounds. Understanding speech depends on the detection of the envelopes of sounds, especially over the range of <50 Hz (Shannon et al. 1995; Smith et al. 2002). Choppers have been demonstrated to encode amplitude modulation over a wide range of intensities (Frisina et al. 1990; Rhode and Greenberg 1994).

The phasic firing of auditory nerve fibers is preserved or enhanced in other principal cells of the VCN, the bushy and octopus cells. That phasic firing is functionally important because it enhances formant transitions and provides accurate information about the location of sound sources even in reverberant environments, critical features of hearing (Delgutte and Kiang 1984; Devore et al. 2009). If the excitatory input to choppers is phasic, however, the question arises how choppers convert phasic to tonic firing.

Multiple mechanisms enable T stellate cells to make phasic excitation more tonic

The observation that chopping can be generated in T stellate cells simply by applying steady depolarizing current (Oertel et al. 1988) was initially surprising because excitation by auditory nerve fibers would be expected to be large excitatory synaptic currents at the onset of a tone when auditory

nerve fibers fire most rapidly and then to decrease as the firing rate of auditory nerve fibers adapts. It is now clear that five mechanisms conspire to enable tonic firing.

Feedforward excitation of T stellate cells through other T stellate cells

T Stellate cells innervate their own isofrequency lamina within the multipolar cell area of the VCN (Smith et al. 1989; Oertel et al. 1990; Doucet et al. 1997; Friedland et al. 2003). As most of the cells in the vicinity of T stellate cells in the multipolar cell area are T stellate cells, their targets are probably other T stellate cells. Electrophysiological results confirm that conclusion. Shocks to the root of the auditory nerve evoke not only monosynaptic but also disynaptic excitatory input in slices of the VCN (Ferragamo et al. 1998b).

Coactivation of phasic excitation with phasic inhibition

It is likely that the coactivation of phasic inhibition reduces phasic excitation (Paolini et al. 2005). T Stellate cells receive inhibition from D stellate cells ipsilaterally and contralaterally (Ferragamo et al. 1998b; Needham and Paolini 2003). D Stellate cells respond transiently to tones with "onset chopping" patterns (Smith et al. 1989). The rapid firing of D stellate cells at the onset would be expected to produce relatively strong inhibition in T stellate cells at the onset of a tone when excitation from auditory nerve fibers is greatest. The onset of inhibition would be expected to follow the onset of excitation by about 1or 2 ms if auditory nerve fibers are activated synchronously and would therefore be expected to affect T stellate cell responses after one action potential (Oertel et al. 1990). Because D stellate/onset choppers are more broadly tuned than T stellate/chopper cells and often receive input from fibers tuned to higher frequencies, the temporal disparities could be smaller because the cochlear traveling wave delays are

shortest for the highest frequencies (Wickesberg 1996). Inhibition reduces the firing rate within the response area of choppers consistent with choppers receiving input from the more broadly tuned, more phasically responding, glycinergic D stellate cells and from sharply tuned glycinergic neurons in the deep layer of the DCN (Ferragamo et al. 1998b; Wickesberg and Oertel 1990; Caspary et al. 1994; Palmer et al. 1996). Tuberculoventral neurons whose cell bodies lie in the deep layer of the DCN provide sharply tuned inhibition to T stellate cells (Wickesberg and Oertel 1988; Wickesberg et al. 1990). The firing patterns of tuberculoventral cells seem to be variable. Cells likely to be tuberculoventral cells have been reported to respond to tones phasically in anesthetized cats (Rhode 1999). On the other hand, neurons in unanesthetized cats and gerbils cells thought to be tuberculoventral cells have been shown to respond with either phasic and tonic firing patterns (Ding and Voigt 1997; Shofner and Young 1985). Glycinergic inhibition may also arise from the ipsilateral periolivary regions and GABAergic inhibition from periolivary regions bilaterally (Adams et al. 1976; Shore et al. 1991; Ostapoff et al. 1997).

Absence of low-voltage-activated potassium conductance

T Stellate cells lack a low-voltage-activated potassium conductance that helps to make firing transient in bushy and octopus cells (Manis and Marx 1991; Bal and Oertel 2001; Ferragamo and Oertel 2002; McGinley and Oertel 2006; Cao et al. 2007). In contrast with other principal cells of the VCN, bushy and octopus cells, the biophysical properties of T stellate cells allow them to fire steadily at rates that reflect the magnitude of depolarization (Oertel et al. 1990; Ferragamo et al. 2002).

Activation of NMDA receptors

Excitation of T stellate cells activates relatively large currents through NMDA receptors (Cao and Oertel 2010). NMDA receptors require depolarization through AMPA receptors for the relief of the block by Mg^{2+}; they therefore amplify excitation through AMPA receptors (Nowak et al. 1984). In being slower and longer lasting than currents through AMPA receptors, NMDA receptors amplify excitation through AMPA receptors not only in amplitude but also over time. The long-lasting excitation through NMDA receptors thus reduces the phasic nature of excitation and obscures the time course of excitation through AMPA receptors.

Relatively little synaptic depression

The excitatory inputs of T stellate cells show less synaptic depression than those on phasically firing bushy and octopus cells. Trains of shocks to excitatory inputs, largely from auditory nerve fibers but possibly including some from other T stellate cells, show less synaptic depression than those to bushy or octopus cells (Wu and Oertel 1987; Chanda and Xu-Friedman 2010; Cao and Oertel 2010). The excitation of T stellate cells therefore adapts less than in other neurons of the VCN.

The mechanisms that enhance tonic firing obscure the encoding of temporal fine structure of sounds

The onset of the chopper response is dominated by excitation from auditory nerve fibers and would thus be expected to reflect the timing of the arrival of signals through auditory nerve fibers, similarly as in other principal cells of the VCN. Surprisingly, the latency between the onset of a tone and the first spike of chopper responses to tones has a small standard deviation but is about 1 msec longer than that of the other principal cells (van Gisbergen et al. 1975; Young et al. 1988). These authors

suggest that the longer first spike latency reflects a longer integration time in choppers than in other principal cells. The integration window, defined by the biophysical properties of the membrane, is indeed longer for T stellate than for bushy or octopus cells (McGinley and Oertel 2006). It is also possible that the timing of the onset of the response to tones in choppers is affected by inhibition that is activated by higher frequencies and shorter traveling wave delays (Wickesberg 1996). After an initial volley of excitation, feedforward excitation, the activation of NMDA receptors, and inhibition would be expected to sum with incoming excitation and to obscure the fine structure of sounds that is encoded in the ongoing firing of auditory nerve fibers and in the activation of AMPA receptors. After the onset, the timing of firing of choppers is determined by the biophysical properties of T stellate cells rather than by the fine structure of incoming excitation.

T Stellate cells are affected by neuromodulatory as well as driving inputs

T Stellate cells differ from other principal cells of the VCN in their sensitivity to neuromodulatory currents. Their relatively high input resistances allow small currents to cause relatively large voltage changes to produce firing (Fujino and Oertel 2001). T Stellate cells lack the low-voltage-activated potassium conductance that reduces repetitive firing in bushy and octopus cells (Ferragamo et al. 2002; McGinley and Oertel 2006). The low-voltage-activated potassium conductance also makes bushy and octopus cells relatively insensitive to steady currents in comparison with T stellate cells (Oertel and Fujino 2001; McGinley and Oertel 2006). Furthermore, in T stellate cells the hyperpolarization-activated conductance is activated at more hyperpolarized potentials than in bushy or octopus cells so that a smaller fraction is activated at rest. In having relatively high input resistances, T stellate cells respond with relatively large voltage changes to small modulatory currents. As the voltage-sensitivity of the hyperpolarization-activated inward current can be altered through G-protein coupled receptors, the

modulation of the hyperpolarization-activated inward current can itself make T stellate cells more excitable (Rodrigues and Oertel 2006). T Stellate cells have been shown to be sensitive to neuromodulatory currents (Fujino et al. 2001).

Sources of driving inputs

Auditory nerve fibers provide the driving glutamateric excitation for T stellate cells on proximal dendrites and at the soma (Cant 1981; Ferragamo et al. 1998b; Alibardi 1998). Consistent with their narrow tuning, only a few (5 or 6 in mice) auditory nerve fibers contact a T stellate cell (Ferragamo et al. 1998b; Cao and Oertel 2010). In addition they receive glutamatergic excitation from other T stellate cells and glycinergic inhibition from D stellate cells (Ferragamo et al. 1998b). T Stellate cells also receive glycinergic inhibition from tuberculoventral cells in the deep layer of the DCN (Wickesberg et al. 1990; Zhang and Oertel 1993). As the synaptic responses are well defined in intracellular recordings, these probably arise near the cell body in proximal dendrites as illustrated in Figure 3A (Ferragamo et al. 1998).

Neuromodulatory inputs

T Stellate cells also receive modulatory inputs. In contrast with the driving inputs, the neuromodulatory inputs raise or lower the excitability of T stellate cells subtly on a slower time scale, without fast postsynaptic potentials (PSPs) or postsynaptic currents (PSCs). This is interesting because it implies that the conductances associated with the neuromodulatory inputs affect the strength and time course of the driving inputs only minimally. Neuromodulatory inputs that are mediated through G-protein coupled receptors are generally slow even if they arise through terminals near the soma. Anatomical and electrophysiological evidence reviewed below suggests that some neuromodulatory

inputs are mediated by ionotropic receptors and arise on distal dendrites as illustrated schematically in Figure 3A.

GABA may play a neuromodulatory role. GABAergic inhibitory PSPs or inhibitory PSCs have never been observed although T stellate cells have $GABA_A$ receptors and bicuculline, a blocker of $GABA_A$ receptors, increases firing in response to trains of shocks to the auditory nerve in slices (Wu and Oertel 1986; Oertel and Wickesberg 1993; Ferragamo et al. 1998b). The specificity of bicuculline indicates that T stellate cells receive inhibition through $GABA_A$ receptors even when GABAergic IPSPs and IPSCs have not been observed (Ferragamo et al. 1998b). One explanation for these findings is that dendritic filtering obscures GABAergic IPSPs and IPSCs. Golgi cells are GABAergic and lie within the granule cell domains around the VCN and terminate near the fine distal dendrites of T stellate cells (Ferragamo et al. 1998a). Terminals that contain glutamic acid decarboxylase (GAD) have been observed near cell bodies in the multipolar cell area (Adams and Mugnaini 1987). These could be glycinergic terminals at which GAD is colocalized with glycine and that are functionally glycinergic as in the DCN (Kolston et al. 1992; Golding and Oertel 1997). They could also arise from GABAergic neurons in the ipsilateral lateral nucleus of the trapezoid body (LNTB) and dorsomedial periolivary nucleus, neurons whose cell bodies are absent in slices of the cochlear nuclei (Adams et al. 1976; Shore et al. 1991).

Acetylcholine modulates firing of T stellate cells. Cholinergic inputs from collateral branches of olivocochlear neurons in the VNTB terminate in the vicinity of the granule cells, where the tips of dendrites of T stellate cells lie, but distant from most cell bodies in the multipolar cell area (Brown et al. 1991; Sherriff and Henderson 1994; Osen and Roth 1969; Motts et al. 2008) (Fig. 3). T Stellate cells, in contrast with D stellate cells, have both nicotinic and muscarinic acetylcholine receptors (Fujino et al. 2001). Cholinergic inputs to T stellate cells, together with their olivocochlear efferent actions, can enhance the encoding of spectral peaks in noise (Fujino et al. 2001).

Norepinephrine (NE) and serotonin (5-HT) are associated with arousal. Both noradrenergic and serotonergic fibers terminate in the vicinity of T stellate cells (Klepper and Herbert 1991; Thompson et al. 1994; Thompson et al. 1995; Thompson and Thompson 2001; Thompson 2003a; Thompson 2003b). As these fibers have swellings even in the body of the VCN where the principal cells are located, serotonergic and noradrenergic inputs could potentially contact T stellate cells anywhere on the soma or dendrites. T Stellate cells have receptors that sense NE and 5-HT. Figure 3B shows that bath application of 15 µM 5-HT (replicated in 4 cells) or 10 µM NE (replicated in 5 cells) in the presence of blockers of glutamatergic and glycinergic inputs result in increased firing in a T stellate cell. Excitatory synaptic responses would be expected to be slow since adrenergic receptors and most serotonergic receptors are G-protein coupled and act through second messengers. NE and 5-HT can affect either or both presynaptic terminals or postsynaptic cells; in the cell illustrated in Figure 3B these neuromodulators were acting postsynaptically because glutamateric and glycinergic inputs were blocked pharmacologically. Norepinephrine has been shown to affect the release probability at the young calyx of Held (Leao and von Gersdorff 2001). Iontophoretic application of noradrenaline increased the firing rate of choppers (Kössl and Vater 1989; Ebert 1996). 5-HT has been shown to excite or inhibit choppers *in vivo* (Ebert and Ostwald 1992).

T Stellate cells form a major ascending auditory pathway through the brain stem

The prominence of T stellate cells in the brainstem auditory pathways can be appreciated by their projections. T Stellate cells have targets within the cochlear nuclei and in addition form one of the major ascending pathways through the brainstem (reviewed by Doucet and Ryugo 2006). Their projections are summarized in Figure 4.

Axons of T stellate cells exit the VCN through the trapezoid body, cross the midline and ultimately terminate in the contralateral inferior colliculus (Adams 1979). Through collateral branches they innervate several brainstem auditory nuclei, including the DCN, the lateral superior olive, the contralateral VNTB, and the contralateral VNLL (Warr 1969; Smith et al. 1993; Thompson 1998; Doucet and Ryugo 2003). A small proportion of T stellate cells also projects to the ipsilateral intermediate and dorsal nuclei of the lateral lemniscus and inferior colliculus (IC) (Adams 1979; Thompson 1998).

T Stellate cells bring acoustic input to the DCN

It is likely that T stellate cells deliver the bulk of acoustic input to the deep layer of the ipsilateral DCN (Fig. 1). In mice the density of stellate cell terminals is considerably greater than that of auditory nerve fiber terminals (Cao et al. 2008). T Stellate cells innervate their own isofrequency lamina in the DCN (Smith et al. 1989; Oertel et al. 1990; Doucet et al. 1997; Friedland et al. 2003). It has been suggested that the DCN plays a role in using spectral cues to localize sounds (reviewed by Oertel and Young 2004). T Stellate cells that encode spectrum effectively are particularly well suited to provide the acoustic input to neurons in the DCN that are involved in making use of spectral cues for localizing sound sources.

T Stellate cells could bring ipsilateral excitation to the LSO

T Stellate cells project to the lateral superior olive (LSO) raising the possibility that they provide ipsilateral, excitatory, acoustic input to the principal cells of the LSO (Thompson and Thompson 1991a; Thompson 1998; Doucet and Ryugo 2003). LSO neurons detect interaural intensity differences by summing ipsilateral excitation with contralateral inhibition (Tollin and Yin 2002b; Tollin and Yin 2002a).

What the source is of ipsilateral excitation to the principal cells of the LSO is unclear. It is possible that small spherical bushy cells excite LSO neurons (Cant and Casseday 1986). However, T stellate cells also project to the LSO (Thompson and Thompson 1991b; Doucet et al. 2003; Thompson 1998). T Stellate cells have small diameter axons whose relatively slow propagation could balance the rapid propagation over a longer distance and through an additional synapse from the contralateral globular bushy cells through the medial nucleus of the trapezoid body (MNTB) (Joris and Yin 1995). It is noteworthy that ipsilateral excitation in the LSO evokes tonic firing in chopping patterns (Tsuchitani and Johnson 1985). The balance of tonic excitation and more phasic inhibition through globular bushy cells would be expected to result in a balance between excitation and inhibition that changes over the time of a tonal stimulus.

T Stellate cells take part in olivocochlear efferent feedback loops

T Stellate cell input to the VNTB contributes to medial olivocochlear (MOC) feedback loops. Many cholinergic olivocochlear efferent neurons arise from the contralateral VNTB (Sherriff et al. 1994; Motts et al. 2008). T Stellate cells provide acoustic input to neurons in the contralateral VNTB (Warr 1982; Robertson and Winter 1988; Thompson et al. 1991a; Warr 1992; Smith et al. 1993; de Venecia et al. 2005). They also receive input from at least some of those cholinergic neurons through the crossed MOCs (Spangler et al. 1987; Brown et al. 1988; Winter et al. 1989; Shore et al. 1991; Brown and Benson 1992; Sherriff et al. 1994; Warr and Beck 1996). As cholinergic inputs excite T stellate cells, the connections between T stellate cells and the VNTB neurons form a positive feedback loop (Fujino et al. 2001). T Stellate cells are also influenced by medial olivocochlear efferent neurons through the cochlea. This feedback loop is negative because the activation of efferents reduces firing in auditory nerve fibers

which in turn reduces excitation of T stellate cells (Wiederhold and Kiang 1970; Warren III and Liberman 1989).

It is also likely that T stellate cells are involved in lateral olivocochlear feedback loops. T Stellate cells terminate in the vicinity of lateral olivocochlear efferent (LOC) neurons (Warr 1982; Thompson and Thompson 1988; Thompson et al. 1991a; Doucet et al. 2003). As the excitation of T stellate cells is affected through auditory nerve fibers whose activity is influenced by LOC efferent neurons, T stellate cells are part of a feedback loop in which they regulate the activity of LOC neurons which in turn affect excitability of the auditory nerve fibers that drive responses to sound in T stellate cells. LOC neurons are involved in balancing excitability in the circuits associated with inputs from the two ears (Darrow et al. 2006).

T Stellate cells also feed acoustic input to neurons in the VNLL and to the inferior colliculus. The functional consequences of these direct and indirect connections of T stellate cells with the inferior colliculus are not well understood. They do suggest that the list of integrative functions performed by T stellate cells will continue to grow.

Birds have neurons that share many of the features of T stellate cells

The cochlear nuclei have been studied extensively in birds. *Nucleus angularis* receives innervation from auditory nerve fibers and contains neurons that bear a strong resemblance to T stellate cells. The heterogeneous dendritic morphologies indicate that *nucleus angularis* holds multiple types and that not all neurons in *nucleus angularis* bear homology to T stellate cells (Soares and Carr 2001). Neurons in *nucleus angularis* project to the lemniscal nuclei and to the inferior colliculus (Takahashi and Konishi 1988b; Takahashi and Konishi 1988a). They also project to olivocochlear neurons (Conlee and

Parks 1986; Takahashi et al. 1988a; Yang et al. 1999). Extracellular recordings show that the *nucleus angularis* of barn owls contains neurons that are sharply tuned and respond to tones as choppers but other response patterns are also present (Sullivan and Konishi 1984; Sullivan 1985; Köppl and Carr 2003).

In slices some neurons in *nucleus angularis* also respond to depolarizing current pulses with steady, tonic firing (Soares et al. 2002). Like T stellate cells in mammals, cells in *nucleus angularis* have excitatory synaptic responses with relatively large NMDA components (MacLeod and Carr 2005). Furthermore, in contrast with neurons in *nucleus magnocellularis* that resemble mammalian bushy cells, inputs to cells in *nucleus angularis* not only have less synaptic depression but they sometimes show facilitation (MacLeod et al. 2007).

Owls use interaural timing cues to localize sounds in the azimuth and they use intensity or spectral cues in asymmetrically placed ears to localize sounds in elevation. Neurons in *nucleus angularis* process the spectral, but not interaural timing, cues that owls use to localize sound sources (Takahashi et al. 1984). The role of neurons in *nucleus angularis* goes beyond localizing sounds, however. Carr and her colleagues have suggested that neurons in *nucleus angularis* play a role in recognizing and discriminating sounds (Köppl et al. 2003; MacLeod et al. 2005; MacLeod et al. 2007).

Summary

As a population, T stellate cells encode the spectrum of sounds. They receive acoustic input from auditory nerve fibers whose phasic firing emphasizes changes in intensity and convert them to more tonic responses. Several mechanisms contribute to that transformation: Feedforward excitation through other T stellate cells, coactivation of excitation and inhibition, reduction in synaptic depression, and the amplification of excitatory synaptic current over time through NMDA receptors. They deliver that

information to nuclei that make use of spectral information. T Stellate cells terminate in the DCN, to olivocochlear efferent neurons, to the lateral superior olive, to the contralateral nuclei of the lateral lemniscus, and to the contralateral inferior colliculus. These targets use spectral information to localize sounds, to adjust the sensitivity of the inner ear, and to recognize and understand sounds. Birds also process sounds through neurons that resemble T stellate cells in their projections and also in their cellular properties, attesting to the fundamental importance that T stellate-like cells have for hearing in vertebrates.

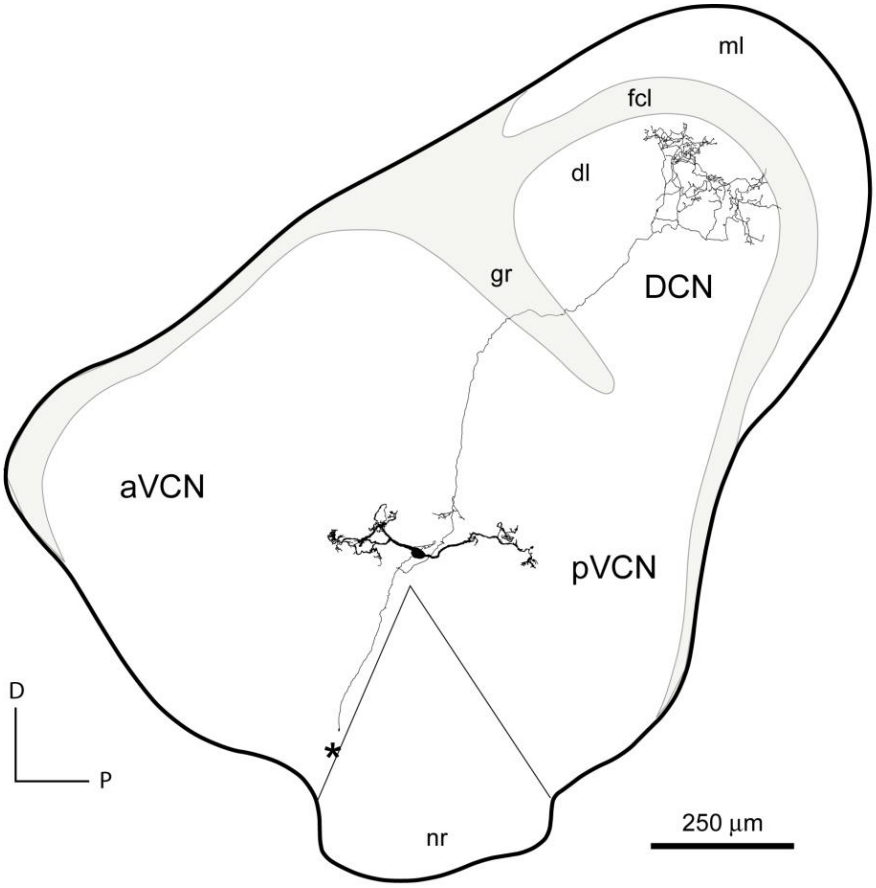

Figure 1

Reconstruction of a T stellate cell in a slice of the cochlear nuclear complex. The cell was labeled with biocytin in a slice of living tissue. The cell was reconstructed with a camera lucida from sections of the slice that had been processed to visualize cells with methods that have been described (Golding et al., 1995). The soma of this cell lies at the indistinct border between the anteroventral (aVCN) and posteroventral (pVCN) cochlear nuclei, just dorsal to the nerve root (nr). As is characteristic of T stellate cells, its dendrites lie parallel to the path of the ascending and descending branches of auditory nerve fibers with the highly branched tips in the vicinity of overlying granule cells. The axon emanates from the cell body. One branch projects dorsally through the granule cell lamina (gr) into the deep layer (dl) of the dorsal cochlear nucleus (DCN). The terminal arbor occupies an isofrequency lamina that crosses the deep layer but does not extend into the fusiform cell layer (fcl) or the molecular layer (ml). The main axon was cut at the medial surface of the slice where it projected into the trapezoid body (*).

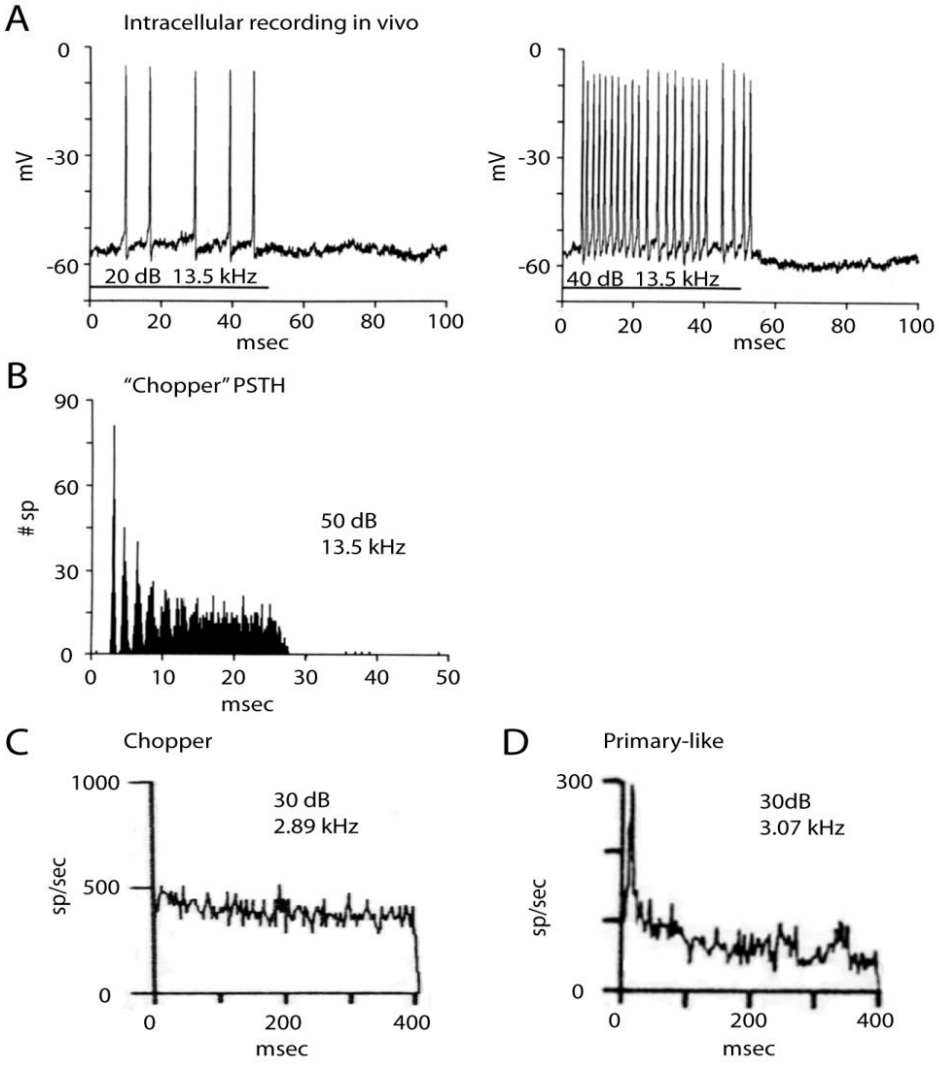

Figure 2

T Stellate cells fire tonically in response to tones. A. An intracellular recording from a T stellate cell in a cat shows that the cell fired steadily for the duration of the 50-msec tone at the cell's characteristic frequency and that the firing became more rapid with increasing intensity. B. Peristimulus time histogram from the same cell as in A generated from responses to 250 repetitions of tones at the characteristic frequency. C. Chopper fires at an almost constant rate for the duration of a 500 msec tone at the characteristic frequency. Bin width for computing histogram was 3.9 ms. D. In contrast with choppers, primary-like neurons fire rapidly at the onset of a tone and then more slowly as they adapt. Figures A and B are by Rhode and Smith, reproduced from the Journal of Neurophysiology, 1986, Am Physiol Soc, used with permission, and C and D are by Blackburn and Sachs, reproduced from the Journal of Neurophysiology, 1989, Am Physiol Soc, used with permission.

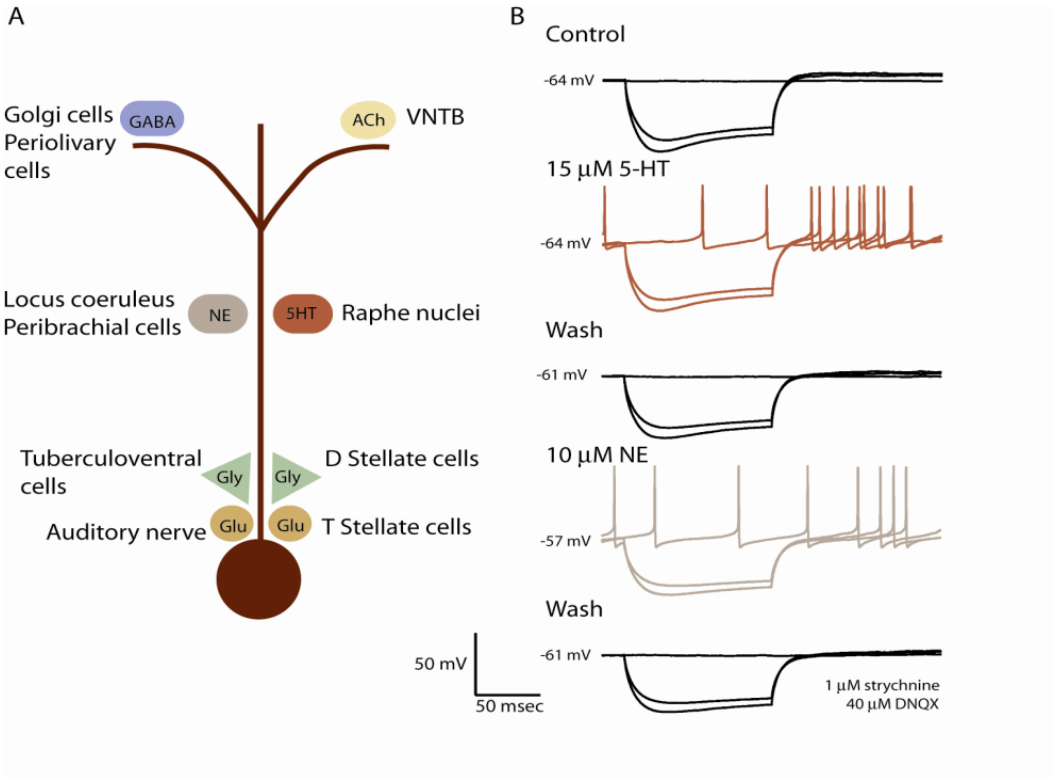

Figure 3

T Stellate cells integrate neuromodulatory with driving inputs. A. Indirect evidence indicates that inputs to T stellate cells are to some extent spatially segregated. Intracellular recordings with electrodes at the soma reveal glutamatergic (Glu) and glycinergic (Gly) synaptic responses. The rapid rise of those synaptic responses is consistent with their being generated near the soma. There are several known sources for these excitatory and inhibitory inputs. Even GABAergic synaptic responses mediated through $GABA_A$ receptors are so slow and small that individual PSPs are difficult to resolve suggesting that they are generated distally in dendrites, which is also consistent with the location of GABAergic terminals from Golgi and Periolivary cells in granule cell regions. T Stellate cells have nicotinic and muscarinic acetylcholine receptors. Cholinergic fibers terminate near the tips of T stellate cell dendrites near the granule cell domains . Noradrenergic and serotonergic fibers course throughout the VCN suggesting that they can contact dendrites of T stellate cells either or both proximally or distally. B. A T stellate cell was excited by the bath-application of neuromodulators. A whole-cell patch-clamp recording made with a pipette that contained a gluconate-based, GTP-containing solution in the presence of 1 µM strychnine and 40 µM 6,7-dinitroquinoxaline-2,3-dione (DNQX) in the extracellular saline solution to block glutamatergic and glycinergic synaptic responses, shows that both serotonin and norepinephrine reversibly evoked spontaneous firing. The application of serotonin did not change the resting potential, shown by the numbers at the left of the traces in mV, and responses to hyperpolarizing current pulses (–0.4 and –0.5 nA) indicate that the change in input resistance was too small to be detected. Serotonin increased firing after the end of the hyperpolarizing pulse. After the serotonin was washed out, norepinephrine increased spontaneous and anode break firing in the same cell. All effects were reversible. Details of the methods have been described previously (Fujino and Oertel, 2001).

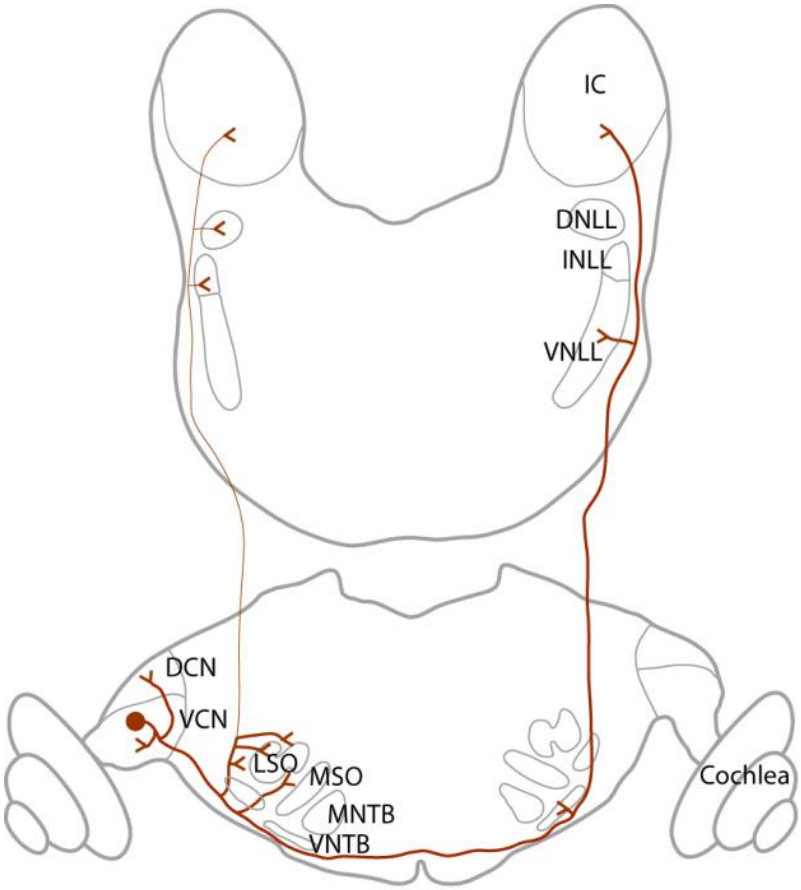

Figure 4

T Stellate cells project widely. Local collaterals innervate the ventral (VCN) and dorsal (DCN) cochlear nuclei. The main axon projects out through the trapezoid body, innervates the region around the ipsilateral lateral superior olivary nucleus (LSO), crosses the midline, innervates the contralateral ventral nucleus of the trapezoid body (VNTB), ventral nucleus of the lateral lemniscus (VNLL) and ultimately terminates in the contralateral inferior colliculus. Occasionally T stellate cells innervate the ipsilateral intermediate nucleus of the lateral lemniscus (INLL), dorsal nucleus of the lateral lemniscus (DNLL) and the ipsilateral inferior colliculus.

Chapter 4

Transmission between End bulbs of Held and Bushy Cells in Mice whose Deafness is caused by a Mutation in Otoferlin

Samantha Wright[1], Youngdeok Hwang[2], Donata Oertel[1].

[1]Department of Neuroscience, University of Wisconsin School of Medicine and Public Health, Madison, WI 53706

[2]I.B.M. Thomas J. Watson Research Center, Yorktown Heights, NY, 10598

Abstract

Mice that carry a mutation in a calcium binding domain of otoferlin, the putative calcium sensor at hair cell synapses, have normal distortion product otoacoustic emissions (DPOAEs) but auditory brain stem responses (ABRs) are absent. In mutant mice transduction is normal but transmission of acoustic information to the auditory pathway is blocked even before the onset of hearing. We reveal that primary auditory neurons adapt in the face of altered excitation. The volumes of ventral cochlear nuclei of mutant mice are reduced by 45% relative to hearing controls. While the tonotopic organization was not detectably changed, the axons to end bulbs of Held and the end bulbs themselves were smaller. In mutant mice the targets of end bulbs, bushy cells, in the anterior ventral cochlear nucleus (aVCN) have the electrophysiological hallmarks of control cells. Spontaneous miniature EPSCs occur with similar frequencies and have similar shapes in deaf as in hearing animals but they are 24% larger. Bushy cells in deaf mutants are contacted by about 2.6 auditory nerve fibers compared to about 2.0 in hearing controls. Furthermore, each fiber delivers more synaptic current, 4.8 nA compared to 3.4 nA, than in hearing littermate animals. The quantal content of evoked EPSCs is not different between mutants and controls; the increase in current delivered in mutants is accounted for by the increased response to the size of the quanta. Responses to shocks presented at long intervals are larger in mutants but they depress more rapidly than in hearing controls.

Introduction

Experimental manipulation of electrical activity in the cochlear nuclei after the onset of hearing has long been known to affect neuronal circuits in the cochlear nuclei (Trune and Morgan 1988; Pasic and Rubel 1989; Ryugo et al. 1998; Redd et al. 2000; Stakhovskaya et al. 2008). However, electrical activity even before the onset of hearing is likely to affect auditory circuits. Before hearing begins, supporting cells in the cochlea induce action potentials in small groups of adjacent inner hair cells that in turn evoke periodic bursts of suprathreshold responses in the auditory nerve that are propagated to the cortex (Johnson et al. 2011; Tritsch et al. 2007; Tritsch et al. 2010; Tritsch and Beurgles 2010). Synaptic transmission between hair cells and spiral ganglion neurons, the cells whose axons are auditory nerve fibers (ANF), depends on the detection of calcium by otoferlin (Roux et al. 2006; Beurg et al. 2010) whereas downstream synapses do not depend on otoferlin. Mice that lack otoferlin are thus naive of most patterned spontaneous activity that originates in the cochlea and propagates throughout the auditory system before the onset of hearing. Here we examine how the reduction of electrical activity from hair cells affects the next synaptic stage.

ANFs innervate the ipsilateral ventral (VCN) and dorsal cochlear nuclei (DCN) tonotopically. Fibers that encode low-frequencies innervate ventral regions and fibers that encode high-frequencies innervate dorsal regions. ANFs terminate on bushy cells in the aVCN with the second largest synapse in the mammalian brain, the end bulb of Held (Held 1893). End bulbs release glutamate which binds to postsynaptic AMPA receptors in the bushy cell membrane (Wang et al. 1998; Gardner et al. 1999; Gardner et al. 2001). We sought to understand how the end bulbs of Held and their target bushy cells are altered by deprivation of input from inner hair cells even before the onset of hearing.

The mice studied in these experiments have a point mutation resulting in a non-conserved substitution of I319N in the second of six calcium domains in the protein otoferlin (Longo-Guess et al.

2007). Otoferlin is thought to sense calcium and regulate synaptic transmission by inner hair cells (Roux et al. 2006; Johnson and Chapman 2010). Otoferlin is a member of the Ferlin family of proteins, all of which have been implicated in calcium regulated membrane fusion events and are membrane-anchored, cytosolic proteins that are involved in vesicle fusion and/or membrane trafficking (Yasunaga et al. 2000; Lek et al. 2011). Mutations in otoferlin were first described from human pathologies in several unrelated, consanguineous Lebanese families (Yasunaga et al. 1999). These deaf individuals have an autosomal recessive, nonsyndromic prelingual form of deafness, DFNB9 (Yasunaga et al. 1999). In humans, otoferlin has multiple long and short, alternatively spliced isoforms but mice have only the long isoform (Yasunaga et al. 1999, 2000). In mice otoferlin appears in inner hair cells (IHCs) at P4, after which it is responsible for the calcium induced exocytosis in IHCs; synaptotagmin isoforms 1, 2 and 7 are also present in IHCs but none appear responsible for calcium induced exocytosis before P3 (Beurg et al. 2010). Otoferlin also mediates synaptic transmission from outer hair cells (Beurg et al 2008).

Materials and Methods

Mice

Otoferlin mutant animals *Otof* ^{deaf5Jcs}*/Kjn*, were purchased from Jackson Labs, stock #006128. An ENU induced point mutation from Thymine to Adenine in exon 10 of the *otoferlin* gene causes a non-conserved amino acid change from isoleucine to asparagine in the second calcium binding domain of the protein. Breeding colonies of mutant mice, on a mixed background of C57BL/6J and C3HeB/FeJ, were maintained by crossing deaf otoferlin mutant males, with hearing, heterozygous females. Their offspring were either homozygous deaf mutants, or hearing heterozygotes and could be distinguished before experiments by the presence or absence of a Preyer reflex. Wild type mice were created by mating heterozygous animals; resulting wild type mice which were bred and maintained separately. Genotypes

of all mice were confirmed *post hoc* (Longo-Guess et al. 2007). Animals of both sexes, aged from P11-60, with the majority of animals aged P17-23, were used for anatomical experiments and P16-22 for the electrophysiological experiments. *Otoferlin* knockout (KO) mice were kindly given to us by Dr. Isabel Roux with permission from Dr. Christine Petit (Roux et al. 2006). Genotyping of these mice were also confirmed *post hoc*. All procedures were approved by the Institutional Animal Care and Use Committee at the University of Wisconsin, Madison.

Solutions

The dissection of the cochlear nuclei from the brainstem was done in a high sucrose extracellular saline solution that contained reduced Na^+ and Ca^{2+} (345 mOsm/kg). The composition of the solution (in mM) is as follows: 99 NaCl, 3 KCl, 1.2 KH_2PO_4, 1 $CaCl_2$, 1.3 $MgSO_4$, 20 $NaHCO_3$, 6 HEPES, 10 glucose, 72 sucrose, pH 7.3. The cutting solution was kept around 28°C.

The extracellular physiological saline (osmolarity 308 mOsm/kg) used to perfuse the tissue (1.5-2 hours) after biocytin injections and also for whole-cell recordings, contained (in mM): 130 NaCl, 3 KCl, 1.2 KH_2PO_4, 2.4 $CaCl_2$, 1.3 $MgSO_4$, 20 $NaHCO_3$, 6 HEPES, 10 glucose, and 0.4 ascorbic acid, pH 7.3. Whole-cell recordings were made in the presence of 10 μM strychnine to block glycinergic inhibition. All salines were saturated with 95% O_2-5% CO_2, and maintained at 32-33°C. Chemicals were from Sigma-Aldrich, except that sucrose was purchased from Fisher.

The internal pipette solution for voltage and current clamp recordings was (in mM): 108 potassium gluconate, 9 HEPES, 9 EGTA, 4.5 $MgCl_2$, 14 phosphocreatinine (Tris salt), 4 ATP (Na salt), and 0.3 GTP (tris salt) that had a final osmolarity ~303 mOsm/kg. The pH was adjusted to 7.4 with KOH. The final holding potentials were corrected for a −10 mV junction potential.

Brain Slices

For electrophysiological studies, parasagittal slices of the left cochlear nucleus were cut from the brainstem with a vibrating microtome (Leica VT 1000S) in sections of 200 μm. Cochlear nuclei were superfused continually at ~ 3-6 ml/min. The temperature was measured with a Thermalert thermometer (IT-23, Physitemp) and was controlled with a custom-made, feedback-controlled heater to remain at 32 or 33°C.

Biocytin injections

For the anatomy, cochlear nuclei were removed bilaterally from the brainstem by hand, via scissors. In a few cases, parasagittal slices up to 420 μm thick of cochlear nuclei were cut with a vibrating microtome (Leica VT 1000S). Tissue was transferred to a holding chamber ~0.6 mL and superfused continually at ~6-8 mL/min for 1.5-2 hours. Temperature was kept at 33^{o}C with a custom-made, feedback-controlled heater that was connected to a Thermalert thermometer (IT-23, Physitemp). Injections were made under the control of a Wild (M5) dissecting microscope.

1% biocytin was dissolved via sonication, in physiological extracellular saline which was used to label auditory nerve fibers. Visualization of the biocytin was made possible with Vectastain ABC Peroxidase Kits (Standard) purchased from Fisher (Golding et al. 1995). Extracellular injections were made with a Picospritzer, through a glass pipette with a tip diameter ~ 5 μm, along the dorsal/ventral axis of the pVCN; some injections were made only at the nerve root, while others were made in groups of three with one made ventrally in the nerve root, one medially in the pVCN and one dorsally in the pVCN. Occasionally single injections into the aVCN were made to visualize the tuberculoventral cell projections,

which also labeled end bulbs. Tissue was fixed in 4% paraformaldahyde, stored at 4°C, cryo-protected in 30% sucrose, embedded in a gelatin-albumin mixture, and resectioned at 60 μm in frozen sections. Tissues were mounted on subbed slides, dehydrated with alcohol and stained with cresyl violet to visualize cellular nuclei. Photomicrographs were taken through a Zeiss Axioskop with a Zeiss Axiocam.

Volume measurements

Quantification of the volumes of the magnocellular regions in the ventral and dorsal cochlear nuclei were made from *camera lucida* reconstructions in serial sections from each nucleus. Images were scanned into a computer, outlined and analyzed with Image J software, wherefrom the final volume measurements were imported into excel and compared by Student's t-tests for statistical analysis. Volumes are presented as means ± standard deviation.

Auditory Brainstem Responses (ABRs) and Distortion Product Otoacoustic Emissions (DPOAEs)

Animals aged between P20 and P60 were anesthetized with Ketaject, 150 mg/kg and Xylazine, 5 mg/kg. Once animals were unresponsive to a paw pinch, they were placed on a heating pad to maintain body temperature. Auditory brainstem responses (ABRs) and distortion product otoacoustic emissions (DPOAEs) were recorded with Tucker Davis Technologies, Sig Gen Software.

To measure ABRs, animals were placed next to a freefield speaker (ES1) positioned 10 cm away from their left ear, grounded by a subcutaneous electrode behind the contralateral pinna and a subcutaneous reference electrode at the apex of the skull and a subcutaneous recording electrode directly behind the left ear, as near as possible to the ear. Animals were presented with clicks, 0.1 msec in duration and of alternating polarity between 90 and 10 dB; or with tones, 5 msec duration, with a 3 msec

gating time, at 4 kHz, 8 kHz, 16 kHz and 32 kHz ranging between 90 to 10 dB SPL. Final traces were averages of 500-1500 individual recordings.

DPOAEs near 16 kHz were measured in response to presentation of two simultaneous tones presented at equal levels through a separate electrostatic speaker (EC1) of frequencies *f1* and *f2*, giving rise to a distortion product.

Electrophysiological Recordings

Whole-cell patch-clamp recordings were made using a Multiclamp 700B amplifier (Axon Instruments) that is under the control of pCLAMP 9 software. Patch electrodes are made from borosilicate glass and have resistances between 3.5 - 8 MΩ. All recordings are digitized at rates more than twice the low-pass limit of the filter to prevent aliasing. Recordings of evoked synaptic currents (eEPSC) were digitized at 40 kHz and low-pass filtered at 10 kHz. Compensation for the capacitance and series resistance of electrodes was done using the automatic features of the amplifier. The series resistance was compensated 65-80% with a 10 μsec lag. EPSCs are evoked by shocks through a Master-8 stimulator and Iso-flex isolator (AMPI, Jerusalem, Israel), are of various voltages from approximately 0.1-10V and delivered through an extracellular-saline-filled glass pipette (~10 μm tip). The stimulating pipette was approximately 50-100 μm away from the bushy cell being recorded from. Tissue was visualized with a Zeiss Axioskop 2 microscope with a 63x water immersion lens using a differential interference contrast microscope and infrared illumination. Analyses was performed using pCLAMP (Clampfit 9.0, Axon Instruments) and with Origin software. All quantifications are presented as means ± standard deviation from the mean.

Clustering Algorithms

Two assessments were made of the number of steps in the growth of shock-evoked EPSCs (eEPSCs) in bushy cells that are an estimate of the number of inputs and of the amount of current delivered per input. The number of steps was estimated by counting the number of jumps in the growth of the peak synaptic current (EPSC) as the shock strength was gradually increased. An estimate of the current delivered by a single input was made from the jump in amplitude between clusters. One count of inputs was made by eye and the second by a new, objective statistical clustering method.

A manual assessment was based on multiple rounds of analysis. Once the border between clusters was established, the smallest and largest currents from each cluster were averaged to obtain the mean current of the cluster and then the amounts of current per input were calculated.

The second method of quantifying number of steps is a customized statistical clustering method. The data analysis in this report is conducted by using R (R Core Team 2013). The quantification is conducted in the following two steps. First, for a set of n observations of individual sweeps of length T, the T×n matrix is factorized by singular value decomposition to find an efficient empirical orthogonal representation of the observations. By choosing the first principal component in the analysis, the overall pattern observed over n sweeps is characterized by the first principal component of length T, while each sweep is characterized by its weight parameter.

Once each sweep is characterized by its weight parameter, then the n parameters are analyzed by a normal mixture model. A normal mixture model is a probabilistic model that assumes the observations are from a mixture of multiple normal distributions. The expectation behind the normal mixture model is that when a distribution has multiple peaks, then we assume that the observations are from multiple normal distributions without labeling which they belong to. The parameters related to the distribution are estimated by using Expectation-Maximization algorithm (Dempster et al. 1977). The estimation of the

number of normal distributions is based on the Bayesian Information Criterion (Schwarz 1978). The Bayesian Information Criterion (BIC) is based on maximized log-likelihood with a penalty on the number of model parameters, where the larger the value of the BIC, the stronger evidence for the model (Fraley and Raftery 2002). Comparing the BIC for different numbers of normal distribution, the method can estimate the number of clusters. The probability of each sweep belonging to different clusters is simultaneously estimated.

Results

Distortion Product Otoacoustic Emissions and Auditory Brainstem Responses

An objective measure of the health of the cochlea in mice as well as in humans is provided by otoacoustic emissions (Avan et al. 2013). In the healthy cochlea, stimulation with pairs of tones produces distortion products that generate traveling waves which can be detected by a microphone in the ear canal as distortion product otoacoustic emissions (DPOAEs). Figure 1A shows recordings of DPOAEs produced by two tones, f_1 = 14,544 Hz, f_2 = 17,440 Hz, from a deaf juvenile mutant mouse. When those tones were presented at relatively low levels, the most prominent distortion product was at $2f_1$-f_2, 11,648 Hz (Fig. 1A, dp). At higher levels a second distortion product was evident at $3f_1$-$2f_2$, 8873 Hz (Fig. 1A, dp_2). Both distortion products disappeared when the animal was killed with an overdose of anesthetic (Figure 1B), indicating that they resulted from the interaction of the tones with a healthy cochlea. This pattern of responses was observed in all mice tested, including otoferlin KO, deaf mutant, heterozygous mutant, and wild type control mice. We conclude that hair cell function in the cochleae of homozygous mutants, KO, heterozygous mutant, and wild type animals are healthy and unaffected by the mutation.

Hearing of mice was further assessed with auditory brainstem responses (ABRs), measurements of electrical activity associated with the propagation of acoustic information through auditory nerve fibers to higher auditory centers. Adult ~P60 and juvenile ~P19-24 mice of each of the three genotypes associated with the *otoferlin* point mutation, Mut (n= 13), Het (n= 11), WT (n=12), and juvenile mice with the complete knock out of otoferlin (n=6) were tested. Figure 2A illustrates typical ABRs from each of the genotypes. All wild type and heterozygote animals responded to clicks with a small positive wave that was followed by larger positive and negative waves. Every homozygous mutant and knock out animal responded to clicks with only a small positive wave. It seems likely that the first small wave that we observe in both homozygous mutant and knock out animals reflects a cochlear microphonic response. The lack of electrical activity after the cochlear microphonic inflection in mice with mutant otoferlin and without otoferlin indicates that brain stem circuits are not activated by clicks, and mice that lack at least one normal *otoferlin* gene are thus deaf. Average thresholds of responses to clicks for hearing and deaf animals are summarized in Figure 2B. Thresholds in responses to pure tone stimuli are summarized in Figure 2C. These measurements indicate that mice with mutant or absent otoferlin are profoundly deaf.

The findings that cochlear function is normal in mutant and KO animals but that ABRs in these same animals are absent indicates that acoustic information is transduced but not transmitted from the cochlea to the brain stem. These findings are consistent with the conclusion from previous studies that otoferlin is required for synaptic transmission between hair cells and their spiral ganglion cell targets (Beurg et al. 2010).

Volume of the Cochlear Nuclei

Having noted that the cochlear nuclei seemed smaller in the mutants than in heterozygotes or wild type, we made measurements of the volumes of the VCN, DCN and of the granule cell areas. Figure 3A

shows a photomicrograph of a parasagittal section of the cochlear nuclei in which the DCN and VCN are outlined. The surface area of the outlined regions multiplied by the thickness of serial sections (60 μm) gave us volumes. Figure 3B shows average volumes from juvenile mice, of the DCN, and VCN (n=15), 5 from each of the three *otoferlin* mutation genotypes. The differences in the average volume of the DCN between hearing and deaf phenotypes were not statistically significant (0.15 ± 0.03 mm^3 in deaf mutants relative to 0.18 ± 0.03 mm^3 in hearing wild type). However, the volumes of the VCN were significantly ($p<0.001$) smaller in the deaf mutants, 0.19 ± 0.03 mm^3, than in hearing mice, 0.35 ± 0.04 mm^3.

End bulbs of Held

Many features of the projection of auditory nerve fibers to the cochlear nuclei appear normal in mutant mice relative to hearing controls. Injections of biocytin into the nerve root and along dorsal-ventral axis of the posterior ventral cochlear nucleus (pVCN) labeled bundles of auditory nerve fibers that innervate the VCN and DCN topographically as demonstrated previously in other strains of mice (data not shown). Labeled fibers that bifurcated ventrally in the nerve root innervated the ventral aVCN and ventral pVCN; fibers that bifurcated dorsally in the nerve root, innervated the dorsal aVCN and dorsal pVCN (Wickesberg and Oertel 1988; Cao et al. 2008). Also as in other strains, ANFs in mutant mice terminated in endings of variable size in the multipolar cell area and in uniformly small boutons in the octopus cell area. In the aVCN where most neurons are bushy cells, auditory nerve fibers end in clusters of boutons that wrap the somas of their targets, end bulbs of Held (Held 1893). Some synaptic terminals of ANFs in the aVCN are conventional terminal boutons.

The morphology of end bulbs of Held differs in hearing and deaf mice. Figure 4A shows end bulbs from hearing mice. These end bulbs are clusters of boutons connected to finger-like projections that encompass the target bushy cell soma. We found that the mutant mice had fewer end bulbs compared

to their hearing controls, which is not surprising when the volume of the VCN was reduced. Figure 4B shows end bulbs from deaf mutant mice. These end bulbs are thinner and more wispy than those of hearing controls. The number of branches per end bulb was counted from 144 end bulbs from hearing mice and 72 in deaf mutant mice; the number of branches per end bulbs in hearing mice was significantly greater in deaf mutant mice. The mean number of branches in hearing mice was 13.7 ± 4.1 compared to 11.2 ± 4 in deaf mice ($p =<0.001$). Our finding that deaf, mutant mice have more wispy end bulbs, is consistent with the work of others that shows that deafness *per se* can affect the sizes and shapes of end bulbs but it does not eliminate them (Ryugo et al. 1997; Redd et al. 2000; Cao et al. 2008).

In order to understand not only the end bulb but also the axon of the ANF leading to the end bulb we made *camera lucida* reconstructions of end bulbs and of the segment of axon between the final branch point of ANF and the end bulb. Figure 5 shows five reconstructions of end bulbs and their axons from each phenotype. The reconstructions show that the axons that lead to the end bulbs of hearing mice (Fig. 5A) were thicker than those of deaf mutant mice (Fig. 5B). Measurements of the thickness of axons near the end bulbs show that the axons in hearing animals (1.36 ± 0.3 μm, n=10) are significantly thicker than the axons of ANFs from deaf mutant animals (0.93 ± 0.31 μm, n=5) ($p=<0.001$).

Intrinsic electrical properties of bushy cells

Bushy cells from deaf mutant mice have biophysical properties that are largely indistinguishable from those in hearing controls as assessed by whole-cell patch recordings. Figure 6A illustrates responses to depolarizing and hyperpolarizing current pulses (Fig. 6B), in a bushy cell from a deaf mutant mouse. As in control hearing mice and in mice of other strains, bushy cells fired one or two action potentials at the onset of the depolarizing current injection and showed rectification (Oertel 1983; Cao et al. 2007). Quantification of the input resistance in bushy cells, based on responses to +10 and -10 pA current pulses,

reveals that there is no significant difference between the phenotypes (Fig. 6C); bushy cells in hearing mice had input resistances of 83.7 ± 32.6 MΩ (n=32), while the input resistances of bushy cells from deaf mutant mice was 96.1 ± 39.1 MΩ (n=27). The resting membrane potentials, too, were not different in hearing and deaf mutant mice (Fig. 6D). The bushy cells in hearing animals rested at -66.8 ± 5.0 mV (n=32) while those in bushy cells from deaf mice rested at 65.9 ± 5.1 mV (n=27).

There was however a significant difference in the rate of depolarization thresholds between bushy cells of hearing and deaf mice. Bushy cells detect the synchronous firing of ANFs; their sensitivity to rate of depolarization is an intrinsic property that is associated with the time window over which spatial summation occurs (McGinley and Oertel 2006). Bushy cells are more likely to fire action potentials when multiple ANFs are activated synchronously and when EPSPs have a steeper slope of depolarization. To measure the threshold rate of depolarization, current pulses with systematically varied ramped onsets that rose to a constant value (Fig. 6G) were presented to bushy cells (Fig. 6F). The slope of depolarization that was just steep enough to cause a bushy cell to fire was defined as the threshold rate of depolarization (Fig. 6F, dark traces). Bushy cells from hearing mice needed to be depolarized on average at least 2.21 ± 0.66 mV/msec to fire action potentials, while those in deaf animals needed to be depolarized on average at least 1.66 ± 0.54 mV/msec to fire action potentials. Bushy cells from deaf mutant mice fire action potentials in response to less steeply rising depolarizations than bushy cells from hearing mice ($p = 0.002$), indicating that their requirements for synchronicity are less stringent than those of bushy cells from mice that hear (Fig. 6E).

Spontaneous EPSCs

We first compared the spontaneous miniature EPSCs (mEPSCs) in bushy cells from mice with differing phenotype and genotypes. Example recordings of spontaneous postsynaptic currents in eleven

overlaid sweeps in representative bushy cells from hearing and deaf mice are displayed in Figures 7A and B respectively. The averaged miniature events in these same bushy cells from hearing and deaf mice are exhibited in Figures 7C and D. To facilitate comparisons, some features of mEPSCs were measured (Figs. 7 E-J, Table 1). The frequency, amplitude, charge, half-width, 10-90% rise time and 100-37% decay tau were quantified. Of these measures, only the average amplitude and charge transferred in each mEPSC was significantly greater in bushy cells of deaf than hearing mice (Fig. 9F and G; Table 1). The average amplitude of mEPSCs in hearing animals was -88 pA, compared with -109 pA in bushy cells of deaf mutant mice. The average charge transferred by a mEPSC in bushy cells of hearing mice was 27 femtocoul compared to 35 femtocoul in deaf mice. The shapes of mEPSCs, described by their half-width, 10-90% rise time, and decay time constants, were not significantly different in hearing and deaf mice (Fig. 9E, H-J; Table 1). In summary, mEPSCs were larger in deaf mice than in hearing controls but their shapes were similar.

Electrically evoked EPSPs

Next we compared how bushy cells respond to activation of their auditory nerve inputs. By placing an extracellular stimulating electrode on a bundle of ANFs near to a bushy cell that was being monitored in a whole-cell patch-clamp recording, in current-clamp and gradually increasing the strength of shocks delivered through the stimulating pipette, we evoked EPSPs that grew in clustered steps (Fig. 8A and B). Since ANFs fire all-or-none action potentials, the steps likely represent the recruitment of fibers that converge on the recorded bushy cell; the counts of the numbers of clusters are thus estimates of the numbers of auditory nerve inputs. We interpret these recordings as showing that both cells have at least two inputs. Most EPSPs in bushy cells from both hearing and deaf mutant mice are suprathreshold. For example, in Figures 8A and B even responses to the weaker shock strengths showed an inflection

(arrows) indicative of electrically active processes. Responses to strong shocks rise more rapidly and reach a higher peak than responses to smaller shocks. When the recording mode was switched to voltage-clamp, electrically evoked EPSCs were recorded in the same cells (Fig. 8C and D). The number of current jumps resolved in the voltage-clamp recordings matched the number of clusters measured in current-clamp recordings, generally. In ~35% of the 45 cells tested, the number of inputs estimated in voltage and current clamp matched. In ~20% of the recordings one extra step appeared in EPSPs, likely because small current jumps were obscured by variability in EPSCs. However, in ~45% of cells the number of steps could not be well resolved in current clamp because direct spiking in the bushy cell occluded the synaptic delay. For this reason, the analysis of differences in synaptic transmission between hearing and deaf animals was done under voltage-clamp.

Electrically evoked EPSCs

We quantified evoked synaptic transmission from end bulbs to bushy cells in hearing and deaf, mutant mice from recordings in voltage clamp. By placing an extracellular stimulating electrode on a bundle of ANFs near to a bushy cell that was being monitored with a whole-cell patch-clamp recording and gradually increasing the strength of shocks delivered through the stimulating pipette, we evoked EPSCs (eEPSCs), that grew in steps (Fig. 9A, B). Shocks were delivered slowly, at 10-15 second intervals, to minimize synaptic depression. As ANFs fire all-or-none action potentials, we interpret each jump in current to represent the bringing to threshold of at least one additional ANF that contacted the bushy cell. The total number of steps is thus an estimate of the number of ANFs that converge on the recorded bushy cell (Cao and Oertel 2010). Many of the current steps are large and likely reflect currents delivered through end bulbs of Held. Figures 9 A, B show four examples of eEPSCs, two cells each from hearing and deaf phenotypes. Figure 9A shows responses from two different bushy cells from hearing,

heterozygote mice whose eEPSC jumped in a single step to a peak of approximately 11 nA; we thus estimate that this bushy cell had a single ANF input. The second example of an eEPSC in a hearing mouse illustrated below grew in two steps, one of 1 nA and the second of 6 nA for a total cumulative current delivered to the cell of about 7 nA (Fig. 9A bottom); we conclude that this bushy cell had at least two inputs. Figure 9B illustrates eEPSCs in bushy cells from two different deaf mutant mice. The top panel illustrates eEPSCs grew in two current steps, one of approximately 10 nA and another of approximately 23 nA, for a peak synaptic current of 33 nA; this cell was likely contacted by at least two end bulbs. Figure 9B bottom, shows a second recording in a bushy cell from a deaf mutant mouse whose eEPSCs grew in three jumps, presumably from the recruitment of three ANFs, which delivered 5 nA, 7 nA, and 6 nA, for a total synaptic current of approximately 18 nA. The variability in the sizes and shapes of eEPSCs presumably results from the stochastic nature of release of neurotransmitter. Because it is possible that multiple fibers have a similar threshold, or that some inputs are not stimulated, or that small inputs are not resolvable when synaptic currents are variable, our estimates of numbers of inputs err on the low side.

Comparisons of eEPSCs in hearing and deaf mice are illustrated in Figures 9 C-E and summarized in Table 2. In Figures 9 C-E, the first assessment of the clustering in synaptic current jumps was determined by eye. The size of a current step was calculated by averaging the amplitudes of the smallest and largest current responses in a cluster. Figure 9C shows that average maximal eEPSCs were significantly larger in bushy cells of deaf than of hearing mice. In hearing mice the average maximal eEPSCs were ~7 nA whereas they were ~13 nA in deaf mice (Table 2). In addition, bushy cells in deaf mice had significantly larger average number of inputs or current jumps than bushy cells in hearing mutant mice (Fig. 9D, Table 2). Bushy cells of hearing mice had on average ~2.1 inputs compared with ~2.7 inputs in deaf mutant mice. The difference between the averaged currents delivered per step in

bushy cells, ~3.3 nA in bushy cells of hearing mice compared to ~4.8 nA in bushy cells of deaf mutant mice, approached but did not reach statistical significance (p=0.06) (Fig. 9E and Table 2).

Because there is considerable physiological variability in the amplitudes of eEPSCs and thus possibly unequal variance in the magnitudes of the eEPSCs we took the natural logarithm of each of the amplitudes of the maximum eEPSCs and also of the estimates of current per input based on count of inputs, and re-ran the ANOVA test using the $\log_e$ numbers (Figs. 9F, G, Table 2). In the resulting statistical test, the maximal eEPSCs remained significantly different between the hearing and deaf phenotypes, and we also found the difference between average current per input to reach statistical significance between the hearing and deaf mice, with the bushy cells from deaf mice again having larger individual eEPSCs per input (Figs. 9F, G, Table 2).

For comparing the number of steps with which eEPSCs grew between phenotypes, it was inappropriate to take the logarithm (O'Hara and Kotze 2010). As an alternative, secondary check to the input count made by the experimenter's eye and experience; a rigorous statistical test was conducted based on permutations (Ernst 2004). The statistical significance was calculated as the fraction of permutation values that are at least as extreme as the test statistic derived from the original data. Using this test with 10,000 permutations, the mean number of current steps in eEPSCs and as such number of inputs, was statistically significantly larger in deaf mutant mice than in hearing controls (p=0.01).

A potential difficulty with the analysis described above is that it depends on an assessment of clustering by the investigator. Cellular responses differed in the clarity of the clustering. We therefore developed a novel objective clustering algorithm with which the investigator's estimate of the number of steps could be compared. The custom clustering algorithm is based on singular value decomposition to find an efficient yet comprehensive representation of the data. To quantify the current delivered per input, determination of the number of inputs must be made first. Table 2 has all of the results from the

clustering algorithm in comparison to the experimenter's assessment. In order to determine how many inputs innervate each bushy cell the clustering algorithm was run on all recordings. A nonparametric permutation was used to quantify inputs between the phenotypes. Throughout, two-sided t-tests were used to assess statistical significance unless otherwise noted (Table 2).

The results of the clustering algorithm parallel the experimenter's assessment; the number of inputs innervating bushy cells in deaf mice was significantly larger than in the hearing mice. The results did vary slightly such that the clustering algorithm often resulted in slightly fewer input counts than the experimenter quantified (Table 2). Figures 10A and B show recordings from two bushy cells in different deaf mutant mice whose clustering is not absolutely clear. The clustering algorithm shows that eEPSCs in the bushy cell illustrated in Figure 10A grew in two steps, each identified by a different color. The EPSCs in Figure 10B grew in three current steps. An additional inference available from this quantification method regarding sample size can be made using simulations. Approximately 25 samples will be enough to achieve the 95% statistical power at significance level 0.05, which provides a justification of our sample sizes (n=27 and n=29 samples per phenotype).

After an input count was assessed the maximal evoked currents and current per input can be quantified, again by averaging the amplitude of the smallest and largest sweeps from each cluster of inputs. Figures 10 C and D show the distribution of maximal evoked synaptic currents and current per input per phenotype, respectively. For assessment of mean current per input, in order to take into account of the unequal number of inputs between phenotypes (74 in the deaf and 53 in the hearing), a weighted least squares method is used. The averages calculated from more observations have low variability and hence get a higher weight (Faraway 2005). Table 2 illustrates the results based on a one-sided t-test with the alternative of the deaf having greater mean current per input.

Quantal Content Estimates

Having assessed the average amount of charge delivered per by mEPSCs from each cell and also the average current delivered from eEPSCs in response to graded extracellular stimulation, estimates of the quantal content can be made (Table 3). In order to do so the charge delivered per spontaneous mEPSC was averaged for each cell and then the charge delivered by each evoked input from each cell was divided by the charge for that cells averaged mEPSC. These resulting estimates of quantal content of steps of eEPSCs were then compared between cells from hearing and deaf animals. There was considerable variation between estimated quantal content of steps, ranging between 3 and 532 quanta; there was not a significant difference between the numbers of quanta released per input in bushy cells from hearing and deaf animals (Table 3). Because of the large physiological variability, the natural logarithm of each of the estimates of quantal content was taken and also tested for statistical significance. In this analysis, too, there was no significant difference in quantal content of inputs between the hearing and deaf phenotypes (Table 3). Since the amplitude of current steps, estimates of the current delivered by one auditory nerve input, was larger in deaf than hearing animals but quantal content was not significantly different, the larger amplitude of EPSCs in deaf animals most likely arose from the upregulation of AMPA receptors at postsynaptic sites in the bushy cells of deaf mutant mice.

Synaptic depression

In order to assess synaptic depression, trains of eEPSCs were recorded from bushy cells in deaf mutant mice and their heterozygote and wild type controls. Five trains, each comprising ten shocks at 100/sec, that produced eEPSCs of maximal amplitude, were delivered five seconds apart, and were then averaged for statistical analysis. Figures 11 A and B show examples of synaptic depression in two hearing mice. Successive eEPSCs generally become smaller than the one before even in hearing animals

but bushy cells from deaf mutant mice show stronger depression and occasional failures (Fig. 11C). The cell shown in Figure 11D shows an unusual pattern in that the magnitudes of eEPSCs are highly variable with intermixed large and small responses. The cell illustrated in Figure 11E shows that some shocks can fail to evoke any response at all. Multiple synaptic failures were seen in 7 of the 19 (37%) bushy cells from deaf mutant mice in which responses to trains of stimuli were recorded. Failures were rare in hearing mice; one synaptic failure was recorded in one heterozygous animal out of 18 bushy cells tested in hearing mice (6%). The paired-pulse ratio (PPR), the amplitude of the second eEPSC divided by the magnitude of the first eEPSC from trains of stimuli, is significantly smaller in deaf mutant cells ($p=0.03$) compared to the hearing controls. The PPR from bushy cells in hearing mice was 0.65 ± 0.20 compared to 0.48 ± 0.25 in deaf mice. A larger PPR ratio is indicative of less synaptic depression and a lower probability of release. We also assessed synaptic depression by taking the average of each of the ten eEPSCs (Figs. 11 G and H) and plotting a time course of depression. The size of EPSCs decays faster in cells from deaf mutant mice than in cells from hearing mice.

Discussion

Otoferlin serves as the major calcium sensor that regulates synaptic transmission between hair cells and their spiral ganglion cell targets. Hair cells in mice that express a non-functional otoferlin or that lack otoferlin transduce sound but are largely unable to release neurotransmitter to activate their auditory nerve targets after P3 (Beurg et al. 2010). Indeed, we find that DPOAEs which assay the function of the cochlea, especially the outer hair cells, are normal in mice with mutant otoferlin and also in mice that lack otoferlin. On the other hand, these same mice have no detectable ABRs, indicating that sensory information from the cochlea fails to be transmitted to the auditory nerve and to brain stem auditory circuits and that these animals are therefore profoundly deaf. Acoustically, there were no

detectable differences between mice in which otoferlin had a point mutation in the second calcium binding domain and those in which the gene for otoferlin was knocked out. Mice that lack functional otoferlin are profoundly deaf.

The absence of synaptic input from early in life affects downstream neuronal circuits. In deaf mutant animals the VCNs are shrunk by nearly half. In deaf otoferlin mutant mice ANFs innervate the cochlear nuclei topographically as in hearing mice but at least some of the endings, the end bulbs of Held that innervate bushy cells, are smaller. Bushy cells from deaf mutant mice receive converging inputs from more ANFs than the hearing controls. Bushy cells in deaf mutants receive input from about 2.6 ANFs while hearing mice receive input from only about 2. And although the terminals of ANFs on bushy cells are smaller in deaf mutant mice than in controls, the synaptic currents each one evokes are larger, about 4.8 nA compared to 3.4 nA in hearing mice. We have evidence for both pre and postsynaptic adaptations of synapses between ANF and bushy cells. As the quantal content is not significantly different in deaf mutants and hearing controls, the increase in synaptic current can be accounted for by in increase in the number of AMPA receptors at synapses of bushy cells, a postsynaptic adaptation. The finding that synapses in bushy cells of deaf mutant mice depress more rapidly and fail far more often indicates that there are presynaptic changes too. Synaptic depression is likely to result from depletion of neurotransmitter presynaptically. The existence of failures suggests that presynaptic fibers may also suffer from conduction block.

Identity of bushy cells

Bushy cells of mammals fall into three distinct types, large spherical, small spherical and globular, that differ not only in histological staining patterns but also, most importantly, in their projection patterns (Osen 1969; Brawer and Morest 1975; Cant and Casseday 1986; Tolbert et al. 1982).

Large spherical bushy cells encode low frequencies, occupy the most anterior pole of the aVCN, and project to the medial superior olivary nuclei bilaterally (Smith et al. 1993). Mice have little low-frequency hearing and correspondingly have few large spherical bushy cells and small medial superior olivary nuclei (Webster and Trune 1982; Willard and Ryugo 1983). While the sizes of large and small spherical bushy cells clearly differ in cats (Osen 1969), they are not obviously different in many other mammals such as mice and guinea pigs for example (Willard and Ryugo 1983; Hackney et al. 1990). Small spherical bushy cells occupy most of the rostral aVCN of mice. They are thought to project to the ipsilateral lateral superior olive (Cant and Casseday 1986). Globular bushy cells are most common in the more posterior aVCN, near the nerve root (Tolbert et al. 1982; Tolbert and Morest 1982a; Tolbert and Morest 1982b). They project across the midline to the contralateral medial nucleus of the trapezoid body (Smith et al. 1991).

Recordings in the present study were made from the anterior aVCN and thus are probably mostly or exclusively from small spherical bushy cells. In hearing mice small spherical and globular bushy cells have been distinguished electrophysiologically by the numbers of auditory nerve inputs, small spherical bushy cells having four or fewer inputs and globular bushy cells having more than four inputs (Cao et al. 2007). Recordings included for analysis in this project were from bushy cells from both hearing and deaf mutant mice that had four or fewer inputs. We did encounter eEPSC recordings from bushy cells which had more than 4 steps in current, that also had smaller current jumps compared to the larger current jumps from cells with <4 steps, we interpreted these to be from GBCs and they were excluded from this analysis. We conclude, therefore, that our recordings were largely or exclusively from small spherical bushy cells.

The bushy cells in deaf otoferlin mutant mice have similar resting potentials and input resistances but they differ in their sensitivity to rate of depolarization relative to hearing control mice. Bushy cells have a threshold rate of depolarization such that depolarizations that are slower than the threshold rate do

not evoke firing (McGinley and Oertel 2006). The deaf otoferlin mutant mice have lower thresholds than hearing mice. These findings imply that smaller, slower or less synchronous EPSPs can lead to firing in deaf mutants relative to hearing controls.

Sources of excitation in bushy cells

Bushy cells receive excitatory input from ANFs through large synaptic terminals, the end bulbs of Held (Held 1893; Cant and Morest 1979; Sento and Ryugo 1989; Ryugo and Sento 1991; Spirou et al. 2005; Lauer et al. 2013). Ultrastructurally it has been shown that synaptic terminals with characteristics of excitatory synapses are of only two or possibly three types (Cant and Morest 1979; Gomez-Nieto and Rubio 2009; Gomez-Nieto and Rubio 2011; Lauer et al. 2013). In mice all glutamatergic synaptic contacts on somas and dendrites contain large round vesicles and arise from the auditory nerve (Lauer et al. 2013). Terminals with small round vesicles could be cholinergic, serotonergic, or nor-adrenergic inputs (Sherriff and Henderson 1994; Motts et al. 2008; Thompson et al. 1995; Klepper and Herbert 1991).

It has also been suggested on the basis of ultrastructural studies that bushy cells cluster and are electrically coupled to other bushy cells (Gomez-Nieto and Rubio 2009; Gomez-Nieto and Rubio 2011). What the functional consequences are of those gap junctions is not known. When labeled with biocytin, labeling has not been reported to spread between bushy cells (Cao et al. 2007). If the coupling were weak, shocks might evoke small inputs through adjacent cells; if coupling were strong, it would be difficult to distinguish direct inputs to the recorded cell from inputs to coupled neighbors. The small total number of inputs detected in bushy cells in our experiments would suggest that coupled bushy cells, together, receive input from only few inputs.

Deafness and loss of volume in the VCN

In young animals cochlear ablation leads to apoptosis or shrinkage of cochlear nuclear neurons, to changes in patterns of Nissl staining, protein synthesis, proliferation of glial cells and processes, and axonal sprouting; cochlear ablation in older animals generally produce less drastic changes (Powell and Erulkar 1962; Wenthold and Gulley 1977; Trune 1982a; Trune 1982b; Steward and Rubel 1985; Moore and Kowalchuk 1988; Rubel and MacDonald 1992; Lustig et al. 1994; Tierney et al. 1997; Mostafapour et al. 2000; Harris and Rubel 2006; Meidinger et al. 2006). The consequences of cochlear ablation vary as a function of the age at cochlear ablation, being more drastic when cochleae are ablated in younger than in older animals. Cochlear ablations are artificial manipulations that differ from physiological deafness in that it destroys spiral ganglion cells and causes complete degeneration of the auditory nerve.

It is not the absence of spiral ganglion neurons *per se* but rather the lack of electrical activity in the circuitry of the VCN that causes it to shrink. Deafness caused by the failure of transduction by hair cells genetically or pharmacologically or from a conductive hearing loss leaves spiral ganglion neurons intact but deprived of sensory input from the onset of hearing. The *deafness* mouse (*dn/dn*) which has a mutation in TMC1 and the *jerker* mouse (*je/je*) which lacks espin (Sekerkova et al. 2011) have shrunken VCNs (Webster 1985; Cao et al. 2008). Normally hearing mice that are deprived of hearing, too, have shrunken neurons (Evans et al. 1983). Here the otoferlin point mutants reveal the importance of calcium induced exocytosis from the IHCs of the cochlea before and after hearing onset. With even severe cochlear ablations, we see an almost parallel significant reduction in VCN volume, with a 55% reduction in the deaf otoferlin point mutant mice, having lost prehearing patterned spontaneous activity after P4 compared to hearing controls, versus an almost 60% reduction in VCN volume with total cochlear ablations in mice at P5 (Mostafapour et al. 2000). This result speaks volumes for the importance of

prehearing patterned spontaneous activity, because without it there is almost equal principal neuronal volume loss in the VCN between these two methodologies. Since the DCN receives somatosensory innervation, significant volume reductions were not expected in the DCN from deafness.

The size and appearance of neurons in the VCN of mice are also altered by a conductive hearing loss (Trune and Morgan 1988) and by blocking action potentials in the auditory nerve with tetrodotoxin (Pasic and Rubel 1989). Adult *deafness* mice (*dn/dn*), mice which cannot transduce sound and which have degenerated organs of Corti but which still retain 23% of spiral ganglion neurons (SGNs) that have been shown to have no spontaneous activity (Youssoufian et al. 2005), have shrunken VCNs whose volumes that were reduced 37% (Webster 1985). Deaf otoferlin mutant mice showed a reduction in volume of the VCN that was 55%. The larger loss of volume in otoferlin mutant mice could be a consequence of having not just posthearing but also prehearing deficits in electrical activity but it is impossible to exclude the possibility that differences in numbers reflect differences in ages and strains of mice measured.

End Bulb Morphology

We show that otoferlin mutant mice have thin axons that terminate in wispy end bulbs compared to the large, almost hand-like terminals that encompass the bushy cell soma in the hearing mice. The differences are reminiscent of the findings in cats by Ryugo and colleagues (Ryugo et al. 1997; Redd et al. 2000). *Camera lucida* reconstructions and measurements of the segment of axon of ANFs that leads up to the end bulbs, is significantly thinner in deaf otoferlin mutants than in hearing controls.

Deaf white cats have a form of non-syndromic, congenital deafness that mimics the Scheibe deformity in humans, characterized by degeneration of the organ of Corti early in life; with some spiral

ganglion atrophy as well (Heid et al. 1998). End bulbs from deaf white cats that never hear have withered end bulb morphologies that cover less of the target soma with smaller networks of filamentous processes (Ryugo et al. 1997; Redd et al. 2000). The authors report that the normally hearing cats have approximately double the synaptic area per end bulb as deaf white cats. Synapses of hearing cats have round, clear synaptic vesicles, and small, round or oval postsynaptic densities along the bushy cell membrane, typically protruding in a convex manner into the end bulb active zone. The end bulbs of deaf white cats varied in synaptic vesicle densities and postsynaptic densities were unusually long and thick and did not form convex bulges into the active zone of the end bulb.

Synaptic Transmission

The spontaneous mEPSCs in the deaf mutants are larger in amplitude and they carry more charge than mEPSCs in hearing controls. Our finding suggests more AMPA receptors in deaf otoferlin mutant mice are activated by the contents of one synaptic vesicle. AMPA receptors in bushy cells are composed of GluA3 and 4 isoforms as flop splice variants (Wang et al. 1998; Gardner et al. 2001). Knocking out GluA4, but not GluA3, dramatically affects synaptic transmission in targets of bushy cells and that GluA2 can substitute for GluA3 but not for GluA4 (Yang et al. 2011).

As measured by trains of stimulation, the probability of release is increased from end bulbs in deaf mutant mice. A lower PPR as found in the deaf mice is indicative of a higher probability of release; as well we found that the time constant of decay for synaptic depression from trains was much shorter in the deaf mutants. Both of these measures indicate a possible adaptive mechanism to increase the potential for releasing glutamate and thus activating bushy cells in a supra-threshold manner to preserve their activation and maintain stimulation in the rest of the auditory pathway in deaf mice.

From mature mice an additional investigation of probability of release from the end bulb reveals that the end bulb has a high release probability and that synaptic depression decreases as animals mature (Wang and Manis 2008). Depression of AMPA and NMDA receptors has two phases of recovery; the fast component of AMPA receptors is likely from desensitization while the fast component from NMDA receptors is likely from saturation, while the slow component is probably presynaptic in origin (Yang and Xu-Friedman 2008). Dynamic clamp experiments revealed that increasing synaptic depression of the end bulb leads to lower probability of bushy cells spiking (Yang and Xu-Friedman 2009). From these data we can see that even in hearing animals the end bulb bushy cell interface is adaptive in the face of various intensities of stimulation.

Concluding Remarks

The cellular adaptations presented here are likely to reflect mechanisms of homeostatic plasticity. Homeostatic plasticity causes neurons to modify their biophysical properties in response to synaptic activation. Regulation of ion channels, number and type of neurotransmitter receptors and modulation of neurotransmitter release, is matched to levels of activity to preserve optimal levels of neuronal activation (Shah et al. 2010; Turrigiano 1999).

Table 1. Spontaneous mEPSCs

smEPSCs	Amplitude (pA)	Charge (femtocoul)	Frequency (per sec)	Half-width (msec)	10-90% Rise Time (msec)	100-37% Decay Tau (msec)
Average Hearing	88.2±38.0 (n=35)	26.9±8.3 (n=35)	58.9±42.5 (n=35)	0.27±0.1 (n=35)	0.13±0.04 (n=35)	0.2±0.1 (n=33)
Average Deaf	108.7±29.7 (n=31)	34.9±8.6 (n=31)	62.1±90.1 (n=31)	0.26±0.1 (n=31)	0.15±0.16 (n=31)	0.24±0.1 (n=31)
p-value	p=0.02	p=0.0003	p=0.8	p=0.6	p=0.6	p=0.2

Table 2. Evoked EPSCs

Eye Count	Number of Inputs	Current per Input (nA)	Maximum Current (nA)	**Statistical Clustering Algorithm**	Number of Inputs	Current per Input (nA)	Maximum Current (nA)
Statistical Test	ANOVA	ANOVA	ANOVA	**Statistical Test**	Permutation Test	2 sample t-test	2 sample t-test
Average Hearing	2.11 ± 0.97 (n=27)	3.33 ± 3.70 (n=57)	7.03 ± 6.29 (n=27)	**Average Hearing**	1.96±0.81 (n=27)	3.49±4.08 (n=53)	6.81±5.83 (n=27)
Average Deaf	2.68 ± 0.89 (n=29)	4.77 ± 4.95 (n=78)	12.81 ± 9.91 (n=29)	**Average Deaf**	2.55±0.87 (n=29)	4.92±5.13 (n=74)	12.55±9.46 (n=29)
p value	p=0.02	p=0.06	p=0.01	**p value**	p=0.009	p=0.09	p=0.009
Statistical Test		ANOVA Ln of values	ANOVA Ln of values	**Statistical Test**		Weighted Least Square of Ln values	2 sample t-test of Ln values
Ln Average Deaf		7.98±1.1	9.17±0.81	**Ln Average Deaf**		7.97±1.16	9.16±0.79
p value		p=0.02	p=0.004	**p value**		p=0.03	p=0.002

Table 3. Quantal Content

Quantal Content			Statistical test
n	Hear=57 inputs from 27 bushy cells	Deaf=78 inputs from 29 bushy cells	ANOVA
Mean vesicles per input	Hearing 72.28±78.0	Deaf 97.87±99.09	p-value p=0.1
Natural log of vesicles per input	Hearing 3.78±1.06	Deaf 4.12±1.0	p-value p=0.07

Figure 1

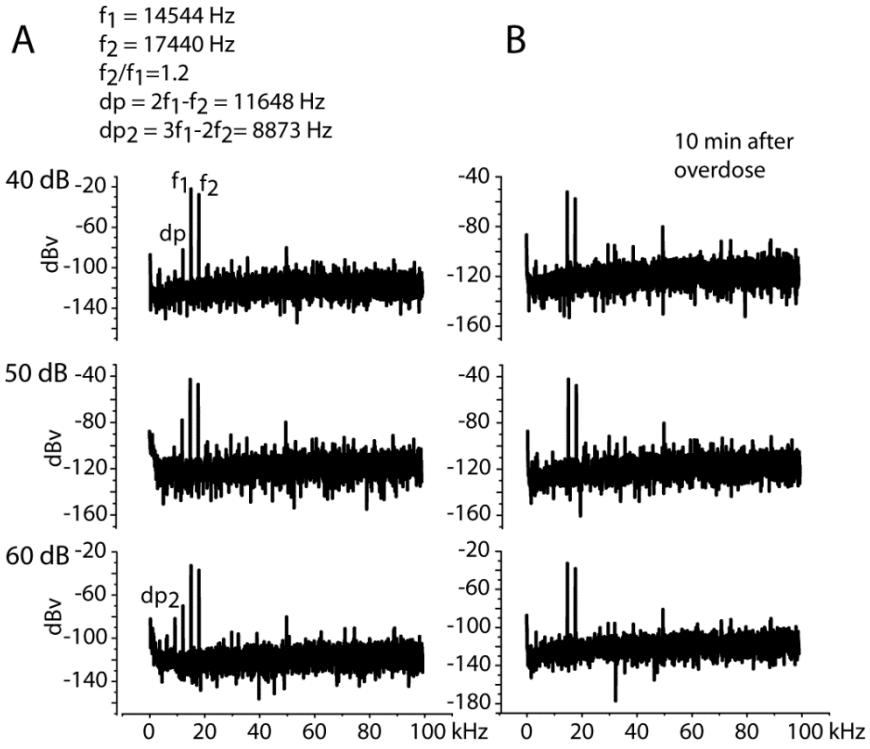

Figure 1 Distortion Product Otoacoustic Emissions

A) Two tones were delivered to one ear and the distortion products were measured at three different sound pressure levels, two distortion products were detected, 2f1-f2 (dp) and 3f1-2f2 (dp2).

B) The same animal was then lethally overdosed without moving the tone probes or microphone. Ten minutes later the same two tones were delivered but these resulted in no distortion products.

Figure 2

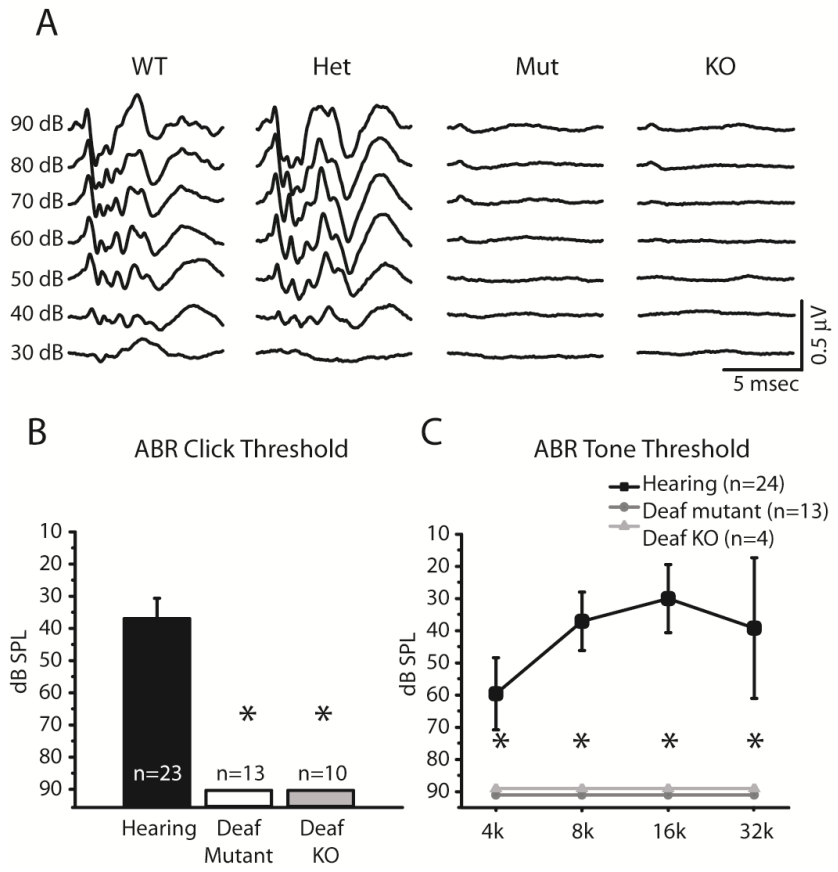

Figure 2 Auditory Brainstem Responses

A) Clicks, 0.1 msec and alternating in polarity, evoked a series of positive and negative waves that reflect the activity of neurons in the brain stem in the hearing genotypes, wild type (WT) and heterozygote (Het) otoferlin mutant mice. Those waves became smaller as the sound pressure levels were reduced; their disappearance was used to measure the threshold of hearing. The otoferlin mutant and knock out animals lacked all but a small positive-going wave in responses to the same acoustic stimuli. The brief inflection at the beginning of each trace is likely a remnant of the cochlear microphonic potential. The absence of electrical waves in the deaf mutant animal and full knock out animal indicate that acoustic signals fail to propagate through the circuits of the brain stem and shows that these animals are deaf.

B) The averaged hearing thresholds for the click stimuli are depicted in the histogram.

C) The hearing thresholds for the tone stimuli at 4 KHz, 8 KHz, 16 KHz and 32 KHz are represented graphically and show that wild type and heterozygote hearing controls hear best at about 16 kHz and that homozygous mutants and otoferlin KO do not hear at any frequency.

Figure 3

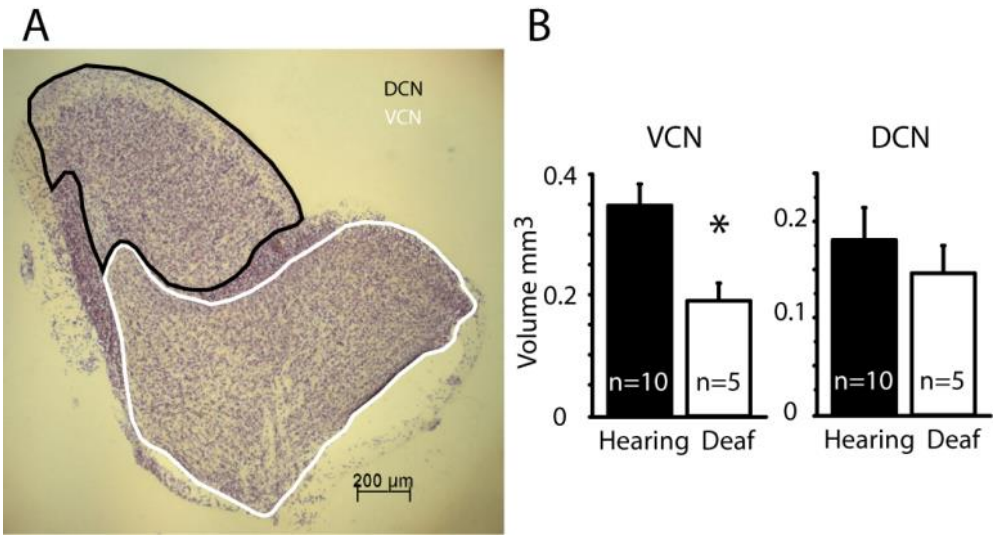

Figure 3 Volumes of Cochlear Nuclei

A) Photomicrograph of a parasagittal section, 60 µm thick, through the cochlear nucleus that had been stained with cresyl violet. The ventral cochlear nucleus (VCN) and dorsal cochlear nucleus (DCN) are outlined.

B) The areas were summed across serial sections and multiplied by 60 µm. Average volumes are shown in histograms illustrating the average volume difference of 5 mice from each otoferlin genotype. The volumes of the VCN were significantly different between the hearing and deaf phenotypes with a p-value < 0.001. The difference in the volumes of the DCN was not significant.

Figure 4

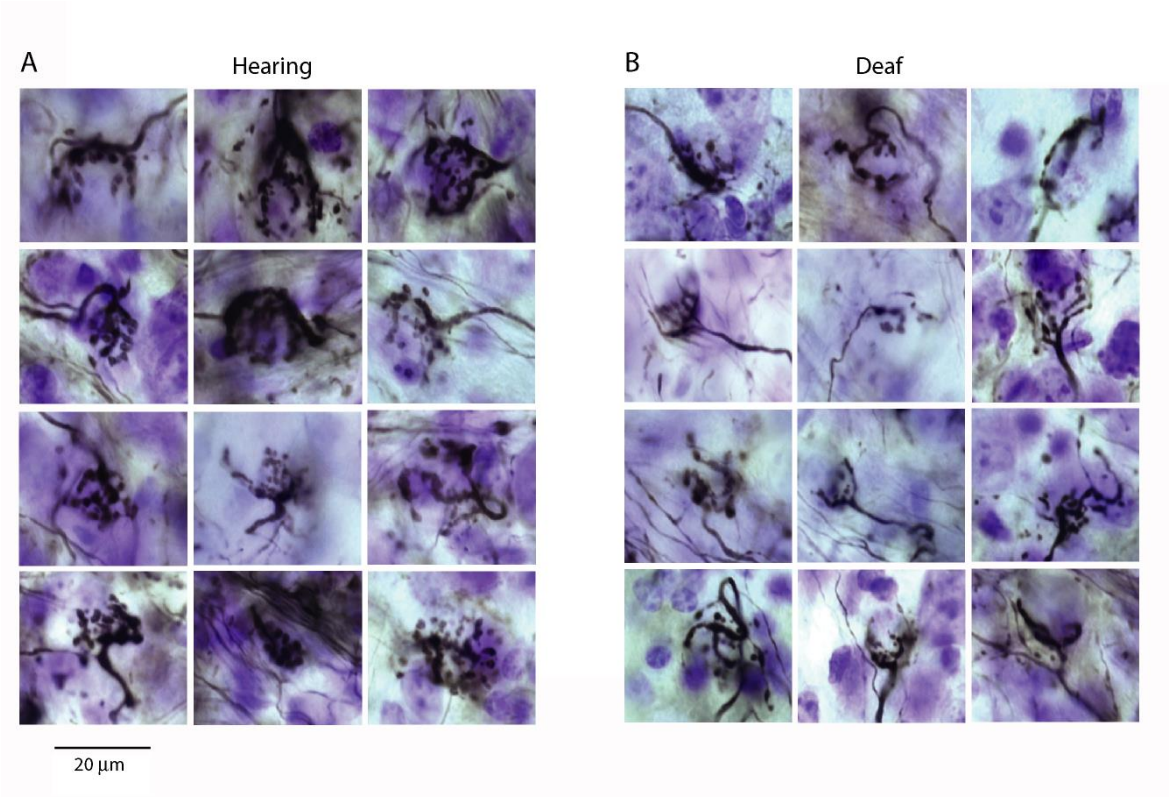

Figure 4 Auditory Nerve Fibers and their End Bulb Terminals
Photomicrographs of end bulbs labeled with extracellular injections of 1% biocytin into either the nerve root or into the aVCN.
A) End bulbs from hearing mice comprise highly branched clusters of boutons that engulf the cell body of target bushy cells.
B) End bulbs from the deaf mice and the axons that lead to the end bulbs are smaller and thinner.

Figure 5

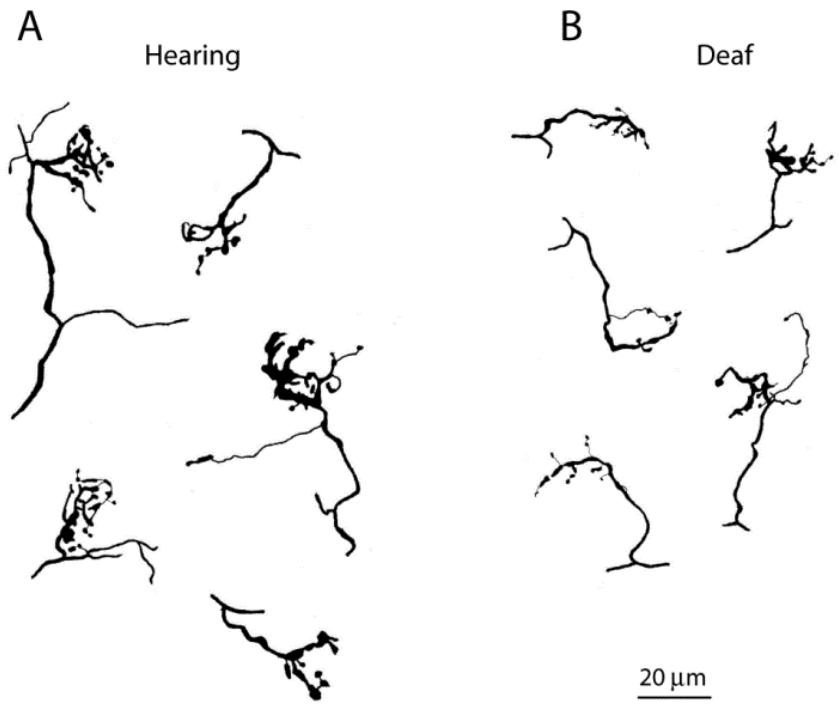

Figure 5 ***Camera Lucida*** **reconstructions of End Bulbs**
A) End bulbs were reconstructed to the branch of the parent auditory nerve fiber which illustrate the difference in the end bulbs of hearing and deaf animals
(B) Measurements of the thickness of axons near the end bulb show that axons are significantly thicker in the hearing compared to the deaf mice. In hearing mice axons were on average 1.36 ± 0.3 µm compared to 0.93 ± 0.31µm in deaf mutant mice. The values differ significantly ($p = 0.00003$).

Figure 6

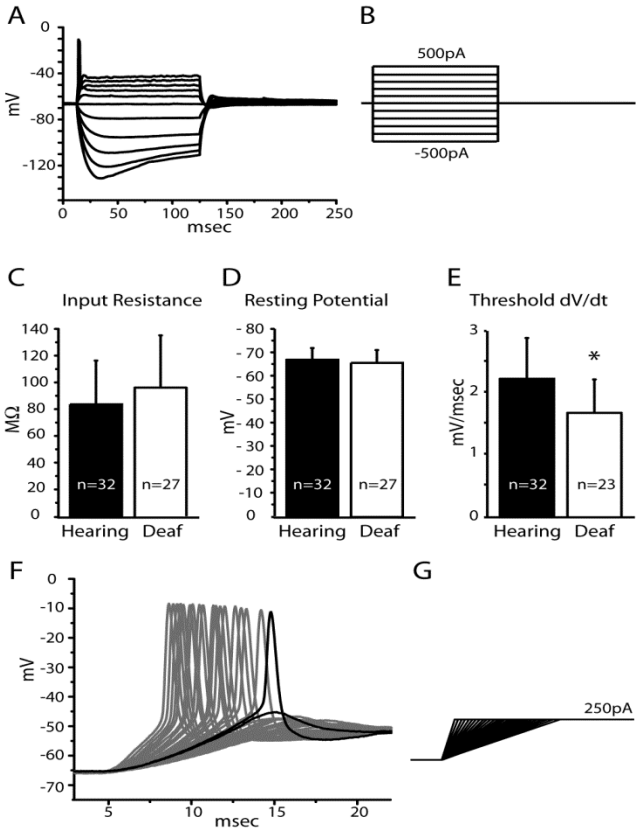

Figure 6 Intrinsic Properties of Bushy Cells

A) Current clamp recording of a bushy cell from a deaf otoferlin mutant mouse shows superimposed responses to current pulses of various amplitudes.

B) The depolarizing and hyperpolarizing current steps injected into the bushy cell illustrated in A.

C) The average input resistances from bushy cells in hearing and deaf mice calculated from responses to 10pA and -10 pA current steps were not significantly different between the bushy cells in hearing and deaf mutant mice. The mean input resistance from hearing mice was 83.7 ± 32.6 MΩ. The mean input resistance from deaf mice was 96.0 ± 39.0 MΩ.

D) The average resting membrane potentials in bushy cells was not significantly different between the hearing and deaf mice. Bushy cells from hearing mice sat at an average of -66.8 ± 5.0 mV and deaf mice rested at mean= -65.9 ± 5.1mV.

E) The rate-of-depolarization threshold was significantly lower in the bushy cells of deaf than those of hearing mice. The bushy cells from hearing mice require a significantly steeper depolarization to fire action potentials compared to bushy cells from deaf mice. The average depolarization threshold in hearing mice was 2.2 ± 0.7 mV/msec whereas in the deaf mice it was 1.7 ± 0.5 mV/msec ($p = 0.002$).

F) A representative current clamp recording from a hearing mouse illustrates how the rate-of-depolarization thresholds were measured. The black traces are the responses to the current ramp that were just suprathreshold and just subthreshold.

G) The ramped depolarizing current pulses that were injected into the bushy cell in F.

Figure 7

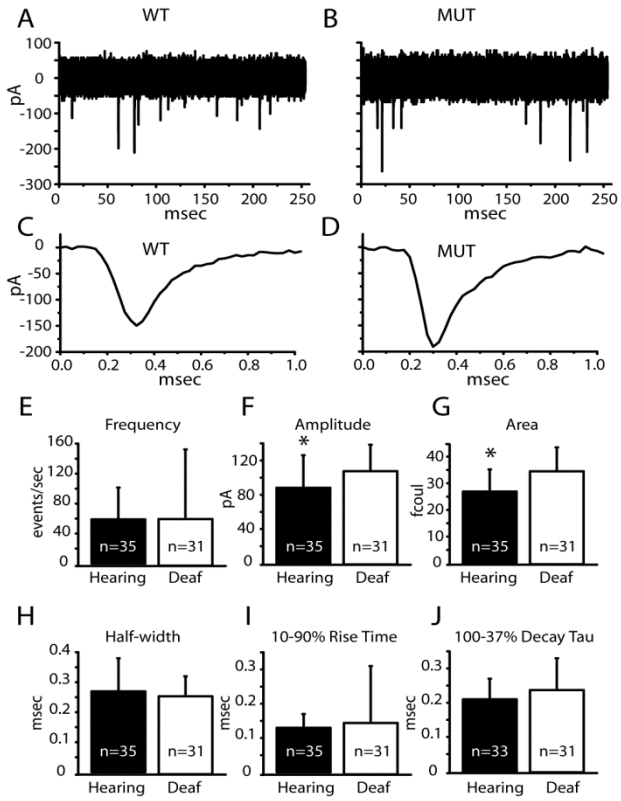

Figure 7 smEPSCs and Characteristics

A) Eleven superimposed traces illustrate spontaneous synaptic currents in a bushy cell from a hearing mouse.

B) Eleven superimposed traces from a bushy cell of a deaf mutant mouse show spontaneous synaptic currents in a bushy cell from a deaf mouse.

C) The average of all of the individual mEPSCs in panel A.

D) The average of all of the individual mEPSCs in panel B.

E) The average frequency of mEPSCs was not significantly different between bushy cells in hearing (58.9 ± 42.5 events/sec) and deaf mice (62.1 ±90.1 events/sec).

F) The average amplitude of mEPSCs was significantly smaller in bushy cells of hearing (-88.21 ± 38.0 pA) than of deaf mice (-108.7 ± 29.7 pA) ($p = 0.02$).

G) The average area of mEPSCs corresponding charge transferred was significantly smaller in hearing (26.9 ± 8.3 fcoul) than in deaf mice (34.9 ± 8.6 fcoul) ($p = 0.0003$).

H) The average half-width of the mEPSCs between the phenotypes was not significantly different. In bushy cells of hearing mice it was 0.27 ±0.11 msec and in deaf animals was 0.26 ±0.06 msec.

I) The average 10-90% rise time of the mEPSCs was not significantly different between the hearing and deaf phenotypes. In the bushy cells from the hearing mice it was 0.13 ± 0.04 msec and in deaf animals was 0.15 ± 0.16 msec.

J) The average 100-37% decay tau was not was not significantly different between the hearing and deaf phenotypes. In the bushy cells from the hearing mice it was 0.21 ±0.06 msec and in deaf animals was 0.24 ±0.09 msec.

Figure 8

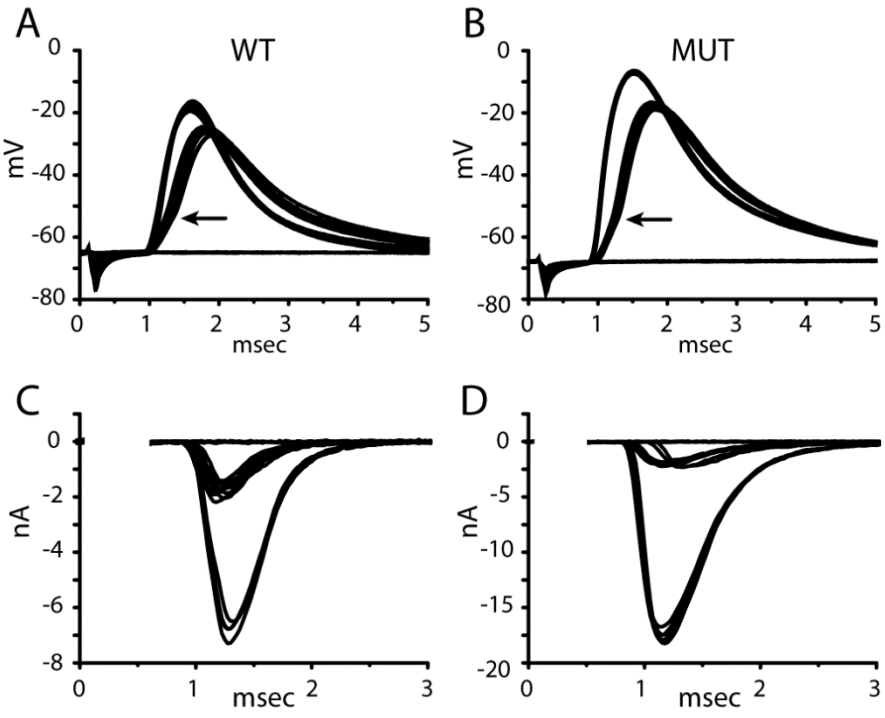

Figure 8 Steps in the growth of shock-evoked EPSPs and EPSCs

As the strength of shocks to fiber bundles near bushy cells was gradually increased, eEPSPs and eEPSCs grew in steps. Numbers of steps were compared in current clamp and voltage clamp.

A) eEPSPs grew with two steps in the same cell from a wild type hearing mouse as in C.

B) eEPSPs grew with two steps in the same bushy cell from a mutant deaf mouse as in D.

C) eEPSCs in the same wild type bushy cell as in A grew in two steps.

D) eEPSCs in the same bushy cell as in B from a homozygous, deaf mutant mouse grew in two steps.

Figure 9

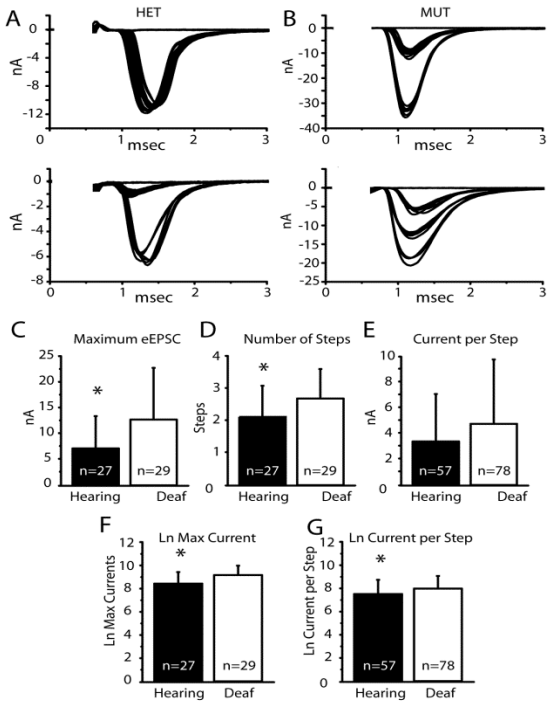

Figure 9 eEPSCs and Characteristics

A) eEPSCs in two bushy cells from heterozygous, hearing mice grew in one step and two steps, forming a single cluster and two clusters of responses.

B) eEPSCs from two bushy cells from deaf mice grew in two steps, forming two clusters of responses, or in three steps.

C) Averaged maximal eEPSCs are significantly larger in deaf than in hearing mice. The average maximal current was quantified by averaging the smallest and largest current sweep from the largest cluster of inputs. In hearing mice the average maximum evoked current was -7.03 ± 6.29 nA and in deaf mice was -12.81 ± 9.91 nA ($p = 0.01$).

D) The average number of steps in eEPSCs was also significantly different between bushy cells in hearing and deaf mice, with eEPSCs in the deaf mice growing in more steps. The number of steps was quantified *post hoc* by eye. In the hearing mice the average number of steps was 2.1 ± 1.0 and in deaf mice was 2.7 ± 0.9 ($p = 0.02$).

E) Differences in the current delivered per step approached significance between the phenotypes but was not significant. Again the amount of current per step was quantified by averaging the smallest and largest current sweeps in a cluster of inputs. In bushy cells from hearing mice the average current delivered per step was -3.33 ± 3.70 nA and in deaf mice it was 4.77 ± 4.95 nA ($p = 0.06$).

F-G) Because the variability in amplitudes of eEPSCs was so large and the possibility that amplitudes are not normally distributed could not be excluded, we tested with ANOVA whether the natural logarithms of amplitudes were the same or different. The average logarithm of maximal eEPSCs in bushy cells from hearing animals was 8.43 ±1 and in deaf mice was 9.17 ±0.81; these were significantly different ($p = 0.004$). The average current delivered per step also became significant. The average logarithm of current per step in hearing mice was 0.64 ± SD 0.48 and in deaf mice was 0.93 ± 0.37; these are significantly different ($p = 0.02$).

Figure 10

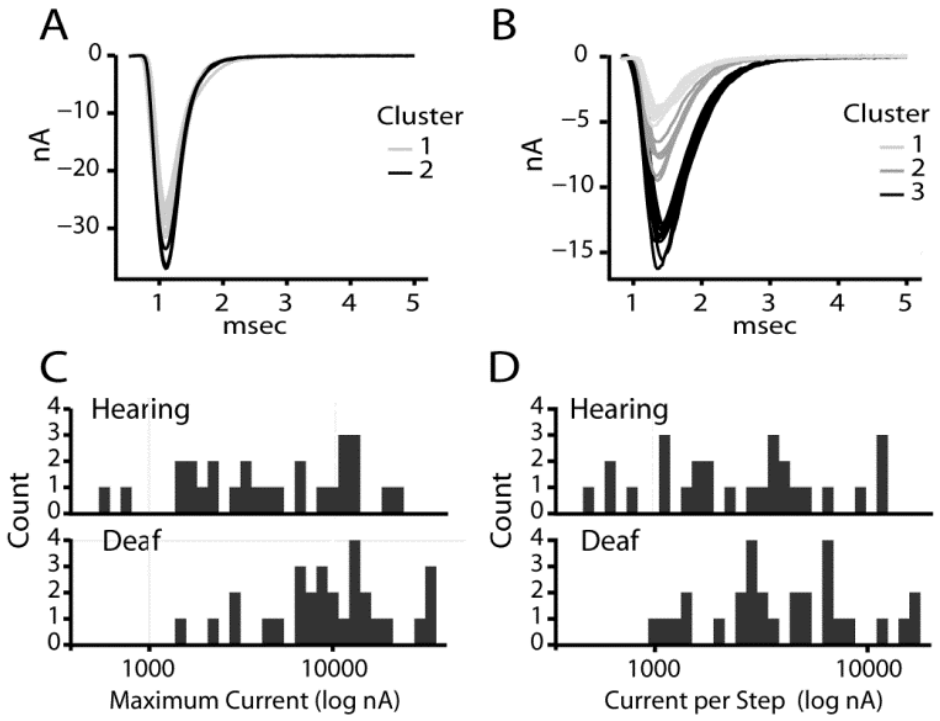

Figure 10 Measuring Steps with a Clustering Algorithm

A) A recording from a bushy cell of a deaf mutant mouse was analyzed with an objective clustering algorithm. This cell's eEPSC grew in two steps.

B) A second recording from a bushy cell of a deaf mutant mouse in which the number of steps was shown by the clustering algorithm to have three steps.

C) The maximal evoked currents between the hearing and deaf mice are illustrated in a log based histogram plot. On average bushy cells from deaf mice (n=29) had maximal evoked currents of 12.55±9.46, and in hearing mice bushy cells had (n=27) 6.81±5.83, p=0.002.

D) After quantifying the number of inputs with the clustering algorithm, we can assess how much current is delivered per input. This is illustrated in a log based histogram plot. In bushy cells from deaf mice (n=74) the average current per input was 4.9 ± 5.1 nA. In bushy cells of hearing mice the average current per input (n=53) was 3.5 ±4.1 nA. Statistically, to deal with the unequal number of samples, different weights were given to a sample with more inputs and as such will be treated as more accurate as it is calculated from more numbers, p=0.03.

Figure 11

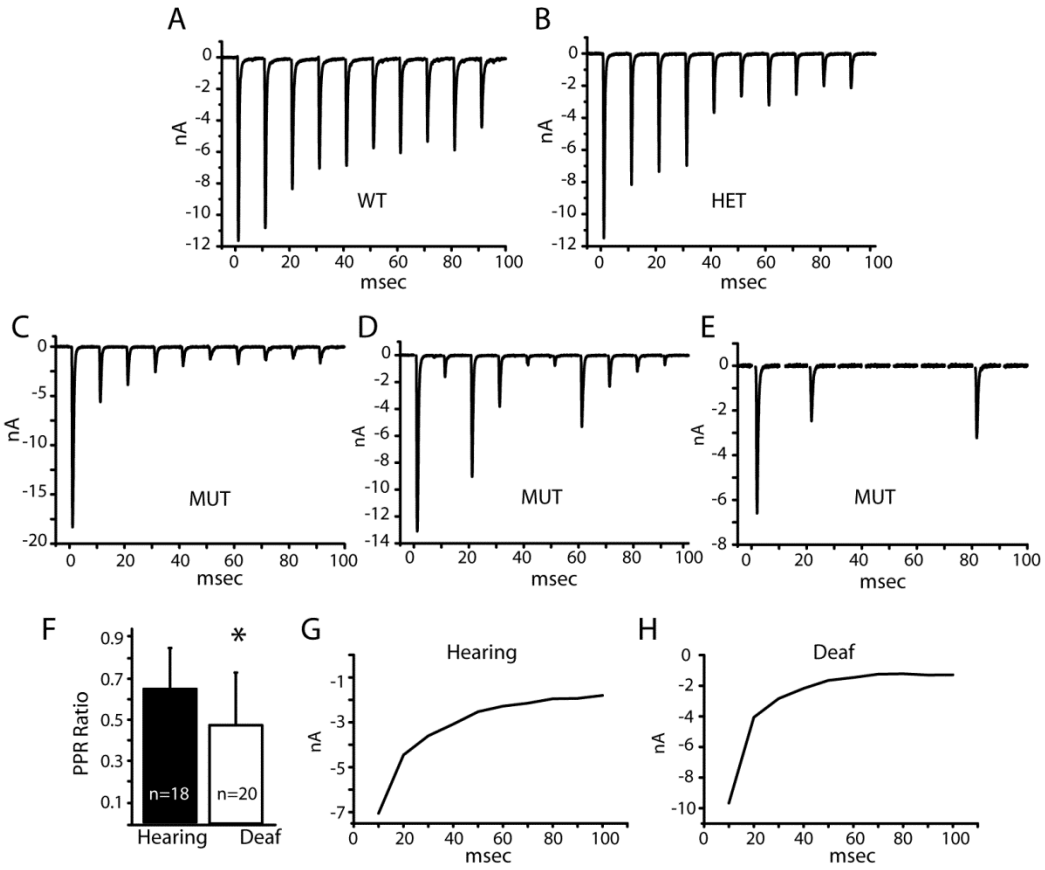

Figure 11 Trains of eEPSCs

A) In a bushy cell from a wild type mouse eEPSCs to a single train of ten shocks at 100 Hz shows that eEPSCs show depression.

B) In a bushy cell from a heterozygote mouse depression was similar as in the wild type.

C-E) eEPSCs in bushy cells from deaf mice in responses to ten stimuli at 100 Hz depress more and sometimes fail altogether.

F) The paired-pulse ratio (PPR), the ratio of the amplitude of the eEPSC in response to the second stimulus divided by the amplitude of the eEPSC to the first stimuli, is a measure of the probability of release and synaptic depression. The hearing animals had higher PPR ratios than the deaf mice. The bushy cells in the hearing mice had PPRs of 0.65 ± 0.2 and the deaf had 0.48 ± 0.25 ($p = 0.03$).

G & H) Average values of eEPSCs in bushy cells from hearing and deaf mice show that depression is greater and faster at end bulb/bushy cell synapses in the deaf mice.

Chapter 5

Future Directions & Conclusions

Future Directions

My investigation of the adaptive changes at the second synapse of the auditory pathway when the first synapse is disrupted raises three issues that are worth addressing in the future. The first would be to measure the exact contribution of low voltage activated potassium conductance (g_{KL}) in bushy cells between the hearing and deaf otoferlin point mutant mice. Second, the findings of large synaptic currents in mutant mice raises the question whether there are measurably more AMPA receptors in the post synaptic densities of the bushy cell membranes in deaf relative to hearing mice. Finally, it would be interesting to quantify the average complexity and volume of the end bulb terminals between the hearing and deaf mice.

Low-voltage Activated Potassium Conductance

Bushy cells are coincidence detectors; they are one of the key neurons involved in localizing sound sources in the azimuth. Their job is to detect coincident stimulation by ANFs, upon which they are activated to fire action potentials and thus excite their targets bilaterally in the medial superior olive where timing of excitation is compared in interaural timing differences and to their targets in the ipsilateral lateral superior olive and contralateral medial nucleus of the trapezoid body where the excitation and inhibition are compared for interaural level differences. Bushy cells detect the synchronous activation of ANFs with the help of the low-voltage activated potassium conductance (g_{KL}). This conductance terminates any depolarization in the bushy cells membrane and brings the cell back to near to its resting membrane potential. This property makes it necessary for bushy cells to be depolarized

by large EPSCs such as those delivered through the end bulb of Held and by the requirement for synchronous synaptic inputs arriving simultaneously. g_{KL} makes bushy cells sensitive to the rate at which they are depolarized (McGinley and Oertel 2006) such that the steeper the rise of the depolarization in the bushy cells membrane the more likely the EPSP will overcome the hyperpolarizing effects of g_{KL} and thus permit the cell to spike. I confirmed in my experiments that bushy cells in otoferlin mice are sensitive to the rate at which they are depolarized and also that the bushy cells from the deaf otoferlin mutant mice are less sensitive to the rate at which they are depolarized, such that they require a less steep slope of depolarization to fire action potentials.

My findings lead me to the hypothesis that a change in the magnitude of g_{KL} results from homeostatic plasticity in response to altered synaptic input. Presumably a decrease in drive from ANFs results in an increase in excitability. In order to measure and quantify the different levels of g_{KL} in bushy cells from hearing and deaf mice, bath application of 65 nM α-dendrotoxin (α-DTX) will fully block g_{KL} (Bal and Oertel 2001; Cao et al. 2007) and by recording from bushy cells before and after α-DTX application, it is possible to measure whether the bushy cell's sensitivity to the rate at which it is depolarized has changed and thereby quantify how much the dv/dt threshold is correlated to g_{KL}. This would allow us to compute how much g_{KL} is present in bushy cells from hearing and deaf mice. Bushy cells from deaf mice most probably will have less g_{KL} because they are less sensitive to the rate at which they are depolarized.

Electron Microscopy

Working on the synapses associated with end bulb terminals has made me curious about what the differences might be in the ultrastructural physical arrangement of the postsynaptic densities in the bushy cell membrane between phenotypes. Electron microscopy (EM) experiments performed on deaf white

cats characterized functional changes to the postsynaptic densities. Ryugo and colleagues found that the postsynaptic densities of the deaf white cats were hypertrophied, being elongated and more numerous compared to the postsynaptic densities in bushy cells of hearing cats (Ryugo et al. 1997; Redd et al. 2000) which is consistent with the upregulation of receptors in response to deafness. Another interesting aspect of the AMPA receptor regulation within the postsynaptic densities between hearing and deaf mice is the composition of individual GluA subunits. After EM, postembedding immunocytochemical methods using specific antibodies to GluA2, GluA3 and GluA4 subunits and colloidal gold particle labeling would make it possible to examine the distribution of AMPA receptor subunits in the postsynaptic densities of bushy cells between the phenotypes (Hermida et al. 2010).

Since the amount of synaptic current per input and the maximal evoked current in bushy cells from deaf otoferlin mutant mice was significantly larger than those of the hearing mice, and since the end bulbs in the deaf otoferlin mutant mice appeared wispy in comparison to those of hearing mice it is a plausible hypothesis that the postsynaptic densities in bushy cells of the deaf otoferlin mutant mice are hypertrophied with a an up-regulation of AMPA receptors, including possible alternations in the distribution of AMPA subunit composition in the deaf otoferlin mutant mice compared to those found in hearing mice. An alternative explanation is that there is more glutamate per synaptic vesicle or possibly more synaptic vesicles associated with individual presynaptic active zones in the deaf animals. In order to be able to definitively recognize end bulb terminals when viewing the EM, extracellular injections of biocytin into the nerve root of the cochlear nucleus made in slice before fixing the tissue and performing the EM would clearly label the ANF terminals.

Complexity and Volume Measurements of End Bulbs

The final and possibly most intriguing aspect of my results concerns the complexity and volume of the end bulbs and their malleability in response to deafness. There is a method to quantify the complexity and a possible way to quantify volumes. The method for quantifying complexity is the form factor used by Sento and Ryugo to analyze the relationship between size of the end bulb and spontaneous firing rate; they divide the end bulb's silhouette area by its silhouette perimeter (Sento and Ryugo 1989; Ryugo and Sento 1991). These measurements were calculated from end bulbs of cats in which the axons of ANFs were labeled with horseradish peroxidase after electrophysiological recordings. They were able to associate the end bulbs' form factor to indicate the ANFs spontaneous discharge rate. They found that in cats, end bulbs with smaller form factors were associated with ANFs of low-medium spontaneous discharge rates and end bulbs with larger form factor ratios are associated with ANFs of high spontaneous discharge rates (Sento and Ryugo 1989) indicating that end bulbs which are more complex in shape, as demarcated by the ratio of area divided by perimeter, have lower spontaneous discharge rates than end bulbs with high spontaneous rates (Ryugo and Sento 1991).

The second method to quantify the volume of end bulbs to compare between the hearing and deaf otoferlin mutant mice is with immunofluorescent labeling. ANFs and their axon terminals, end bulbs, could be labeled with extracellular injections of biocytin in slice, resectioned and then processed with streptavidin Alexa Flour 488 after which they can be visualized with fluorescence microscopy (Song et al. 2012). In order to measure the volume of the end bulb one has to obtain three dimensional images with a confocal microscope and then reconstruct the end bulb in three dimensions, using software like Imaris from Bitplane to calculate the volume. With confocal microscopy there are optical resolution limits due to diffraction limitations of the confocal microscope, and as such we may not be able to resolve the filamentous finger-like projections of the end bulb. Due to this fundamental limit of resolution with this type of microscope these volume measurements may not currently be possible; however there is another confocal variant which can improve the resolution below this diffraction limit. Stimulated emission

depletion microscopy (STED) and some widefield fluorescence microscopy techniques may be used to quantify the volume of the fine projections of the end bulb.

Of these two techniques, the form factor method may be the most useful to measure end bulb complexity, currently. Each end bulb terminal would be reconstructed by hand with camera lucida in serial sections and then the volumes quantified with the SigmaScan Software. In time with improvements in the accessibility and improved resolution ability of fluorescent microscopy the confocal route may be more easily implemented.

Conclusions

Otoferlin

Hearing Assessment

Measurements of DPOAEs and ABRs in otoferlin mutants and in otoferlin knock out animals show that in these mice, cochlear function is normal but transmission of information from the cochlea to the brain is prevented. These findings have many implications. First of which is that the second calcium binding domain of otoferlin is required for the process of sensing local nanodomains of calcium and thus directly triggering vesicle exocytosis at the highly efficient ribbon synapse of inner hair cells. Second, it is likely then that the downstream adaptations in the second synapse of the auditory pathway and beyond, which we find in the deaf otoferlin point mutant mice, will also be present in the complete knock outs, as a result of having disrupted acoustically driven and prehearing patterned spontaneous activity. Third, by showing that both mutations result in complete deafness, it is likely that my work on the point mutant is relevant to other pathological mutations in otoferlin, including a complete absence of the protein. My work is thus entirely and directly relatable to the numerous human mutations in otoferlin and other similar

types of pathologies resulting in DFNB9 and possibly other nonsyndromic, prelingual forms of deafness. The main goal of this work is to understand how the brain, specifically the central auditory system adapts when deprived of spontaneous prehearing and acoustically driven excitation.

Volume Loss in the Ventral Cochlear Nucleus

It has been documented rigorously before that deafness results in a reduction of the volume of the ventral cochlear nucleus but many of those studies involved severe, unphysiological perturbations such as cochlear ablations or pharmacological destruction of hair cells and spiral ganglion neurons. It was therefore interesting to find that such large volume reductions are observed under more physiological conditions. It has been shown before that the volume changes were greater when cochlear function was disrupted earlier in development (Steward and Rubel 1985; Lustig et al. 1994). Not only is the acoustically driven excitation from the outside environment absent, but most of the prehearing patterned spontaneous activity originating in the cochlea after P4 is also missing. This in itself in an indication of how valuable the prehearing patterned spontaneous activity from the developing cochlea is for the maturation and survival of principal neurons downstream in the auditory system.

End Bulbs of Held

End bulbs are a wonderful example of the exquisite beauty of the nervous system. These presynaptic terminals, the second largest in the mammalian brain, are adapted for precision in the transmission of acoustic information. Their job is to faithfully convey reliable spike timing information, requiring meticulously encrypted sustained high frequency transmission in some sounds. How is it that these terminals which are needed to reliably and faithfully encode temporal precision are so adaptable in

the face of diminished excitation? Without a resolute way to quantify the reduced complexity and/or volumes of end bulbs resulting from deafness makes it tricky to describe the morphological flexibility observed in these adaptive presynaptic terminals. Luckily, the naked eye is reliable enough to roughly assess the physiological modifications observed in end bulbs as a result of deafness with the distinction of robust versus wispy morphology in the end bulbs from hearing and deaf mice, respectively, which is striking even to a naive observer. Also needed is a dependable way to quantify the apparent reduction in numbers of end bulbs in the deaf otoferlin mutant mice compared to hearing mice. It is possible that the reduction in end bulbs seen in deaf mice could be related to how many bushy cells survive and not be due to the reduced numbers of end bulbs themselves.

Bushy Cells

What is it about these masters of precision in temporal encoding that is so fundamentally distinct? Not only do they have to receive and interpret acoustic transmission with acuity but they have to project and relay that signal to the principal neurons in the superior olivary complex for comparisons in excitation and inhibition which is based solely on timing and intensity in arrival of the stimulus. How do bushy cells amend themselves when they are denied of regular driven stimulation? Homeostatic plasticity is a well-studied phenomenon where neurons adapt in the face of altered activity patterns in order to preserve and maintain optimal levels of activation both individually and systemically. The most interesting question is exactly what are these neurons adjusting and regulating and by what mechanisms do they sense and self-prescribe these plastic rearrangements. From my experiments I see the results of at least two plastic adjustment mechanisms. First, the regulation of bushy cells' sensitivity to the rate at which they are depolarized, which is most likely due to alterations in the low-voltage activated potassium conductance (g_{KL}), being less in the bushy cells from the deaf otoferlin mutant mice. The activation and

participation of g_{KL} was not directly investigated in my thesis project; however it has been studied and measured in the lab from regular hearing animals and is known to be responsible for bushy and octopus cell's sensitivity to the rate at which they are depolarized (Ferragamo and Oertel 2002; McGinley and Oertel 2006). The second adaptation to diminished levels of excitation is the way bushy cells respond to activation of the auditory nerve.

Synaptic Innervation of Bushy Cells

Bushy cells in deaf mutant mice respond to shocks of the auditory nerve with more synaptic inputs that deliver larger eEPSCs. A possible interpretation is that a lack or decrease in synaptic pruning occurs during development in order to preserve as much synaptic innervation and excitation to the acoustically starved bushy cells from deaf otoferlin mutant mice. In addition, more postsynaptic AMPA receptors would account for the larger maximal and individual eEPSCs we find in the deaf mutant mice. It would also account for the larger amplitude and greater charge transfer associated with the spontaneous miniature EPSCs. Regardless of whether the number of steps was assessed by eye or by a custom made algorithm, my results show that the number of ANF inputs is greater in bushy cells of deaf mice, about 2.6 compared to bushy cells of hearing mice, which had about 2 inputs on average. I also found that maximal evoked EPSCs, which represented the sum of inputs, are considerably larger in deaf than in hearing mice. Maximal EPSCs were over 12 nA on average in deaf mutant mice compared to about 7 nA in hearing mice.

eEPSPs

I was able to estimate the number of inputs in bushy cells in current clamp as well as in voltage clamp. In current clamp I measured the slope of the evoked depolarization; each group or clustering of depolarizations is likely to reflect the recruitment of an input. Direct spiking in bushy cells evoked by the extracellular stimulation eliciting action potentials in the bushy cell's dendrites or axon, evident as responses that lacked a synaptic delay, sometimes obscured changes in slope, however. Because of this my conclusions of synaptic innervation are based on the number and magnitude of current steps that I could resolve in voltage-clamp measurements.

Natriuretic peptide receptor 2 (Npr2)

In the *Npr2* mutant mice we find altered spatial organization of auditory circuits and unreliable action potential conduction but the temporal precision of the acoustic transmission was largely intact. *Npr2* mutant mice lack the ability for ANFs to bifurcate normally in the nerve root of the VCN, the ANFs however do seem to be able to send collateral branches. All the while the peripheral spiral ganglion neuronal innervation into the cochlea remains normal in the *Npr2* mutant mice. These facts make *Npr2* mutant mice a good tool for studying central auditory processing disorders in humans which can be difficult to diagnose because the patients can still detect sounds. In *Npr2* mutant mice ABR measurements are comparable to those of control mice; however the topographic innervation of auditory nerve fibers into the nerve root of the VCN is severely disrupted as well as the second order topographic inhibitory innervation of tuberculoventral cell projection from the DCN to their isofrequency laminae in the VCN. Indicating normal auditory nerve wiring is not required for basic sound perception, although sound perception is very unlikely normal in the *Npr2* mutant mice. There was a propensity for the ANFs in the *Npr2* mutant mice to prefer innervating the descending branch towards the pVCN and DCN over the ascending branch into aVCN. The synaptic formation also appears normal as assessed by the

undistinguishable end bulb morphology between mutant and control mice. There was however slightly less convergence of ANF numbers onto both T stellate and bushy cells in the VCN in *Npr2* mutant mice compared to controls as assessed by jumps in synaptic current responses from evoked EPSCs. Another abnormal feature in the *Npr2* mutant mice was synaptic failures in response to trains of e evoked EPSCs. These synaptic failures were likely due to action potential conduction block at the branch point of ANFs because branch points are known as sources of conduction block. The synaptic failures found in *Npr2* mutant mice were relieved by a K^+ blocker which strengthens the action potential and thus alleviates the conduction block.

References

Adams JC. (1979) Ascending projections to the inferior colliculus. J Comp Neurol 183:519-538.

Adams JC, Mugnaini E. (1987) Patterns of glutamate decarboxylase immunostaining in the feline cochlear nuclear complex studied with silver enhancement and electron microscopy. J Comp Neurol 262:375-401.

Adams JC, Warr WB. (1976) Origins of axons in the cat's acoustic striae determined by injection of horseradish peroxidase into severed tracts. J Comp Neurol 170:107-121.

Ahmmed AU, Ahmmed AA, Bath JR, Ferguson MA, Plack CJ, et al. (2014) Assessment of Children With Suspected Auditory Processing Disorder: A Factor Analysis Study. Ear Hear.

Alibardi L. (1998) Ultrastructural and immunocytochemical characterization of neurons in the rat ventral cochlear nucleus projecting to the inferior colliculus. Ann Anat 180:415-426.

Appler JM, Goodrich LV. (2011) Connecting the ear to the brain: Molecular mechanisms of auditory circuit assembly. Progress in Neurobiology 93:488-508.

Avan P, Buki B, Petit C. (2013) Auditory distortions: origins and functions. Physiol Rev 93:1563-1619.

Bal R, Oertel D. (2001) Potassium currents in octopus cells of the mammalian cochlear nuclei. J Neurophysiol 86:2299-2311.

Bang SJ, Jensen P, Dymecki SM, Commons KG. (2011) Projections and interconnections of genetically defined serotonin neurons in mice. European J Neurosci 35:85-96.

Barbour, Boris. Electronics for electrophysiologists. April 22, 2011. www.biologie.ens.fr/~barbour/electronics_for_electrophysiologists.pdf

Bartels CF, Bükülmez H, Padayatti P, Rhee DK. (2004) Mutations in the Transmembrane Natriuretic Peptide Receptor NPR-B Impair Skeletal Growth and Cause Acromesomelic Dysplasia, Type Maroteaux. Am J Hum Genet. 75:27-34.

Bernatchez P, Sharma A, Kodaman P, Sessa W (2009) Myoferlin is critical for endocytosis in endothelial cells. Am J Physiol Cell Physiol 297:484-492.

Beurg M, Michalski N, Safieddine S, Bouleau Y, Schneggenburger R, Chapman ER, Petit C, Dulon D. (2010) Control of exocytosis by synaptotagmins and otoferlin in auditory hair cells. J Neurosci 30:13281-13290.

Beurg M, Safieddine S, Roux I, Bouleau Y, Petit C, Dulon D. (2008) Calcium- and otoferlin-dependent exocytosis by immature outer hair cells. J Neurosci 28:1798-1803.

Blackburn CC, Sachs MB. (1990) The representations of the steady-state vowel sound /e/ in the discharge patterns of cat anteroventral cochlear nucleus neurons. J Neurophysiol 63:1191-1212.

Blackburn CC, Sachs MB. (1989) Classification of unit types in the anteroventral cochlear nucleus: PST histograms and regularity analysis. J Neurophysiol 62:1303-1329.

Bourk TR, Mielcarz JP, Norris BE. (1981) Tonotopic organization of the anteroventral cochlear nucleus of the cat. Hearing Res 4:215-241.

Brandt N, Kuhn S, Munkner S, Braig C, Winter H, Blin N, Vonthein R, Knipper M, Engel J. (2007) Thyroid hormone deficiency affects postnatal spiking activity and expression of Ca2+ and K+ channels in rodent inner hair cells. J Neurosci 27:3174-3186.

Brawer JR, Morest DK. (1975) Relations between auditory nerve endings and cell types in the cat's anteroventral cochlear nucleus seen with the Golgi method and Nomarski optics. J Comp Neurol 160:491-506.

Brawer JR, Morest DK, Kane EC. (1974) The neuronal architecture of the cochlear nucleus of the cat. J Comp Neurol 155:251-300.

Brenowitz S, Trussell LO. (2001a) Minimizing Syanptic Depression by Control of Release Probability. J Neurosci 21:1857-1867.

Brenowitz S, Trussell LO. (2001b) Maturation of Synaptic Transmission at End-Bulb Synapses of the Cochlear Nucleus. J Neurosci 21:9487-9498.

Brown MC, Benson TE. (1992) Transneuronal labeling of cochlear nucleus neurons by HRP-labeled auditory nerve fibers and olivocochlear branches in mice. J Comp Neurol 321:645-665.

Brown MC, Liberman MC, Benson TE, Ryugo DK. (1988) Brainstem branches from olivocochlear axons in cats and rodents. J Comp Neurol 278:591-603.

Brown MC, Ledwith JV III. (1990) Projections of thin (type-II) and thick (type-I) auditory-nerve fibers into the cochlear nucleus of the mouse. Hear Res 49:105-18.

Brown MC, Pierce S, Berglund AM. (1991) Cochlear-nucleus branches of thick (medial) olivocochlear fibers in the mouse: a cochleotopic projection. J Comp Neurol 303:300-315.

Brownell WE. (1990) Outer hair cell electromotility and otoacoustic emissions. Ear Hear 11:82-92.

Brugge JF, O'Connor TA. (1984) Postnatal functional development of the dorsal and posteroventral cochlear nuclei of the cat. J Acoust Soc Am 75:1548-1562.

Bucher D, Goaillard J-M. (2011) Beyond faithful conduction: Short-term dynamics, neuromodulation, and long-term regulation of spike propagation in the axon. Progress in Neurobiology 94:307-346.

Cajal SR. (1909) In Histologie du Systeme Nerveux de l'Homme et des Vertebres, (Paris: A. Maloine).

Cant NB. (1981) The fine structure of two types of stellate cells in the anterior division of the anteroventral cochlear nucleus of the cat. Neurosci 6:2643-2655.

Cant NB, Benson CG. (2003) Parallel auditory pathways: projection patterns of the different neuronal populations in the dorsal and ventral cochlear nuclei. Brain Res Bull 60:457-474.

Cant NB, Casseday JH. (1986) Projections from the anteroventral cochlear nucleus to the lateral and medial superior olivary nuclei. J Comp Neurol 247:457-476.

Cant NB, Morest DK. (1979) The bushy cells in the anteroventral cochlear nucleus of the cat. A study with the electron microscope. Neuroscience 4:1925-45.

Cant NB, Morest DK. (1974) The Sturctural Basis for Stimulus Coding in the cochlear Nucleus of the Cat. In Hearing Science, Recent Advances, C.I. Berlin, ed. (San Diego: College-Hill Press), pp. 371-421.

Cao XJ, McGinley MJ, Oertel D. (2008) Connections and synaptic function in the posteroventral cochlear nucleus of deaf jerker mice. J Comp Neurol 510:297-308.

Cao XJ, Oertel D. (2010) Auditory nerve fibers excite targets through synapses that vary in convergence, strength, and short-term plasticity. J Neurophysiol 104:2308-2320.

Cao XJ, Shatadal S, Oertel D. (2007) Voltage-sensitive conductances of bushy cells of the mammalian ventral cochlear nucleus. J Neurophysiol 97:3961-3975.

Caspary DM, Backoff PM, Finlayson PG, Palombi PS. (1994) Inhibitory inputs modulate discharge rate within frequency receptive fields of anteroventral cochlear nucleus neurons. J Neurophysiol 72:2124-2133.

Chanda S, Xu-Friedman MA. (2010) A Low-affinity antagonist reveals saturation and desensitization in mature synapses in the auditory brainstem. J Neurophysiol 103:1915-1926.

Clandinin TR, Feldheim DA. (2009) Making a visual map: mechanisms and molecules. Curr Opin Neurobiol 19: 174–180.

Clause A, Nguyen T, Kandler K. (2011) An acoustic startle-based method of assessing frequency discrimination in mice. J Neuroscience Methods 200:63-67.

Coate TM, Kelley MW. (2013) Making connections in the inner ear: Recent insights into the development of spiral ganglion neurons and their connectivity with sensory hair cells. Seminars in Cell and Developmental Biology: 459–468.

Coate TM, Raft S, Zhao X, Ryan AK, Iii EBC, Kelley MW. (2012) Otic Mesenchyme Cells Regulate Spiral Ganglion Axon Fasciculation through a Pou3f4/EphA4 Signaling Pathway. Neuron 73:49-63.

Conlee JW, Parks TN. (1986) Origin of ascending auditory projections to the nucleus mesencephalicus lateralis pars dorsalis in the chicken. Brain Res 367:96-113.

Crins TT, Rusu SI, Rodriguez-Contreras A, Borst JG. (2011) Developmental changes in short-term plasticity at the rat calyx of held synapse. J Neurosci 31:11706-11717.

Dallos P. (1996) Overview: Cochlear Neurobiology. In The Cochlea, P. Dallos, A.N. Popper, and R.R. Fay, eds. (New York: Springer), pp. 1-43.

Dallos P, He DZ, Lin X, Sziklai I, Mehta S, Evans BN. (1997) Acetylcholine, outer hair cell electromotility, and the cochlear amplifier. J Neurosci 17:2212-2226.

Darrow KN, Maison SF, Liberman MC. (2007) Selective removal of lateral olivocochlear efferents increases vulnerability to acute acoustic injury. J Neurophysiol 97:1775-1785.

Darrow KN, Maison SF, Liberman MC. (2006) Cochlear efferent feedback balances interaural sensitivity. Nat Neurosci 9:1474-1476.

de Venecia RK, Liberman MC, Guinan JJ, Jr., Brown MC. (2005) Medial olivocochlear reflex interneurons are located in the posteroventral cochlear nucleus: a kainic acid lesion study in guinea pigs. J Comp Neurol 487:345-360.

Delgutte B, Kiang NY. (1984) Speech coding in the auditory nerve: IV. Sounds with consonant-like dynamic characteristics. J Acoust Soc Am 75:897-907.

del Rio T, Nishitani AM, Yu W-M, Goodrich LV. (2013) In Vivo Analysis of Lrig Genes Reveals Redundant and Independent Functions in the Inner Ear Barsh GS, ed. PLoS Genet 9:e1003824.

Dempster AP, Laird N M, Rubin DB. (1977). Maximum likelihood for incomplete data via the EM algorithm (with discussion). Journal of Royal Statistical Society 39: 1–38.

Devore S, Ihlefeld A, Hancock K, Shinn-Cunningham B, Delgutte B. (2009) Accurate sound localization in reverberant environments is mediated by robust encoding of spatial cues in the auditory midbrain. Neuron 62:123-134.

Ding J, Voigt HF. (1997) Intracellular response properties of units in the dorsal cochlear nucleus of unanesthetized decerebrate gerbil. J Neurophysiol 77:2549-2572.

Doucet JR, Ryugo DK. (1997) Projections from the ventral cochlear nucleus to the dorsal cochlear nucleus in rats. J Comp Neurol 385:245-264.

Doucet JR, Ryugo DK. (2003) Axonal pathways to the lateral superior olive labeled with biotinylated dextran amine injections in the dorsal cochlear nucleus of rats. J Comp Neurol 461:452-465.

Doucet JR, Ryugo DK. (2006) Structural and functional classes of multipolar cells in the ventral cochlear nucleus. Anat Rec A Discov Mol Cell Evol Biol 288:331-344.

Dror AA, Avraham KB. (2009) Hearing Loss: Mechanisms Revealed by Genetics and Cell Biology. Annu Rev Genet 43: 411–437.

Dulon D, Safieddine S, Jones SM, Petit C. (2009) Otoferlin is critical for a highly sensitive and linear calcium-dependent exocytosis at vestibular hair cell ribbon synapses. J Neurosci 29:10474-10487.

Duncker SV, Franz C, Kuhn S, Schulte U, Campanelli D, Brandt N, Hirt B, Fakler B, Blin N, Ruth P, Engel J, Marcotti W, Zimmerman U, Knipper M. (2013) Otoferlin Couples to Clathrin-Mediated Endocytosis in Mature Cochlear Hair Cells. J Neurosci 33:9508-19.

Dunn J, Blight A. (2011) Dalfampridine: a brief review of its mechanism of action and efficacy as a treatment to improve walking in patients with multiple sclerosis. Curr Med Res Opin 27:1415-1423.

Ebert U. (1996) Noradrenalin enhances the activity of cochlear nucleus neurons in the rat. Eur J Neurosci 8:1306-1314.

Ebert U, Ostwald J. (1992) Serotonin modulates auditory information processing in the cochlear nucleus of the rat. Neurosci Lett 145:51-54.

Ernst MD. (2004) Permutation methods: A basis for exact inference. Statistical Science 19:676–685.

Evans WJ, Webster DB, Cullen JK, Jr. (1983) Auditory brainstem responses in neonatally sound deprived CBA/J mice. Hear Res 10:269-277.

Faraway JJ. (2005) Linear Models with R (First Edition). London: Chapman & Hall/CRC.

Feller MB, Butts DA, Aaron HL, Rokhsar DS, Shatz CJ. (1997) Dynamic processes shape spatiotemporal properties of retinal waves. Neuron 19:293-306.

Ferragamo M, Golding NL, Gardner SM, Oertel D. (1998a) Golgi cells in the superficial granule cell domain overlying the ventral cochlear nucleus: Morphology and eletrophysiology in slices. J Comp Neurol 400:519-528.

Ferragamo MJ, Golding NL, Oertel D. (1998b) Synaptic inputs to stellate cells in the ventral cochlear nucleus. J Neurophysiol 79:51-63.

Ferragamo MJ, Oertel D. (2002) Octopus cells of the mammalian ventral cochlear nucleus sense the rate of depolarization. J Neurophysiol 87:2262-2270.

Fekete DM, Rouiller EM, Liberman MC, Ryugo DK. (1984) The central projections of intracellularly labeled auditory nerve fibers in cats. J Comp Neurol 229:432-450.

Fraley C, Raftery AE. (2007). Bayesian regularization for normal mixture estimation and model-based clustering. Journal of Classification 24:155–181.

Friedland DR, Pongstaporn T, Doucet JR, Ryugo DK. (2003) Ultrastructural examination of the somatic innervation of ventrotubercular cells in the rat. J Comp Neurol 459:77-89.

Frisina RD, Smith RL, Chamberlain SC. (1990) Encoding of amplitude modulation in the gerbil cochlear nucleus: I. A hierarchy of enhancement. Hear Res 44:99-122.

Fujino K, Oertel D. (2001) Cholinergic modulation of stellate cells in the mammalian ventral cochlear nucleus. J Neurosci 21:7372-7383.

Gardner SM, Trussell LO, Oertel D. (2001) Correlation of AMPA receptor subunit composition with synaptic input in the mammalian cochlear nuclei. J Neurosci 21:7428-7437.

Gardner SM, Trussell LO, Oertel D. (1999.) Time course and permeation of synaptic AMPA receptors in cochlear nuclear neurons correlate with input. J Neurosci 19:8721-8729.

Golding NL, Ferragamo MJ, Oertel D. (1999) Role of intrinsic conductances underlying responses to transients in octopus cells of the cochlear nucleus. J Neurosci 19:2897-2905.

Golding NL, Oertel D. (1997) Physiological identification of the targets of cartwheel cells in the dorsal cochlear nucleus. J Neurophysiol 78:248-260.

Golding NL, Robertson D, Oertel D. (1995) Recordings from slices indicate that octopus cells of the cochlear nucleus detect coincident firing of auditory nerve fibers with temporal precision. J Neurosci 15:3138-3153.

Gomez-Nieto R, Rubio ME. (2011) Ultrastructure, synaptic organization, and molecular components of bushy cell networks in the anteroventral cochlear nucleus of the rhesus monkey. Neurosci 179:188-207.

Gomez-Nieto R, Rubio ME. (2009) A Bushy Cell Network in the Rat Ventral Cochlear Nucleus. J Comp Neurology 516:241-263.

Gregory FD, Quinones PM. (2011) Deciphering the roles of C(2)-domain-containing proteins (synaptotagmins and otoferlin) in the inner ear. J Neurosci 31:4765-4767.

Hackney CM, Osen KK, Kolston J. (1990) Anatomy of the cochlear nuclear complex of guinea pig. Anat-Embryol-(Berl) 182:123-149.

Hama H, Kurokawa H, Kawano H, Ando R, Shimogori T, Noda H, Fukami K, Sakaue-Sawano A, Miyawaki A. (2011) Scale: a chemical approach for fluorescence imaging and reconstruction of transparent mouse brain. Nat Neurosci 14:1481-1488.

Han R, Campbell KP. (2007) Dysferlin and muscle repair. Curr Opin Cell Biol 19:409-416.

Hansen KB, Yuan H, Traynelis SF. (2007) Structural aspects of AMPA receptor activation, desensitization and deactivation. Curr Opin Neurobiol 17:281-8.

Harris JA, Rubel EW. (2006) Afferent regulation of neuron number in the cochlear nucleus: cellular and molecular analyses of a critical period. Hear Res 216-217, 127-137.

Heid S, Hartmann R, Klinke R. (1998) A model for prelingual deafness, the congenitally deaf white cat- population statistics and degenerative changes. Hear Res 115:101-112.

Heidrych P, Zimmermann U, Kuhn S, Franz C, Engel J, Duncker SV, Hirt B, Pusch CM, Ruth P, Pfister M, Marcotti W, Blin N, Knipper M. (2009) Otoferlin interacts with myosin VI: implications for maintenance of the basolateral synaptic structure of the inner hair cell. Hum Mol Genet 18:2779-2790.

Held H. (1893) Die zentrale Gehoerleitung. Arch Anat Physiol 201-248.

Hermida D, Mateos JM, Elezgarai I, Puente N, Bilbao A, Bueno-López JL, Streit P, Grandes P. (2010) Spatial compartmentalization of AMPA glutamate receptor subunits at the calyx of Held synapse. J Comp Neurol 518:163-74.

Hind SE, Haines-Bazrafshan R, Benton CL, Brassington W, Towle B, et al. (2011) Prevalence of clinical referrals having hearing thresholds within normal limits. Int J Audiol 50: 708–716.

Imai T, Yamazaki T, Kobayakawa R, Kobayakawa K, Abe T, et al. (2009) Pre-Target Axon Sorting Establishes the Neural Map Topography. Science 325: 585–590.

Irving S, Moore DR, Liberman MC, Sumner CJ. (2011) Olivocochlear efferent control in sound localization and experience-dependent learning. J Neurosci 31:2493-2501.

Jahan I, Kersigo J, Pan N, Fritzsch B. (2010) Neurod1 regulates survival and formation of connections in mouse ear and brain. Cell Tissue Res 341:95-110.

Johnson CP, Chapman ER. (2010) Otoferlin is a calcium sensor that directly regulates SNARE-mediated membrane fusion. J Cell Biol 191:187-197.

Johnson SL, Eckrich T, Kuhn S, Zampini V, Franz C, Ranatunga KM, Roberts TP, Masetto S, Knipper M, Kros CJ, Marcotti W (2011) Position-dependent patterning of spontaneous action potentials in immature cochlear inner hair cells. Nat Neurosci 14:711-7.

Joris PX, Smith PH, Yin TC. (1998) Coincidence detection in the auditory system: 50 years after Jeffress. Neuron 6:1235-8.

Joris PX, Smith PH, Yin TC. (1994) Enhancement of neural synchronization in the anteroventral cochlear nucleus. II. Responses in the tuning curve tail. J Neurophysiol 71:1037-1051.

Joris PX, Yin TC. (1995) Envelope coding in the lateral superior olive. I. Sensitivity to interaural time differences. J Neurophysiol 73:1043-1062.

Kandler K, Clause A, Noh J. (2009) Tonotopic reorganization of developing auditory brainstem circuits. Nat Neurosci 12:711-717.

Kiang NY. (1965) Discharge Patterns of Single Fibers in the Cat's Auditory Nerve. The M.I.T. Press, Cambridge, Massachusetts.

Kim JH, Renden R, Gersdorff von H. (2013) Dysmyelination of Auditory Afferent Axons Increases the Jitter of Action Potential Timing during High-Frequency Firing. J Neurosci 33:9402-9407.

Klepper A, Herbert H. (1991) Distribution and origin of noradrenergic and serotonergic fibers in the cochlear nucleus and inferior colliculus of the rat. Brain Res 557:190-201.

Kolston J, Osen KK, Hackney CM, Ottersen OP, Storm-Mathisen J. (1992) An atlas of glycine- and GABA-like immunoreactivity and colocalization in the cochlear nuclear complex of the guinea pig. Anatomy & Embryology 186:443-465.

Kopp-Scheinpflug C, Dehmel S, Dorrscheidt GJ, Rubsamen R. (2002) Interaction of excitation and inhibition in anteroventral cochlear nucleus neurons that receive large endbulb synaptic endings. J Neurosci 22:11004-11018.

Köppl C, Carr CE. (2003) Computational diversity in the cochlear nucleus angularis of the barn owl. J Neurophysiol 89:2313-2329.

Kössl M, Vater M. (1989) Noradrenaline enhances temporal auditory contrast and neuronal timing precision in the cochlear nucleus of the mustached bat. J Neurosci 9:4169-4178.

Koundakjian EJ, Appler JL, Goodrich LV. (2007) Auditory Neurons Make Stereotyped Wiring Decisions before Maturation of Their Targets. J Neurosci 27:14078-14088.

Lauer AM, Connelly CJ, Graham H, Ryugo DK. (2013) Morphological Characterization of Bushy Cells and Their Inputs in the Laboratory Mouse (Mus musculus) Anteroventral Cochlear Nucleus. PLoS ONE 8:e73308.

Leao RM, von Gersdorff H. (2001) Noradrenaline increases high-frequency firing at the calyx of held synapse during development by inhibiting glutamate release. J Neurophysiol 87:2297-2306.

Lek A, Evesson FJ, Sutton RB, North KN, Cooper ST. (2011) Ferlins: Regulators of Vesicle Fusion for Auditory Neurotransmission, Receptor Trafficking and Membrane Repair. Traffic.

Levic S, Bouleau Y, Dulon D. (2011) Developmental acquisition of a rapid calcium-regulated vesicle supply allows sustained high rates of exocytosis in auditory hair cells. PLoS. One. *6*, e25714.

Liberman MC. (1991) Central projections of auditory-nerve fibers of differing spontaneous rate. I. Anteroventral cochlear nucleus. J Comp Neurol 313:240-258.

Liberman MC. (1978) Auditory-nerve response from cats raised in a low-noise chamber. J Acoust Soc Am 63:442-455.

Lin KH, Oleskevich S, Taschenberger H. (2011) Presynaptic Ca2+ influx and vesicle exocytosis at the mouse endbulb of Held: a comparison of two auditory nerve terminals. J Physiol 589:4301-4320.

Longo-Guess C, Gagnon LH, Bergstrom DE, Johnson KR. (2007) A missense mutation in the conserved C2B domain of otoferlin causes deafness in a new mouse model of DFNB9. Hear Res 234:21-28.

Lorente de No R. (1933) Anatomy of the eigth nerve. III. General plans of structure of the primary cochlear nuclei. Laryngoscope 43:327-350.

Lorente de Nó R. (1981) The Primary Acoustic Nuclei. Raven Press, New York.

Lorteije JAM, Borst JGG. (2010) Contribution of the mouse calyx of Held synapse to tone adaptation. European J Neurosci 33:251-258.

Lu CC, Appler JM, Houseman EA, Goodrich LV. (2011) Developmental profiling of spiral ganglion neurons reveals insights into auditory circuit assembly. J Neurosci 31:10903-10918.

Lustig LR, Leake PA, Snyder RL, Rebscher SJ. (1994) Changes in the cat cochlear nucleus following neonatal deafening and chronic intracochlear electrical stimulation. Hear Res 74:29-37.

MacLeod KM, Carr CE. (2005) Synaptic physiology in the cochlear nucleus angularis of the chick. J Neurophysiol 93:2520-2529.

MacLeod KM, Horiuchi TK, Carr CE. (2007) A role for short-term synaptic facilitation and depression in the processing of intensity information in the auditory brain stem. J Neurophysiol 97:2863-2874.

Mahdieh N, Shirkavand A, Rabbani B, Tekin M, Akbari B, Akbari MT, Zeinali S. (2012) Screening of OTOF mutations in Iran: A novel mutation and review. International J Pediatric Otorhinolaryngology 76:1610-1615.

Manis PB, Marx SO. (1991) Outward currents in isolated ventral cochlear nucleus neurons. J Neurosci 11:2865-2880.

Maricich SM, Xia A, Mathes EL, Wang VY, Oghalai JS, Fritzsch B, Zoghbi HY. (2009) Atoh1-Lineal Neurons Are Required for Hearing and for the Survival of Neurons in the Spiral Ganglion and Brainstem Accessory Auditory Nuclei. J Neurosci 29:11123-11133.

Marty NJ, Holman CL, Abdullah N, Johnson CP. (2013) The C2 Domains of Otoferlin, Dysferlin, and Myoferlin Alter the Packing of Lipid Bilayers. Biochemistry 52:5585-92.

May BJ, Prell GS, Sachs MB. (1998) Vowel representations in the ventral cochlear nucleus of the cat: effects of level, background noise, and behavioral state. J Neurophysiol 79:1755-1767.

McGinley MJ, Liberman MC, Bal R, Oertel D. (2012) Generating Synchrony from the Asynchronous: Compensation for Cochlear Traveling Wave Delays by the Dendrites of Individual Brainstem Neurons. J Neurosci 32:9301-9311.

McGinley MJ, Oertel D. (2006) Rate thresholds determine the precision of temporal integration in principal cells of the ventral cochlear nucleus. Hear Res 216-217, 52-63.

Meidinger MA, Hildebrandt-Schoenfeld H, Illing RB. (2006) Cochlear damage induces GAP-43 expression in cholinergic synapses of the cochlear nucleus in the adult rat: a light and electron microscopic study. Eur J Neurosci 3187-99.

Merchan-Perez A, Liberman MC. (1996) Ultrastructural differences among afferent synapses on cochlear hair cells: correlations with spontaneous discharge rate. J Comparative Neurology 371:208-221.

Melcher JR, Guinan JJ Jr, Knudson IM, Kiang N. (1996) Generators of the brainstem auditory evoked potential in cat. II. Correlating lesion sites with waveform changes. Hearing Research 93:28-51.

Miko IJ, Nakamura PA, Henkemeyer M, Cramer KS. (2007) Auditory brainstem neural activation patterns are altered in EphA4- and ephrin-B2-deficient mice. J Comp Neurol 505:669-681.

Molea D, Rubel EW. (2003) Timing and topography of nucleus magnocellularis innervation by the cochlear ganglion. J Comp Neurol 466:577-591.

Molecular Devices, Resources Center. November 29, 2010. http://mdc.custhelp.com/app/answers/detail/a_id/18716/~/correcting-for-pipette-capacitance-using-a-multiclamp%E2%84%A2-amplifier

Moore JW, Westerfield M. (1983) Action potential propagation and threshold parameters in inhomogeneous regions of squid axons. J Physiology 336:285-300.

Moore DR, Kowalchuk NE. (1988) Auditory brainstem of the ferret: effects of unilateral cochlear lesions on cochlear nucleus volume and projections to the inferior colliculus. J Comp Neurol 272:503-15.

Mostafapour SP, Cochran SL, Del Puerto NM, Rubel EW. (2000) Patterns of Cell Death in Mouse Anteroventral Cochlear Nucleus Neurons After Unilateral Cochlea Removal. J Comp Neurol 426:561-571.

Motts SD, Slusarczyk AS, Sowick CS, Schofield BR. (2008) Distribution of cholinergic cells in guinea pig brainstem. Neurosci 154:186-195.

Muniak MA, Ryugo DK. (2013) Tonotopic organization of vertical cells in the dorsal cochlear nucleus of the CBA/J mouse. J Comp Neurol 522:937-49.

Needham K, Paolini AG. (2003) Fast inhibition underlies the transmission of auditory information between cochlear nuclei. J Neurosci 23:6357-6361.

Nelken I, Young ED. (1994) Two separate inhibitory mechanisms shape the responses of dorsal cochlear nucleus type IV units to narrowband and wideband stimuli. J Neurophysiol 71:2446-2462.

Nouvian R, Neef J, Bulankina AV, Reisinger E, Pangrsic T, Frank T, Sikorra S, Brose N, Binz T, Moser T. (2011) Exocytosis at the hair cell ribbon synapse apparently operates without neuronal SNARE proteins. Nat Neurosci 14:411-413.

Nowak L, Bregetovski P, Ascher P, Herbet P, Prochiantz A. (1984) Magnesium gates glutamate-activated channels in mouse central neurones. Nature 307:462-465.

Oertel D. (1983) Synaptic responses and electrical properties of cells in brain slices of the mouse anteroventral cochlear nucleus. J Neurosci 3:2043-2053.

Oertel D, Bal R, Gardner SM, Smith PH, Joris PX. (2000) Detection of synchrony in the activity of auditory nerve fibers by octopus cells of the mammalian cochlear nucleus. Proc Nat Acad Sci USA 97:11773-11779.

Oertel D, Fujino K. (2001) Role of biophysical specialization in cholinergic modulation in neurons of the ventral cochlear nuclei. Audiol Neurootol 6:161-166.

Oertel D, Wickesberg RE. (1993) Glycinergic inhibition in the cochlear nuclei: evidence for tuberculoventral neurons being glycinergic. In: Merchan,M.A., Juiz,J.M., Godfrey,D.A. (Eds.), The Mammalian Cochlear Nuclei: Organization and Function. Plenum Publishing Corp., New York.

Oertel D, Wright S, Cao XJ, Ferragamo M, Bal R. (2011) The multiple functions of T stellate/multipolar/chopper cells in the ventral cochlear nucleus. Hear Res 276:61-69.

Oertel D, Wu SH, Garb MW, Dizack C. (1990) Morphology and physiology of cells in slice preparations of the posteroventral cochlear nucleus of mice. J Comp Neurol 295:136-154.

Oertel D, Wu SH, Hirsch JA. (1988) Electrical characteristics of cells and neuronal circuitry in the cochlear nuclei studied with intracellular recordings from brain slices. In: Edelman,G.M., Gall,W.E., Cowan,W.M. (Eds.), Auditory Function. John Wiley & Sons, Inc., New York, pp. 313-336.

Oertel D, Young ED. (2004) What's a cerebellar circuit doing in the auditory system? Trends Neurosci 27:104-110.

O'Hara RB, Kotze DJ. (2010) Do not log-transform count data. Methods in Ecology and Evolution 1:118-122.

Oleskevich S, Clements J, Walmsley B. (2000) Release probability modulates short-term plasticity at a rat giant terminal. J Physiology 524:513-523.

Osen KK. (1970a) Afferent and efferent connections of three well-defined cell types of the cat cochlear Nuclei. In Excitatory Synaptic Mechanisms, P. Andersen, and J.K.S. Jansen, eds. Oslo: pp. 295-300.

Osen KK. (1970b) Course and termination of the primary afferents in the cochlear nuclei of the cat. Arch Ital Biol 108:21-51.

Osen KK. (1969) Cytoarchitecture of the cochlear nuclei in the cat. J Comp Neurol 136:453-484.

Osen KK, Roth K. (1969) Histochemical localization of cholinesterases in the cochlear nuclei of the cat, with notes on the origin of acetylcholinesterase-positive afferents and the superior olive. Brain Res 16:165-185.

Ostapoff EM, Benson CG, Saint Marie RL. (1997) GABA- and glycine-immunoreactive projections from the superior olivary complex to the cochlear nucleus in guinea pig. J Comp Neurol 381:500-512.

Palmer AR, Jiang D, Marshall DH. (1996) Responses of ventral cochlear nucleus onset and chopper units as a function of signal bandwidth. J Neurophysiol 75:780-794.

Palombi PS, Caspary DM. (1992) GABAA receptor antagonist bicuculline alters response properties of posteroventral cochlear nucleus neurons. J Neurophysiol 67:738-746.

Pangrsic T, Lasarow L, Reuter K, Takago H, Schwander M, Riedel D, Frank T, Tarantino LM, Bailey JS, Strenzke N, Brose N, Muller U, Reisinger E, Moser T. (2010) Hearing requires otoferlin-dependent efficient replenishment of synaptic vesicles in hair cells. Nat Neurosci 13:869-876.

Pangrsic T, Reisinger E, Moser T. (2012) Otoferlin: a multi-C_2 domain protein essential for hearing. Trends in Neurosci 35: 671-680.

Paolini AG, Clarey JC, Needham K, Clark GM. (2005) Balanced inhibition and excitation underlies spike firing regularity in ventral cochlear nucleus chopper neurons. Eur J Neurosci 21:1236-1248.

Pasic TR, Rubel EW. (1989) Rapid changes in cochlear nucleus cell size following blockade of auditory nerve electrical activity in gerbils. J Comp Neurol 283:474-80.

Pfeiffer RR. (1966) Classification of response patterns of spike discharges for units in the cochlear nucleus: tone-burst stimulation. Exp Brain Res 1:220-235.

Pienkowski M, Eggermont JJ. (2012) Reversible long-term changes in auditory processing in mature auditory cortex in the absence of hearing loss induced by passive, moderate-level sound exposure. Ear and hearing 33:305-314.

Powell TP, Erulkar SD. (1962) Transneuronal cell degeneration in the auditory relay nuclei of the cat. J Anat 96:249-68.

R Core Team (2013) R: A language and environment for statistical computing. R Foundation for Statistical Computing, Vienna, Austria. URL http://www.R-project.org/.

Rajan R. (1988) Effect of electrical stimulation of the crossed olivocochlear bundle on temporary threshold shifts in auditory sensitivity. I. Dependence on electrical stimulation parameters. J Neurophysiol 60:549-568.

Ramakrishnan NA, Drescher MJ, Drescher DG. (2009) Direct interaction of otoferlin with syntaxin 1A, SNAP-25, and the L-type voltage-gated calcium channel Cav1.3. J Biol Chem 284:1364-1372.

Ray RS, Corcoran AE, Brust RD, Kim JC, Richerson GB, Nattie E, Dymecki SM. (2011) Impaired Respiratory and Body Temperature Control Upon Acute Serotonergic Neuron Inhibition. Science 333:637-642.

Redd EE, Pongstaporn T, Ryugo DK. (2000) The effects of congenital deafness on auditory nerve synapses and globular bushy cells in cats. Hear Res 147:160-174.

Reisinger E, Bresee C, Neef J, Nair R, Reuter K, Bulankina A, Nouvian R, Koch M, Buckers J, Kastrup L, Roux I, Petit C, Hell SW, Brose N, Rhee JS, Kugler S, Brigande JV, Moser T. (2011) Probing the functional equivalence of otoferlin and synaptotagmin 1 in exocytosis. J Neurosci 31:4886-4895.

Rhode WS. (1999) Vertical cell responses to sound in cat dorsal cochlear nucleus. J Neurophysiol 82:1019-1032.

Rhode WS, Greenberg S. (1992) Physiology of the cochlear nuclei. In Auditory Research, Volume 2: The Physiology of the Mammalian Auditory Central Nervous System, R.R. Fay, and A.N. Popper, eds. pp. 94-152.

Rhode WS, Greenberg S. (1994) Encoding of amplitude modulation in the cochlear nucleus of the cat. J Neurophysiol 71:1797-1825.

Rhode WS, Oertel D, Smith PH. (1983) Physiological response properties of cells labeled intracellularly with horseradish peroxidase in cat ventral cochlear nucleus. JComp Neurol 213:448-463.

Rhode WS, Smith PH. (1986) Encoding timing and intensity in the ventral cochlear nucleus of the cat. J Neurophysiol 56:261-286.

Robertson D, Winter IM. (1988) Cochlear nucleus inputs to olivocochlear neurones revealed by combined anterograde and retrograde labelling in the guinea pig. Brain Res 462:47-55.

Rodrigues ARA, Oertel D. (2006) Hyperpolarization-activated currents regulate excitability in stellate cells of the mammalian ventral cochlear nucleus. J Neurophysiol 95:76-87.

Roux I, Safieddine S, Nouvian R, Grati M, Simmler MC, Bahloul A, Perfettini I, Le GM, Rostaing P, Hamard G, Triller A, Avan P, Moser T, Petit C. (2006) Otoferlin, defective in a human deafness form, is essential for exocytosis at the auditory ribbon synapse. Cell 127:277-289.

Rubel EW, MacDonald GH. (1992) Rapid growth of astrocytic processes in N. magnocellularis following cochlea removal. J Comp Neurol 318:415-25.

Rushton W. (1951) A theory of the effects of fibre size in medullated nerve. J Physiology 115:101-122.

Rutherford MA, Pangrsic T. (2012) Molecular anatomy and physiology of exocytosis in sensory hair cells. Cell Calcium 52: 327-37.

Ryugo DK, Pongstaporn T, Huchton DM, Niparko JK. (1997) Ultrastructural analysis of primary endings in deaf white cats: morphologic alterations in endbulbs of Held. J Comp Neurol 385:230-244.

Ryugo DK, Rosenbaum BT, Kim PJ, Niparko JK, Saada AA. (1998) Single unit recordings in the auditory nerve of congenitally deaf white cats: morphological correlates in the cochlea and cochlear nucleus. J Comp Neurol 397:532-548.

Ryugo DK, Sento S. (1991) Synaptic connections of the auditory nerve in cats: relationship between endbulbs of Held and spherical bushy cells. J Comp Neurol 305*:*35-48.

Ryugo DK, Spirou GA. (2009) Auditory System: Giant Synaptic Terminals, Endbulbs, and Calyces. In Encyclopedia of Neuroscience, Elsevier), pp. 759-770.

Safieddine S, Wenthold RJ. (1999) SNARE complex at the ribbon synapses of cochlear hair cells: analysis of synaptic vesicle- and synaptic membrane-associated proteins. Eur. J Neurosci 11:803-812.

Schmidt H, Rathjen FG. (2010) Signalling mechanisms regulating axonal branching in vivo. Bioessays 32:977-985.

Schmidt H, Stonkute A, Jüttner R, Koesling D, Friebe A, Rathjen FG. (2009) C-type natriuretic peptide (CNP) is a bifurcation factor for sensory neurons. Proc Natl Acad Sci USA 106:16847-16852.

Schmidt H, Stonkute A, Jüttner R, Schäffer S, Buttgereit J, Feil R, Hofmann F, Rathjen FG. (2007) The receptor guanylyl cyclase Npr2 is essential for sensory axon bifurcation within the spinal cord. J Cell Biology 179:331-340.

Schneggenburger R, Meyer AC, Neher E. (1999) Released fraction and total size of a pool of immediately available transmitter quanta at a calyx synapse. Neuron 23:399-409.

Schug N, Braig C, Zimmermann U, Engel J, Winter H, Ruth P, Blin N, Pfister M, Kalbacher H, Knipper M. (2006) Differential expression of otoferlin in brain, vestibular system, immature and mature cochlea of the rat. Eur J Neurosci 24:3372-3380.

Schwarz G. (1978). Estimating the dimension of a model. The Annals of Statistics 6: 461–464.

Sento S, Ryugo DK. (1989) Endbulbs of held and spherical bushy cells in cats: morphological correlates with physiological properties. J Comp Neurol 280:553-562.

Sekerkova G, Richter CP, Bartles JR (2011) Roles of the espin actin-bundling proteins in the morphogenesis and stabilization of hair cell stereocilia revealed in CBA/CaJ congenic jerker mice. PLoS Genet 7:e1002032.

Shah MM, Hammond RS Hoffman DA (2010) Dendritic ion channel trafficking and plasticity. *TINS* 33:307-316.

Shannon RV, Zeng FG, Kamath V, Wygonski J, Ekelid M. (1995) Speech recognition with primarily temporal cues. Science 270:303-304.

Sherriff FE, Henderson Z. (1994) Cholinergic neurons in the ventral trapezoid nucleus project to the cochlear nuclei in the rat. Neurosci 58:627-633.

Shofner WP, Young ED. (1985) Excitatory/inhibitory response types in the cochlear nucleus: relationships to discharge patterns and responses to electrical stimulation of the auditory nerve. J Neurophysiol 54:917-939.

Shore SE, Helfert RH, Bledsoe SC, Jr., Altschuler RA, Godfrey DA. (1991) Descending projections to the dorsal and ventral divisions of the cochlear nucleus in guinea pig. Hear Res 52:255-268.

Silver RA, Momiyama A, Cull-Candy SG. (1998) Locus of frequency-dependent depression identified with multiple-probability fluctuation analysis at rat climbing fibre-Purkinje cell synapses. J Physiology 510:881-902.

Slepecky N. (1996) Structure of the Mammalian Cochlea. P. Dallos, A.N. Popper, and R.R. Fay, eds. (New York: Springer), pp. 44-129.

Smith PH, Joris PX, Banks MI, Yin TC. (1993) Responses of cochlear nucleus cells and projections of their axons. In: The Mammalian Cochlear Nuclei, Organization and Function (Merchan MA, Juiz JM, Godfrey DA, Mugnaini E, Eds), pp 349-360. New York and London: Plenum Press.

Smith PH, Joris PX, Carney LH, Yin TC. (1991) Projections of physiologically characterized globular bushy cell axons from the cochlear nucleus of the cat. J Comp Neurol 304:387-407.

Smith PH, Joris PX, Yin TC. (1993) Projections of physiologically characterized spherical bushy cell axons from the cochlear nucleus of the cat: evidence for delay lines to the medial superior olive. J Comparative Neurology 331:245-260.

Smith PH, Rhode WS. (1989) Structural and functional properties distinguish two types of multipolar cells in the ventral cochlear nucleus. J Comp Neurol 282:595-616.

Smith PH, Spirou GA. (2002) From the Cochlea to the Cortex and Back. In Integrative Functions in the Mammalian Auditory Pathway, R.R. Fay, A.N. Popper, and D. Oertel, eds. (New York: Springer), pp. 6-71.

Smith ZM, Delgutte B, Oxenham AJ. (2002) Chimaeric sounds reveal dichotomies in auditory perception. Nature 416:87-90.

Soares D, Carr CE. (2001) The cytoarchitecture of the nucleus angularis of the barn owl (Tyto alba). J Comp Neurol 429:192-205.

Soares D, Chitwood RA, Hyson RL, Carr CE. (2002) Intrinsic neuronal properties of the chick nucleus angularis. J Neurophysiol 88:152-162.

Song C, Detert JA, Sehgal M, Moyer JR. (2012) Trace fear conditioning enhances synaptic and intrinsic plasticity in rat hippocampus. J Neurophysiol 107:3397-3408.

Spangler KM, Cant NB, Henkel CK, Farley GR, Warr WB. (1987) Descending projections from the superior olivary complex to the cochlear nucleus of the cat. J Comp Neurol 259:452-465.

Spirou GA, Rager J, Manis PB. (2005) Convergence of auditory-nerve fiber projections onto globular bushy cells. Neurosci 136:843-863.

Stakhovskaya O, Hradek GT, Snyder RL, Leake PA. (2008) Effects of age at onset of deafness and electrical stimulation on the developing cochlear nucleus in cats. Hear Res 243:69-77.

Steward O, Rubel EW. (1985) Afferent influences on brain stem auditory nuclei of the chicken: cessation of amino acid incorporation as an antecedent to age-dependent transneuronal degeneration. Comp Neurol 231:385-95.

Sullivan WE. (1985) Classification of response patterns in cochlear nucleus of barn owl: correlation with functional response properties. J Neurophysiol 53:201-216.

Sullivan WE, and Konishi M. (1984) Segregation of stimulus phase and intensity coding in the cochlear nucleus of the barn owl. J Neurosci 4:1787-1799.

Taberner AM, Liberman MC. (2005) Response properties of single auditory nerve fibers in the mouse. J. Neurophysiol 93:557-569.

Takahashi T, Moiseff A, Konishi M. (1984) Time and intensity cues are processed independently in the auditory system of the owl. J Neurosci 4:1781-1786.

Takahashi TT, Konishi M. (1988a) Projections of nucleus angularis and nucleus laminaris to the lateral lemniscal nuclear complex of the barn owl. J Comp Neurol 274:212-238.

Takahashi TT, Konishi M. (1988b) Projections of the cochlear nuclei and nucleus laminaris to the inferior colliculus of the barn owl. J Comp Neurol 274:190-211.

Ter-Avetisyan G, Rathjen FG, Schmidt H. (2014) Bifurcation of Axons from Cranial Sensory Neurons Is Disabled in the Absence of Npr2-Induced cGMP Signaling. J Neurosci 34:737-747.

Tessier-Lavigne M. (1995) Eph receptor tyrosine kinases, axon repulsion, and the development of topographic maps. Cell 82:345-348.

Thompson AM. (1998) Heterogeneous projections of the cat posteroventral cochlear nucleus. J Comp Neurol 390:439-453.

Thompson AM. (2003a) A medullary source of norepinephrine in cat cochlear nuclear complex. Exp Brain Res 153:486-490.

Thompson AM. (2003b) Pontine sources of norepinephrine in the cat cochlear nucleus. J Comp Neurol 457:374-383.

Thompson AM, Moore KR, Thompson GC. (1995) Distribution and origin of serotoninergic afferents to guinea pig cochlear nucleus. J Comp Neurol 351:104-116.

Thompson AM, Thompson GC. (1988) Neural connections identified with PHA-L anterograde and HRP retrograde tract-tracing techniques. J Neurosci Method 25:13-17.

Thompson AM, Thompson GC. (1991a) Posteroventral cochlear nucleus projections to olivocochlear neurons. J Comp Neurol 303:267-285.

Thompson AM, Thompson GC. (1991b) Projections from the posteroventral cochlear nucleus to the superior olivary complex in guinea pig: Light and EM observations with the PHA-L method. J Comp Neurol 311:495-508.

Thompson AM, Thompson GC. (2001) Serotonin projection patterns to the cochlear nucleus. Brain Res 907:195-207.

Thompson GC, Thompson AM, Garrett KM, Britton BH. (1994) Serotonin and serotonin receptors in the central auditory system. Otolaryngol.Head Neck Surg 110:93-102.

Tierney TS, Russell FA, Moore DR. (1997) Susceptibility of developing cochlear nucleus neurons to deafferentation-induced death abruptly ends just before the onset of hearing. J Comp Neurol 378:295-306.

Tolbert LP, Morest DK. (1982a) The neuronal architecture of the anteroventral cochlear nucleus of the cat in the region of the cochlear nerve root: electron microscopy. Neurosci 7:3053-3067.

Tolbert LP, Morest DK. (1982b) The neuronal architecture of the anteroventral cochlear nucleus of the cat in the region of the cochlear nerve root: Golgi and Nissl methods. Neurosci 7:3013-3030.

Tolbert LP, Morest DK, Yurgelun-Todd DA. (1982) The neuronal architecture of the anteroventral cochlear nucleus of the cat in the region of the cochlear nerve root: horseradish peroxidase labelling of identified cell types. Neurosci 7:3031-3052.

Tollin DJ, Yin TC. (2002a) The coding of spatial location by single units in the lateral superior olive of the cat. I. Spatial receptive fields in azimuth. J Neurosci 22:1454-1467.

Tollin DJ, Yin TC. (2002b). The coding of spatial location by single units in the lateral superior olive of the cat. II. The determinants of spatial receptive fields in azimuth. J Neurosci 22:1468-1479.

Tritsch NX, Bergles DE. (2010) Developmental regulation of spontaneous activity in the Mammalian cochlea. J Neurosci 30:1539-1550.

Tritsch NX, Rodriguez-Contreras A, Crins TT, Wang HC, Borst JG, Bergles DE. (2010) Calcium action potentials in hair cells pattern auditory neuron activity before hearing onset. Nat Neurosci 13:1050-1052.

Tritsch NX, Yi E, Gale JE, Glowatzki E, Bergles DE. (2007) The origin of spontaneous activity in the developing auditory system. Nature 450:50-55.

Tritsch NX, Zhang YX, Ellis-Davies G, Bergles DE. (2010b) ATP-induced morphological changes in supporting cells of the developing cochlea. Purinergic Signal 6:155-166.

Trune DR. (1982a) Influence of neonatal cochlear removal on the development of mouse cochlear nucleus: I. Number, size, and density of its neurons. J Comp Neurol 209:409-424.

Trune DR. (1982b) Influence of neonatal cochlear removal on the development of mouse cochlear nucleus: II. Dendritic morphometry of its neurons. J Comp Neurol 209:425-434.

Trune DR, Morgan CR. (1988) Influence of developmental auditory deprivation on neuronal ultrastructure in the mouse anteroventral cochlear nucleus. Brain Res 470:304-8.

Tsuchitani C, Johnson DH. (1985) The effects of ipsilateral tone burst stimulus level on the discharge patterns of cat lateral superior olivary units. J Acoust Soc Am 77:1484-1496.

Tsuji T. (2005) A Loss-of-Function Mutation in Natriuretic Peptide Receptor 2 (Npr2) Gene Is Responsible for Disproportionate Dwarfism in cn/cn Mouse. J Biological Chemistry 280:14288-14292.

Turrigiano GG. (1999) Homeostatic plasticity in neuronal networks: the more things change, the more they stay the same. Trends Neurosci 22:221-227.

Turrigiano GG. (2008) The self-tuning neuron: synaptic scaling of excitatory synapses. Cell 135:422- 435.

van Gisbergen JA, Grashuis JL, Johannesma PI, Vendrik AJ. (1975) Statistical analysis and interpretation of the initial response of cochlear nucleus neurons to tone bursts. Exp Brain Res 23:407-423.

Wang Y, Manis PB. (2008) Short-Term Synaptic Depression and Recovery at the Mature Mammalian Endbulb of Held Synapse in Mice. J Neurophysiol 100:1255-1264.

Wang YX, Wenthold RJ, Ottersen OP, Petralia RS. (1998) Endbulb synapses in the anteroventral cochlear nucleus express a specific subset of AMPA-type glutamate receptor subunits. J Neurosci 18:1148-1160.

Wang H, Yin G, Rogers K, Miralles C, De Blas AL, Rubio ME. (2011) Monaural conductive hearing loss alters the expression of the GluA3 AMPA and glycine receptor alpha1 subunits in bushy and fusiform cells of the cochlear nucleus. Neurosci 199:438-451.

Warr WB. (1969) Fiber degeneration following lesions in the posteroventral cochlear nucleus of the cat. Exp Neurol 23:140-155.

Warr WB. (1982) Parallel ascending Pathways from the cochlear nucleus: Neuroanatomical evidence of functional specialization. In: Contributions to Sensory Physiology. Academic Press, New York, pp. 1-38.

Warr WB. (1992) Organization of Olivocochlear Efferent Systems in Mammals. In The Mammalian Auditory Pathway: Neuroanatomy, D. Webster, A.N. Popper, and R.R. Fay, eds. (New York: Springer), pp. 410-448.

Warr WB, Beck JE. (1996). Multiple projections from the ventral nucleus of the trapezoid body in the rat. Hear. Res. 93: 83-101.

Warren EH, III, Liberman MC. (1989) Effects of contralateral sound on auditory-nerve responses. I. Contributions of cochlear efferents. Hear Res 37:89-104.

Watt AJ, Cuntz H, Mori M, Nusser Z, Sjöström PJ, Häusser M. (2009) Traveling waves in developing cerebellar cortex mediated by asymmetrical Purkinje cell connectivity. Nat Neurosci 12:463-73.

Webster DB. (1985) The spiral ganglion and cochlear nuclei of deafness mice. Hear Res 18:19-27.

Webster DB, Trune DR. (1982) Cochlear nuclear complex of mice. Am. J. Anat. 163, 103-130.

Wegener JW. (2001) cGMP-Dependent Protein Kinase I Mediates the Negative Inotropic Effect of cGMP in the Murine Myocardium. Circulation Research 90:18-20.

Wenthold RJ, Gulley RL. (1977) Aspartic acid and glutamic acid levels in the cochlear nucleus after auditory nerve lesion. Brain Res. 138:111-23.

Whiting B, Moiseff A, Rubio ME. (2009) Cochlear nucleus neurons redistribute synaptic AMPA and glycine receptors in response to monaural conductive hearing loss. Neurosci 163:1264-1276.

Wickesberg RE. (1996) Rapid inhibition in the cochlear nuclear complex of the chinchilla. J Acoust Soc Am 100:1691-1702.

Wickesberg RE, Oertel D. (1990) Delayed, frequency-specific inhibition in the cochlear nuclei of mice: A mechanism for monaural echo suppression. J Neurosci 10:1762-1768.

Wickesberg RE, Oertel D. (1988) Tonotopic projection from the dorsal to the anteroventral cochlear nucleus of mice. J Comp Neurol 268:389-399.

Wiederhold ML, Kiang NY. (1970) Effects of electric stimulation of the crossed olivocochlear bundle on single auditory-nerve fibers in the cat. J Acoust Soc Am 48:950-965.

Willard FH, Ryugo DK. (1983) Anatomy of the central auditory system. In: The Auditory Psychobiology of the Mouse (Willott JF, ed), pp 201-304. Springfield: Charles C Thomas.

Winter IM, Robertson D, Cole KS. (1989) Descending projections from auditory brainstem nuclei to the cochlea and cochlear nucleus of the guinea pig. J Comp Neurol 280:143-157.

Wu SH, Oertel D. (1987) Maturation of synapses and electrical properties. Hear Res 30:99-110.

Wu SH, Oertel D. (1986) Inhibitory circuitry in the ventral cochlear nucleus is probably mediated by glycine. J Neurosci 6:2691-2706.

Wu SH, Oertel D. (1984) Intracellular injection with horseradish peroxidase of physiologically characterized stellate and bushy cells in slices of mouse anteroventral cochlear nucleus. J Neurosci 4:1577-88.

Xia C, Nguyen M, Garrison AK, Zhao Z, Wang Z, Sutherland C, Ma L. (2013) CNP/cGMP signaling regulates axon branching and growth by modulating microtubule polymerization. Devel Neurobio 73:673-87.

Yang YM, Aitoubah J, Lauer AM, Nuriya M, Takamiya K, Jia Z, May BJ, Huganir RL, Wang LY. (2011) GluA4 is indispensable for driving fast neurotransmission across a high-fidelity central synapse. J Physiol 589:4209-4227.

Yang L, Monsivais P, Rubel EW. (1999) The superior olivary nucleus and its influence on nucleus laminaris: a source of inhibitory feedback for coincidence detection in the avian auditory brainstem. J Neurosci 19:2313-2325.

Yang H, Xu-Friedman MA. (2009) Impact of synaptic depression on spike timing at the endbulb of Held. J Neurophysiol 102:1699-710.

Yang H, Xu-Friedman MA. (2008) Relative roles of different mechanisms of depression at the mouse endbulb of Held. J Neurophysiol 99:2510-21.

Yasunaga S, Grati M, Chardenoux S, Smith TN, Friedman TB, Lalwani AK, Wilcox ER, Petit C. (2000) OTOF encodes multiple long and short isoforms: genetic evidence that the long ones underlie recessive deafness DFNB9. Am J Hum Genet 67:591-600.

Yasunaga S, Grati M, Cohen-Salmon M, El-Amraoui A, Mustapha M, Salem N, El-Zir E, Loiselet J, Petit C. (1999) A mutation in OTOF, encoding otoferlin, a FER-1-like protein, causes DFNB9, a nonsyndromic form of deafness. Nat Genet 21:363-369.

Yin TC. (2002) Neural mechanisms of encoding binaural localization cues in the auditory brainstem. In Integrative Functions in the Mammalian Auditory Pathway, D. Oertel, R.R. Fay, and A.N. Popper, eds. (NY: Springer), pp. 99-159.

Young ED, Oertel D. (2004) Cochlear Nucleus. In The Synaptic Organization of the Brain, G.M. Shepherd, ed. (New York: Oxford), pp. 125-163.

Young ED, Robert JM, Shofner WP. (1988) Regularity and latency of units in ventral cochlear nucleus: implications for unit classification and generation of response properties. J Neurophysiol 60:1-29.

Youssoufian M, Oleskevich S, Walmsley B. (2005) Development of a robust central auditory synapse in congenital deafness. J Neurophysiol 5:3168-80.

Zak M, Pfister M, Blin N. (2011) The otoferlin interactome in neurosensory hair cells: Significance for synaptic vesicle release and trans-Golgi network (Review). International J Molec Medicine. 28:311-314.

Zhang S, Oertel D. (1993) Tuberculoventral cells of the dorsal cochlear nucleus of mice: intracellular recordings in slices. J Neurophysiol 69:1409-1421.

Zhao Z, Ma L. (2009) Regulation of axonal development by natriuretic peptide hormones. Proc Natl Acad Sci USA 106:18016-18021.

Zhao Z, Wang Z, Gu Y, Feil R, Hofmann F, Ma L. (2009) Regulate axon branching by the cyclic GMP pathway via inhibition of glycogen synthase kinase 3 in dorsal root ganglion sensory neurons. Journal of Neuroscience 29:1350-1360.